Escola de Camins
Escola Tècnica Superior d'Enginyeria de Camins, Canals i Ports
UPC BARCELONATECH

TREBALL FINAL DE GRAU

NUMERICAL SIMULATION OF SEA WAVES AND THEIR IMPACT AGAINST BREAKWATERS FOR ASSESSING COASTAL PROTECTION SYSTEMS

Autor

Sergi Rabasseda Alcaide

Tutors:

Alessandro Franci

Pavel Ryzhakov

Departament d'Enginyeria Hidràulica Marítima i Ambiental

Barcelona, febrer 2022

INDEX

LIST OF TABLES

LIST OF FIGURES

LIST OF EQUATIONS

ACKNOWLEDGEMENTS

The personal motivation for doing this project was the interest caused by the related courses I took during the Civil Engineering degree at UPC, Spain, and during my exchange period at Aalto University, Finland. These courses gave me the necessary background knowledge to do the project. Then, I would like to express my gratitude to all the professors and associates who generated my interest in maritime engineering through their teaching.

I would like to especially express my thanks to my tutors during the project, the research professors at CIMNE Alessandro Franci and Pavel Ryzhakov, for the engagement, attention and understanding they took with me during these intense six months. I am very grateful for the material they provided me, the support they provided whenever I had any problem, and their helpful teaching throughout the whole time the project took, making sure I understood everything needed.

Also, I would like to acknowledge the solidarity of Centro Internacional de Métodos Numéricos en la Ingeniería (CIMNE) for letting me use its software and server for doing these studies. The authors are grateful to the technical staff at the Coastal Research Center, Hannover, and the Leichtweiß-Institute for Hydraulic Engineering and Water Resources who greatly eased conducting experiments at large-scale. The cost of operation of the large wave flume at Coastal Research Center is jointly covered by the Leibniz University Hannover and Technische Universität Braunschweig. The support of the Volkswagen Foundation (project 'Beyond Rigidity - Collapsing Structures in Experimental Hydraulics', No. 93826) through a grant held by N. Goseberg is greatly acknowledged.

Outside the university, I give my thanks to Berrysar S.L., the engineering consultancy I worked at while doing this project for their flexibility and understanding when letting me combine and balance both work and studies, and to my friends for being there despite the pandemic situation that, unfortunately, accompanied me during all the project.

In particular, in this last stage of the degree, I would like to express my thanks and love to my parents, not just for financially supporting me during all the degree, the TFG within it, but for all the patience and understanding they had with me during all these years.

It has been a nice journey.

ABSTRACT

This work studies water waves propagation and their interaction with solid structures using an innovative numerical method, the Particle Finite Element Method (PFEM). A numerical method is a simulation model equivalent to a physical one able of simulating reality. For the case of PFEM, the numerical method solves the Navier-Stokes equations with a Lagrangian strategy to recreate a physical problem. PFEM is a useful for determining the development of fluid flows with free surfaces and describes the fluid-solid interaction with good accuracy. This, is a suitable method for studying the impact of waves with structures such as breakwaters or groins.

To do the numerical method simulation, the study uses two software. GID software is used for the pre-processing and post-processing procedure. It is the interface where the inputs are determined and where the results are displayed. Kratos Multiphysics software carries the computational process that solves the governing equations.

To validate the numerical method in the given area of application, this project compares the results obtained by PFEM with experimental results from laboratory analysis. It also compares the results with the ones conducted with another numerical method, the Eulerian Finite Element Method (FEM). To do so, four different analyses are performed.

The first analysis consists of solitary small-amplitude wave propagation analysis. It is based on the study of tsunamis. The model is run through PFEM and is compared to the experimental results conducted at the experimental laboratory channel in Braunschweig (Hitzegrad, 2019). The results obtained validate the numerical method for the case and demonstrate the mesh size and time-step size convergence. They also show how errors increase with time, as they are accumulated.

The second analysis studies the case of a more complex system. It consists of a big-amplitude solitary wave with a more complex solid boundary geometry where the wave breaks. The case is also run by PFEM and compared with a laboratory experiment carried out in Japan by Arikawa in the large Hydro Geo-Flume facility (Arikawa, 2009). The results validate PFEM for the case and introduce the possibility of using a mesh refinement to improve the problem computational cost-accuracy relation.

The third analysis performs a simulation by PFEM of a wave train and compares its results with an already validated Eulerian FEM analysis. It also focuses on the effects of a slip or non-slip analysis type of the numerical methods, which determines the behaviour of the fluid on the vicinity of the solid. For the case of PFEM, it is natural to do a no-slip analysis while the FEM can easily account for slip and no-slip. The analysis also does a mesh convergence study to prove that the appropriate mesh for a FEM analysis is not necessarily the one of the PFEM and suggests a refinement structure that shows a more optimum solution to the problem.

The fourth analysis studies the behaviour of waves in the presence of breakwaters on PFEM. It consists of a wave train that impacts and overtops a breakwater placed far from the beach shore. The study illustrates the beneficial effect of breakwaters upon diminishing the wave heights.

This work allows concluding that PFEM can be applied as a complementary tool to experimental studies to analyse wave propagation and its interaction with structures such as the beach

bottom and breakwater with the possibility of overtopping. This work has also shown some aspects of the numerical method that may be improved in future developments.

1. INTRODUCTION

Humans have been interacting with seas and oceans since the beginning of history as these water basins provide numerous resources and are useful transportation media for human development. However, water masses are highly unpredictable and carry many dangerous factors related to their many physical aspects to consider. It is a very aggressive media so, to exploit it, it is necessary to find solutions to the many problems it causes. This problem-solution finding process gave birth to the engineering branch called maritime engineering.

Maritime engineering is based on the study of all the physical aspects related to an ocean. It comprehends the study of its elemental features such as wave generation, tides, currents, water pressures and designing the structures that can interact with these phenomena (like mobile constructions such as ships, submarines etc. or static ones as coastal structures like harbours, groins, breakwaters etc. and offshore structures).

There have been many methods for studying maritime engineering problems, from the directly trial-and-error mechanism to laboratory experimental analysis and recently, from the 70s of the XX century, numerical methods. The new analysis tool is capable of simulating virtually real physical models. This new mechanism opens the possibility of highly more economical studies of maritime phenomena. The methods are still being developed so, nowadays, it is needed to complement the numerical results with experimental ones. Numerical methods are strongly affected by the type of physical aspects which they study, so it is necessary to develop many numerical methods or implement variations and extensions to study different phenomena. However, the improvement of numerical methods can bring many benefits not only for the maritime engineering branch but also for other engineering and scientific.

Within all numerical methods, there are some used for maritime engineering, focusing on the study of waves behaviour and its interaction with structures. These types of numerical methods were born in the 90s. Within these numerical methods, they stand out the ones based on VOF (Volume of fluid) (Hirt & Nichols, 1981) and Level-Set (Osher & Fedkiw, 2001). More recently the Particle Finite Element Method (PFEM) was introduced. This method allows predicting the behaviour of fluids evolving and their interactions with solid structures and describing their free surface. This type of model is useful for the study of maritime processes where the action of waves is the main force actor to consider.

The correct setting of the numerical method depends highly on the appropriate determination of the wave parameters and especially on the wave generation method. There are many methods for generating waves on the numerical method and they have to be as equal as possible with the real physical state of the waves that are being studied. The wave generation system depends on the wave parameters and the adequate location at which it is placed. Then, background knowledge on wave theories is needed for the correct usage of the numerical method.

To sum up, we can conclude that the use of a numerical method is a complex procedure that needs to be determined and set accurately to obtain meaningful results. Nevertheless, as described, there is a high interest in its development as it is an optimum possibility for studying waves and has a bright future perspective. The present project will study a specific numerical method, the Particle Finite Element Method (PFEM), applied to maritime engineering. It will try

to determine its strengths and weaknesses when applied. To do so, the project establishes the following objectives:

- To test and validate PFEM for regular solitary waves.
- To test and validate PFEM for regular wave trains.
- To compare PFEM and Eulerian FEM numerical methods.
- To get the insights of the impact of breakwaters upon the wave height in the vicinity of the beaches.

2. THEORETICAL FRAMEWORK

2.1. WAVE THEORY BASICS

2.1.1. WAVE PARAMETERS

A sea wave or water wave can be defined as a liquid surface perturbation that propagates as an undulation of a free surface. Waves can be generated by different forcing factors, the wind being the most common one.

Waves have some defined parameters that describe their characteristics and shape (Airy, 1842). First of all, the higher point of the wave is called the *crest* while the bottom is called the *trough*, the vertical distance between the crest and the trough is called the *wave height* (*H*). The distance between the mean level, as if water were still (SWL or MWL), and the water surface is called the *free surface elevation* (*η*) and the distance between the bottom and the SWL is the *water depth* (*d*). The vertical distance between the SWL and the crest or the trough is the wave *amplitude* (*a*). For the case of regular waves, if the water depth remains constant the wave height is unaltered and the wave amplitude is equal to half the wave height.

In a longitudinal section, the *wave phase* (ϑ), is the relative position inside the wave from *0* to 2π. The distance between two consecutive crests is the *wavelength* (*L*). The *wavenumber* is ($2\pi/L$) and the *wave steepness* (*s*) is the ratio between the wave height and *wavelength*. The *wave period* (*T*) is the necessary time for two points with the same wave phase to coincide on the same location. The inverse of the period is the *wave frequency* (*f*) and it represents the number of waves that pass through a point per unit of time. In wave theory, usually, the *angular frequency* (*ω*) is used more often and it is equal to ($2\pi/T$).

Finally, *wave celerity* (*c*) is the velocity at which the wave propagates over the surface of the water. By definition, ($c = L/T$), and has units of (*m/s*). The above-described parameters can be seen in *Figure 1*.

Figure 1. Wave parameters, from (Conejo, 2021)

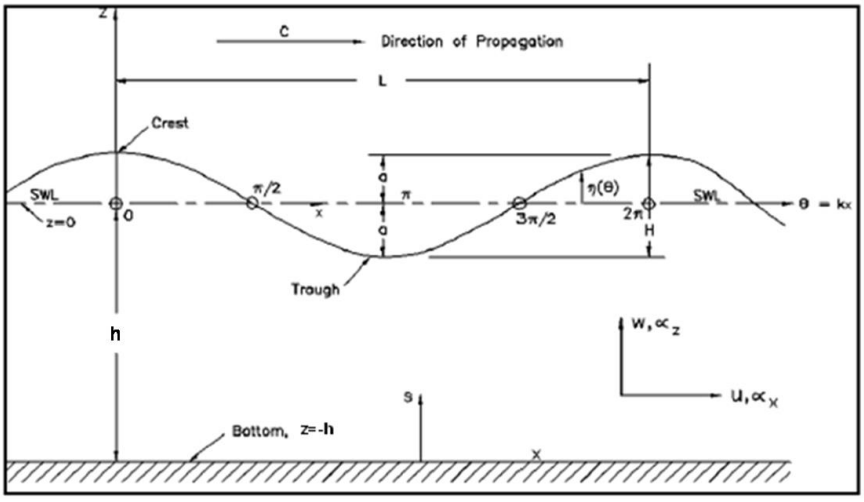

2.1.2. WAVE THEORY HYPOTHESES

Wave theories are approximations of reality that describe the behaviour of waves by satisfying certain hypotheses. The most basic wave theory is the linear wave theory, developed by (Airy, 1842), which gives a simple wave model under the following simplifying assumptions:

- Homogeneous and incompressible fluid (density ρ constant).
- Negligible surface tension.
- Negligible Coriolis effect (due to Earth rotation).
- Pressure at the free surface is uniform and constant
- Ideal fluid (without viscosity).
- Irrotational flow.
- Horizontal, fixed and impermeable bottom.
- Plane waves or long-crested waves (two-dimensional).
- Small wave amplitude (wave steepness s <<1) and the shape of the waves does not vary either in time or space.

These simplifications allow obtaining a wave theory formula (Equation 1)

Equation 1. Wave theory formula.

$$L = \frac{gT^2}{2\pi}\tanh\left(\frac{2\pi h}{L}\right)$$

Waves can be classified depending on the relative depth (h/L) in which they propagate. If (*h/L>0.5*) the wave is in *deep water*, then it follows Equation 2 and Equation 3.

Equation 2. Linear wave theory formula for deep waters

$$L_o = \frac{gT^2}{2\pi}$$

Equation 3 Linear wave theory celerity for deep waters

$$c_o = \frac{gT}{2\pi}$$

On the other hand, if (*h/L < 0.05*), the wave is in *shallow water*, and follows Equation 4 and Equation 5.

Equation 4. Linear wave theory formula for shallow waters

$$L = T\sqrt{gh}$$

Equation 5. Linear wave theory celerity for shallow waters

$$c = \sqrt{gh}$$

In the intermediate case, (*0.05<h/L<0.5*), the wave is in transitional or intermediate water and follows Equation 1.

2.2. WAVE ANALYSIS METHODS

Maritime waves have high impacts on the coast and the structures built on it. The collision of waves on the coastal structures cause erosion and can waste or even break them. The structures should be able to resist the constant impact of these waves not just on their regular state but also during the storm events, where the force impact and height of waves increase notoriously.

Furthermore, waves cause an important accretion or erosion in different places according to the beach orientation, wave direction and currents generated. Several structures can be built to avoid or control this effect including groins and detached breakwaters.

Then, before designing a certain coastal structure it is appropriate to study the maritime properties of the place. Usually, the structure is designed to resist a certain storm event with a specific return period.

An incorrect design of coastal structures can cause big economic and social effects, as it can determine many aspects of the harbour or beach functionality, stability and safety. For all these reasons, to accomplish good designs of coastal structures it is of great importance to study the wave behaviour of the specific place treated. It is necessary to study aspects such as the floor geometry and the typical wave heights, periods, wavelengths etc. that the structure is supposed to withstand and how these waves are going to develop in contact with the future structure.

To predict the development of waves, generically, two types of analysis can be performed, namely laboratory experimental analysis and numerical simulations.

2.2.1. EXPERIMENTAL ANALYSIS

In maritime and coastal engineering studies, to study the behaviour of waves and their effects on coastal structures, it is useful to do experimental studies in a laboratory (Hughes, 1993). These laboratories typically contain hydraulic channels with a paddle that generates waves. The channels can be of different dimensions depending on the scale at which they are recreating the case and its real geometric magnitude (Ursell, et al., 2006).

The wave generation is based on the movement of a paddle. The paddle can have a different shape and movement. There are two common paddles for the generation of regular waves (Oliveira, 2012):

- *Flap*: mainly used to produce deep water waves where the orbital particle motion decreases with depth and there is negligible motion at the bottom. Typical applications include analysis of floating structures in deep water and investigating the physics of ocean waves (Figure 2). Often the hinge of the paddle is mounted on a ledge some distance above the tank floor.

Figure 2. Flap paddle generation for deep water waves, from (Edinburg Designs, 2016)

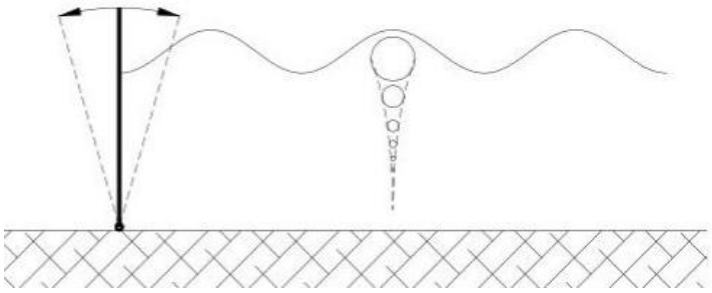

- *Piston*: used to produce shallow-water waves. Here, the orbital particle motion is compressed into an ellipse and there is significant horizontal motion on the floor of the tank (Figure 3). This type of paddle is used to generate waves for modelling coastal structures, harbours and shore mounted wave energy devices.

Figure 3. Piston paddle generation for deep water waves, from (Edinburg Designs, 2016)

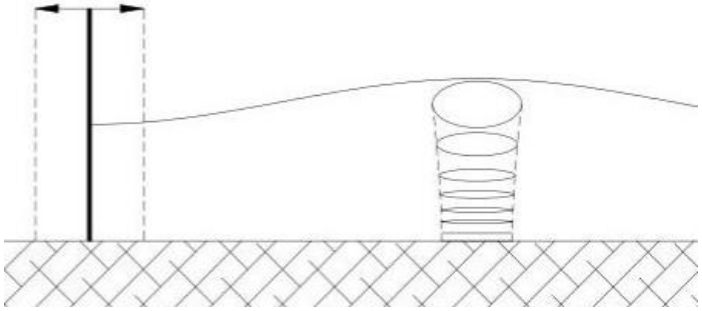

Apart from these two wave paddles, there are more designs such as displacement pistons, sliding wedges and other more complex machines like double-hinged flaps. See (Oliveira, 2012) for details.

The design goal is to try to match paddle motion to the water motion and minimise the evanescent waves immediately in front of the paddle. These unwanted waves decay naturally but reducing their amplitude minimises the unusable space in front of the paddle. Then, the adequate type of paddle can vary for each type of study considered.

The laboratory channels can contain structures to study the impact of waves on coastal constructions such as dykes or offshore constructions. With the addition of sand or other sediments on the bottom, they can also study the effects of sediment transportation, erosion and accretion.

Usually, when analysing the behaviour of waves, the most important wave feature to obtain is the development of the wave-free surface. To do so, the wave height at certain points is obtained by the installation of wave gauges. This device can measure other wave parameters as the period and velocity, for sets of wave gauges.

2.2.2. NUMERICAL METHODS OF WAVE GENERATION

Another option for the analysis of waves is the use of numerical methods. We understand as a numerical method a model equivalent to a physical one able of simulating reality (Oliveira, 2012). For the case of a numerical wave flume, they require to recreate the generation of waves, their propagation and their interaction with structures.

Numerical methods are still being developed but their use is exponentially increasing as numerous cases and improvements are acquiring their reliability. Within the many fields, they can work on maritime engineering aspects, such as the study of the waves for designing coastal and port structures.

There are many different numerical methods for the prediction of waves. They can be divided by the governing equations they used.

On the one hand, there are the ones that are based on the Non-Linear Shallow Water Equations (NLSW). They can predict the behaviour of the wave-free surface for shallow waters. Its equations define the depth and horizontal velocity of the wave in time and space by omitting the vertical velocity of water and considering the hydrostatic pressure as the total pressure (Oliveira, 2012). Its limitations are the need for the wave to be in shallow waters (*h/L <0.05*) and their obligation to have the waves on their breaking phase. The numerical methods based on NLSW are the oldest and they are useful to determine wave reflection, run-up and overflow and their impact on coastal structures. Furthermore, they present a low computational cost.

On the other hand, there are numerical methods based on the Navier-Stokes equations, a partial differential equation that describes the flow of incompressible fluids. The free surface evolution can be tracked by several techniques, mainly Volume of Fluid (VOF) and Level-Set methods, but also exist others such as the Particle Finite Element Method (PFEM) on which the project is going to be based.

PFEM is a numerical method developed to solve problems with large deformation of the domain. Its idea is to combine the Eulerian FEM with a Lagrangian basis where all the information is stored on the mesh nodes. PFEM relies on solving the Navier-Stokes equations on a moving Lagrangian grid (Equation 6) (Cremonesi, et al., 2020). After each solution step, the mesh is regenerated. Mesh nodes are treated as material particles that can merge or separate from the computational domain. PFEM was originally introduced by Idelsohn and Oñate (Idelsohn, et al., 2003).

Equation 6. Navier-Stokes equations

$$\rho \frac{Du}{Dt} - \nabla p + \mu \nabla u = \rho g$$

$$\nabla u = 0$$

2.3. BREAKWATERS

Breakwaters are coastal structures that aim at decreasing the wave height while breaking it to offer protection to the beach at which they are placed (Meer, et al., 2005).

The wave breaking structure is composed of elements distributed in the subsequent layer. Its exterior layer withstands the wave load (Figure 4). They have to withstand the impact and erosion that cause waves during long periods, to do so, they usually have the following parts:

- Core: it is a set of materials that puts weight into the structure but don't have much resistance.
- Filters: they are usually two layers that prevent core skipping outside the structure and provide a solid surface for the armour
- Armour: it is the external layer of the breakwater. It has the function of resisting the impact of waves. This layer is built of rocks or concrete blocks.
- Base: it is the foundation where the breakwater is placed. It is normally built of sand or silt and it avoids differential settlements on the structure.
- Berm or toe: they are placed on the exterior part of the breakwater, in contact with the waves and has the function of defending the structure from undertone, so the breakwater elements are not grabbed to the sea. They also decrease the wave runup on the structure.
- Crest: it is the top part of the structure. The size of their rocks on this part has to be great enough to handle the wave loads.

Figure 4. Breakwater section example (Conejo, 2021)

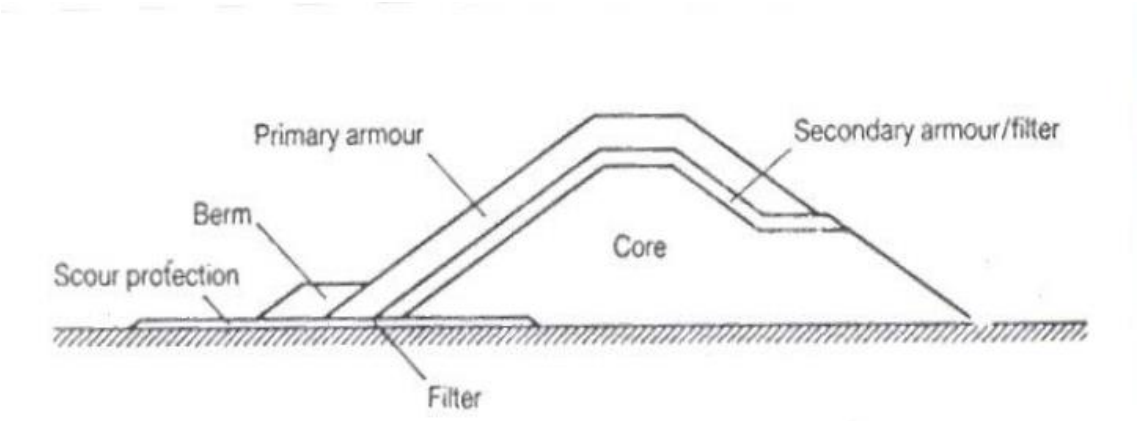

An important parameter on the breakwater is the *freeboard* (*Rc*), the distance from the SWL to the top of the structure, and the *wave runup* (*Ru*), the distance the waves goes up when crashing on the breakwater. If the wave runup is bigger than the freeboard for a specific case, there will be an overtopping, water will pass above the breakwater.

Different types of breakwaters can be distinguished depending on their shape:

- Berm breakwaters: its structure incorporates a berm on its external face to diminish the wave runup.

- Reef breakwaters: on this breakwater, its elements are directly placed on the sea distributed so they reach equilibrium by themselves under storm events.
- Low-crested breakwaters: this type of breakwater present low values on its freeboard, so they usually allow wave overtopping, they are used for coastal and structure protection.

On the other hand, depending on its functionality we can distinguish between:

- Rubble-Mound Breakwaters: their main function is to warrantee the maximum level of agitation inside harbours.
- Groins: they are used for coastal protection.
- Detached breakwaters: they do not have direct contact with the beach as they are placed at some distance from the shoreline.
- Jetty: this type of structure main function is to provide a navigable breach between a river and the sea.
- Submerged: they are low crested breakwater that allows waves to flow on top of it while decreasing its amplitude.
- Revetment: this type of breakwater is placed so they prevent and control the erosion on a certain beach by interfering with the wave currents.

To study the performance of a breakwater an important factor to study is wave transmission. It is defined by the *transmission coefficient* (K_t) (Meer, 1995). It is defined as the fraction between the transmitted wave height and the incident one (H_f). It mainly depends on the permeability of the breakwater, its change in depth and the wave overtopping on the structure. For the case of trapezoidal breakwaters, Van Der Meer formulation suggests the transmission coefficient of the breakwater to follow Equation 7.

Equation 7. Transmission Coefficient (K_t) for trapezoidal breakwaters

$$Kt = 0.8\,, for -2 < \frac{Rc}{Hf} < -1.33$$

$$Kt = 0.46 - 0.3\frac{Rc}{Hf}\,, for -1.33 < \frac{Rc}{Hf} < 1.2$$

$$Kt = 0.1\,, for\ 1.2 < \frac{Rc}{Hf} < 2.0$$

Breakwaters are designed specifically for each case depending on the wave characteristics of the zone they have to withstand. As waves may vary on different parts of the same breakwater, for example, because of orientation changes, it is possible to change the cross-section along with the coastal structure.

3. METHODOLOGY

In this chapter, the methodology used in this work is described. In particular, this part explains how the different numerical methods, PFEM and Eulerian FEM, are used for the cases studied and which are their main characteristics. The different possibilities and types of analyses are also described.

This chapter also described the software that has been used to run the numerical simulations and see the results. For this study, the software used consisted of GID pre and post-processing and Kratos Multiphysics.

3.1. LAGRANGIAN NUMERICAL METHOD (PFEM)

The Particle Finite Element Method (PFEM) is a numerical method designed to model fluids with high deformations on their free surfaces and their possible interactions with solid structures (Cremonesi, et al., 2020). It can solve problems in 2D or 3D. In this work, the analysis will be performed in a 2D space assuming the plane strain hypothesis.

The PFEM solves the fluid governing equations (Navier-Stokes problem, see Equation 6) in a Lagrangian way. This means that the nodes of the mesh are free to move according to governing equations of the problem. In particular, the equations to solve are the mass conservation and the linear momentum equations with the relative boundary conditions (Idelsohn, et al., 2003). These equations are time-dependent and therefore a time integration scheme is required to solve them.

The domain is discretized with a mesh that connects the fluid particles. This mesh is used to solve the governing equations in a standard Finite Element Method (FEM) fashion and uses linear elements for both the velocity and the pressure unknowns. This set if applied to the solution of incompressible material (such as the fluids considered in this work) through the Navier-Stokes equations can lead to pressure fluctuation instability. To solve this effect, PFEM modifies the governing equations with the Finite Calculus (FIC) stabilization technique (Oñate, 2000). More details about the PFEM formulation used in this work can be found in (Oñate, et al., 2014).

Due to its Lagrangian description, the PFEM requires regenerating the mesh at each time-step solution to avoid mesh distortion and therefore a bad FEM solution of the governing equations.

Mesh sizes are commonly generated by the *h* parameter, which describes the desired distance between the nodes, so lower *h* values relate to denser meshes, with more nodes. It is important to notice that the deformation of the mesh experienced in PFEM is the main difference with a standard Eulerian FEM. In fact, in a Lagrangian method such as PFEM, the mesh nodes are attached to the material, so as the material deforms the mesh does too (Donea, et al., 2004). Furthermore, to avoid very irregular shapes of the elements, after each computation time-step the system check if the mesh state is still good, if it is not, the mesh is regenerated (Figure 5).

Figure 5. Mesh deformation mechanism of PFEM

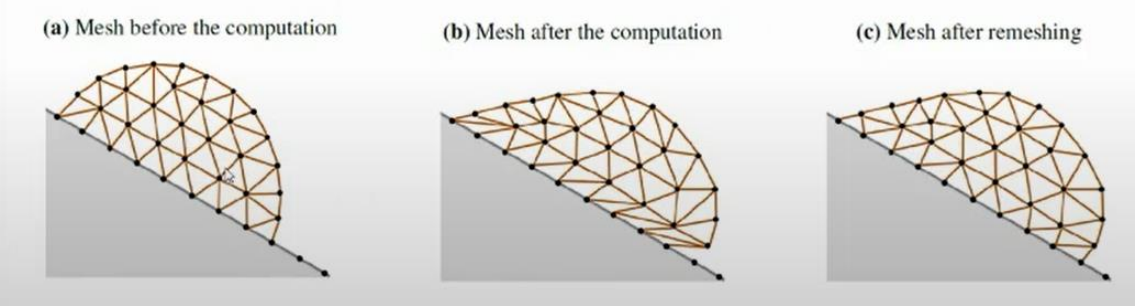

The PFEM uses a Delaunay meshing mechanism generation. The mesh is regenerated at each calculus time-step based on the nodes' location and the boundaries. For the case of this 2D study, the Delaunay triangulation creates a mesh of triangles. To do so, this mechanism first constructs the cloud of points by Voronoi Diagram. Then, it links the nodes by the Delaunay meshing mechanism and finally, to ensure there are no distortional triangles and to make them as equilateral as possible, PFEM uses the Alpha-Shape method (Edelsbrunner & Mücke, 1994).

Using a re-mesh is very useful because it allows to track accurately the deforming material maintaining a good quality of the mesh. However, the re-meshing operations are computationally expensive and have a linear relationship of the time cost and the number of nodes. Moreover, remeshing induces loss of connectivity and induces artificial changes in topology and volume variation which can create water leakage on the system (Cremonesi, et al., 2020).

PFEM is based on storing the information for every node on each time-step to solve the problem unknowns such as velocity and pressure. However, in many problems, such as those studied in this work, an interesting parameter to look at is the free-surface position. To obtain this feature on PFEM, as the mesh remains connected to the material deformation, the mesh determines the fluid boundaries. Then, just looking at the mesh nodes position it is possible to obtain the wave-free surface state.

3.2. EULERIAN NUMERICAL METHOD (FEM)

The Finite Element Method (FEM) is a numerical method widely used in fluid dynamics for solving partial differential equations in 2D or 3D. The FEM can be based both on an Eulerian and a Lagrangian description. The main difference is that in an Eulerian framework, the finite element mesh is fixed, whereas, in a Lagrangian method, the mesh moves according to the solution of the governing equations. Therefore, a Lagrangian FEM may lead to mesh distortion if applied to large deformation problems. For this reason, an Eulerian FEM is generally preferred in fluid mechanics, while a Lagrangian FEM is more adapt for solid mechanics (Ryzhakov & Oñate, 2017) 2017). In this work, an Eulerian FEM will be considered and its results will be compared against those of the PFEM.

The FEM discretizes the system space with a mesh of a finite number of points. It offers great freedom in the selection of discretization, both in the elements that may be used to discretize space, and the basic functions. As already described, the main logic that follows the Eulerian

numerical method is that the mesh remains fixed as the material flows (Donea, et al., 2004). This means that differently from PFEM, nodes are not attached to the material, so the mesh remains constant as the material deforms, it works as a background mesh (Figure 6). This way, in an Eulerian FEM the position of the fluid free surface cannot be determined by the mesh nodes position because they may not coincide with that.

Figure 6. Mesh development mechanism of FEM, from (Rajendran, 2021)

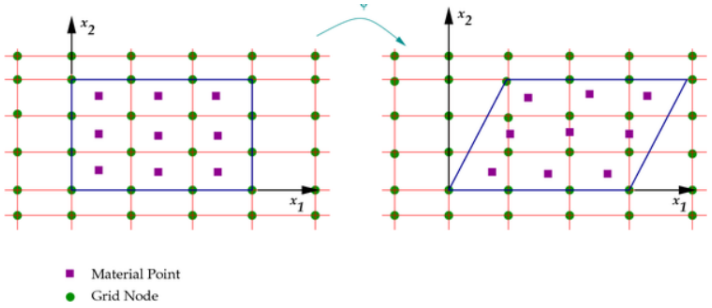

In the Eulerian FEM, the free surface is defined by a distance function that evolves during the problem according to the problem solution and the obtained velocity of the nodes. Initially, the free surface is set for its initial state. Then, as FEM measures the distance that the fluid moves on each calculation point, the free surface can be updated (Hashemi, et al., 2020).

For cases where there are big mesh distortions, it is better to apply the Eulerian numerical method as its mesh remains constant although the mesh needs to be big so the material flow does not leave the mesh domain.

To sum up, the main differences between FEM and PFEM is the meshing mechanism and the detection of the free surface technique. As seen there are shortcomings and advantages both in PFEM and FEM, this is why depending on the case it can be better to use a different technique.

3.3. BOUNDARY CONDITIONS IN LAGRANGIAN AND EULERIAN FRAMEWORKS

The boundary conditions used in the numerical methods for studying fluid flows can be divided into two types depending on how the fluid and solid boundaries interact. Slip conditions consider that the fluid that touches the system walls or boundaries can freely flow without any friction. On the other hand, no-slip conditions consider that the fluid nodes in touch with the wall remain immobile during all the analysis.

Theoretically, there is friction between the walls and the fluid that makes the very first fluid particle in touch with the wall to not move, so it would mean that it has a no-slip behaviour. However, this statement is only correct for the first particle, so to use accurately this method the mesh size should have to be the same size as the fluid particle, which is practically

impossible. On the other hand, applying a no-slip method leads to overestimating this friction effect reducing the fluid velocity. This source of error has a bigger effect on the fluid close to the wall and is more dissipated on the water surface as deeper is the wave. Then, for the same computational mesh resolution, the smaller is the water depth, the higher is the discrepancy between the solutions of the slip or no-slip methods.

Eulerian FEM (from here on, only FEM) and the PFEM have different ways of modelling boundary conditions. The Finite Element Method as the mesh stays still while the material moves, allows to model both boundary conditions (slip and no-slip) in a natural way.

On the other hand, in the Particle Finite Element Method, as the nodes of the wall are also nodes of the water system, they have to remain still to avoid water passing through it. The motion of a wall node would create a hole in that position producing fluid leakage. Then, for PFEM it is only possible to do a no-slip analysis method. Some recent variations allow doing a slip analysis, but it is not on the natural PFEM behaviour.

3.4. SOFTWARE USED FOR THE STUDY

In this work, several cases of waves channels of specific characteristics are studied. The analyses are performed using the Particle Finite Element Method and then compared to the experimental results to validate them. To do the necessary computations, it is needed a system that can read and perform the PFEM computations. Two different software are used for this purpose.

On one side, the software that effectively performs the computations is the PFEM solver implemented in the open-source platform Kratos Multiphysics (Dadvand, et al., 2010). This software is capable of computing the partial differential equations with the needed iterations and then obtaining the properties of each node at each time-step of displacement, pressure and velocity within others.

On the other side, the software in charge of doing the pre-processing and post-processing is GID. This software allows to describe the geometry of the problem, define the mesh desired and describe all the other properties needed for the computation as the time-step size, fluid and structures properties, boundary condition etc. Later, after the case is computed, GID is capable of displaying the results and plot images or videos of the desired fluid properties. GID software is only responsible for describing the nodes distribution of the initial mesh, all the posterior re-meshing will be performed by Kratos.

The computations can be done on a personal computer or an informatics cloud.

Computations for the study of waves can be of very high meshes and low time-steps causing analysis with high computational costs of days or even weeks. For these cases, it is not optimum to run the cases on a personal device but through an external server. in this work, the *Centre Internacional de Mètodes Numèrics a l'Enginyeria* (CIMNE), provided the author with the credits for using the Aquario server to do the necessary studies computations.

4. PROPAGATION OF A SMALL-AMPLITUDE SOLITARY WAVE

4.1. INTRODUCTION

In this first analysis, the numerical solver is used to model the propagation of a solitary wave in a channel reproducing the experimental analysis of (Hitzegrad, 2019) carries out at Braunschweig, Germany.

The numerical analysis is performed by the Lagrangian PFEM method. The computation is done using the Kratos software and the pre and post-processor GID.

The analysis studies the propagation of a small-amplitude wave with simple boundaries and behaviour as it is an interesting first analysis to observe how the numerical method reacts to basic wave analysis.

The analysis will compare the results obtained by the experimental study to the ones obtained with the PFEM numerical method.

4.2. PROBLEM GEOMETRY

The numerical analysis imitates the geometry of the experimental channel. Its dimensions are described in Figure 7. The channel has a length of 237,5 metres with a water depth of 3.6 metres. It has a wave paddle located at the end of the channel that acts as a piston generating a solitary tsunami wave. The height of the wave has been measured experimentally at different wave gauges. In this study, three different gauges will be analysed, at 60, 165.5 and 170 metres from the wave paddle (Figure 7).

Figure 7. Channel geometry of the experimental laboratory channel in Braunschweig (Hitzegrad, 2019)

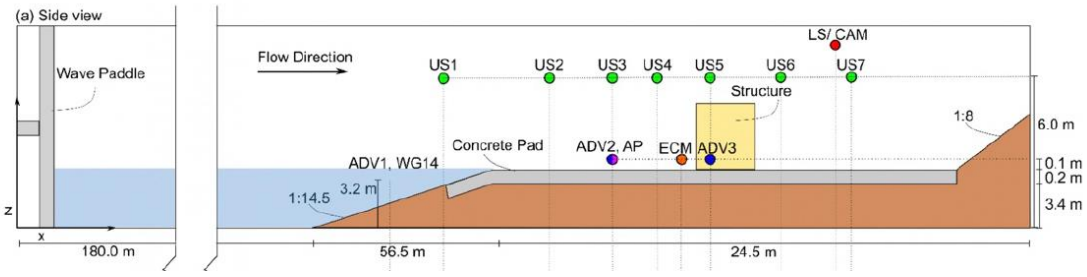

The paddle motion that causes the wave on the experimental channel follows a specific time function (Figure 8)

Figure 8. Small-amplitude solitary wave paddle velocity in time graphic from (Hitzegrad, 2019)

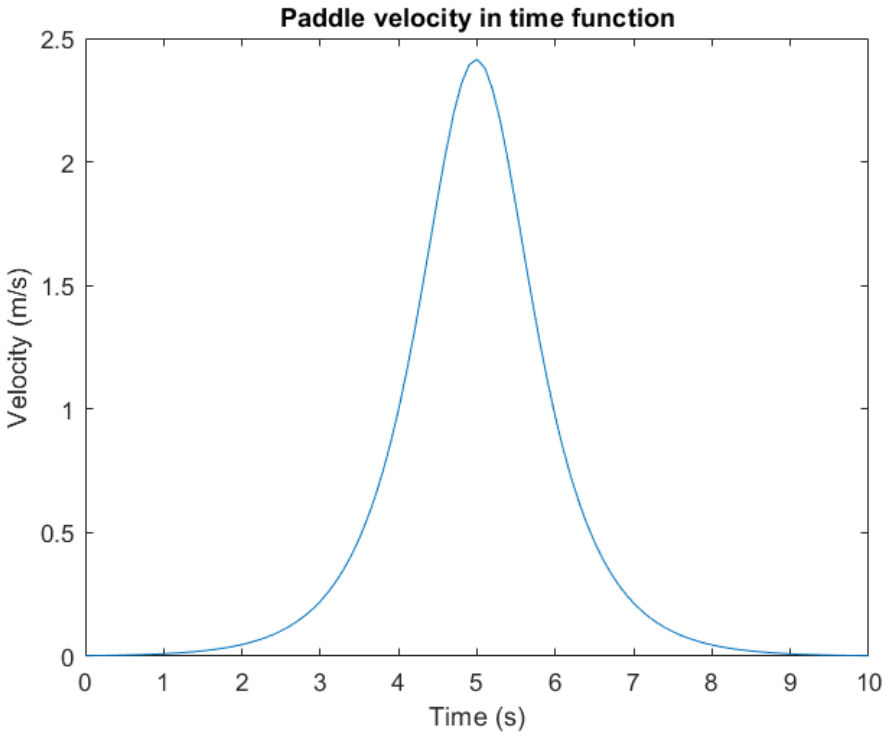

To recreate this laboratory experiment in a numerical method, Kratos software is used with the support of GID pre-processing and post-processing. The geometry of the laboratory channel is created using the GID software (Figure 9).

To represent the problem with this software, first, it is needed to establish the water body as NURBS surface and impose its properties. A Fluid Updated Lagrangian element type with the Newtonian constitutive law used. Water properties consist of a density of 1000 kg/m^3, a dynamic viscosity of 10^{-3} Pa·s and a bulk modulus of $2.1 \cdot 10^9$ Pa.

Then, to solve the problem, rigid walls are imposed as the boundary on the paddle and the bottom of the problem.

Figure 9. Small-amplitude solitary wave analysis geometry on GID software.

The boundary conditions are the following. The bottom walls are fixed and have no-slip conditions. The wave paddle follows a horizontal movement to generate the waves determined in Figure 8 abstracted from Equation 8. The paddle horizontal movement allows the generation of waves while avoiding water flowing out of the boundaries. This paddle movement is programmed to be active during the first 10 seconds of analysis after which it remains still.

Equation 8. Paddle movement in time function of the small-amplitude solitary wave

$$x = -3.12256146 * e^{(-1.54715671*(t+164-168.98849405)} * \frac{-1.54715671}{1.0 + e^{-1.54715671*(t+164-168.98849405)^2}}$$

The geometry is first discretised using the GID software. Then, during the computation, the mesh is regenerated automatically by the PFEM-Kratos software. The total time duration of the analysis is 50 seconds.

After establishing these geometry features of the single wave analysis, Kratos can predict the behaviour of the wave. It will compute the position of each node on each time step and its appropriate velocity and pressure.

To obtain numerical results comparable, an additional function is added to the Kratos scripts which measure the wave height at a given point. This function has several inputs that need to be determined to give correctly the wave height measurement (Table 1). The function main code lines are described in Figure 10.

Figure 10. Function main code lines for obtaining the wave height measurements

```
self.calculate_wave_first_probe = KratosMultiphysics.PfemFluidDynamicsApplication.
CalculateWaveHeightProcess(self.main_model_part,0,1,2, 60, 1.75, 3.6, 0.8, "WaveHeight",0.1)

self.calculate_wave_first_probe.Execute()
```

Table 1. Function for the wave height measurement inputs for the small-amplitude solitary wave.

Point of measurement	Distance from the wave paddle at which the wave height is measured. For this case, there will be three equal functions set to measure the wave height at 60, 165.3 and 170 metres.
Transversal distance of measurement	It is the amplitude at which the wave height is measured. For this case, as the problem is set in 2-D this input is irrelevant.
Reference coordinates	It is the water table height. As established in the geometry it is 3.6 metres
Tolerance	Distance from the point of measurement where the function is going to look for the nodes from which abstract the wave height measurements. Depending on the properties of the problem this input will change
Size of the finite element	For this case, it is set to 1.75
Time-step	Time-step for the function to print the results.
Name of the output	Name of the output where the function is going to print the results

4.3. NUMERICAL RESULTS WITH PFEM

The GID software plotting is used to analyse the global wave movement and acquire a graphic representation of the wave amplitude, pressure and velocity distribution. Thus, we report here some snapshots of the PFEM results. Figure 11, Figure 13, Figure 15, Figure 17 and Figure *19* shows the velocity distribution of the wave at the most important time-steps of the wave propagation at the different time-steps, which are the wave maximums and minimums. Figure 12, Figure 14, Figure 16, Figure 18, and Figure 20 shows the pressure distribution at these time-steps.

Figure 11. Small-amplitude solitary wave maximum height at x=60 metres velocity distribution.

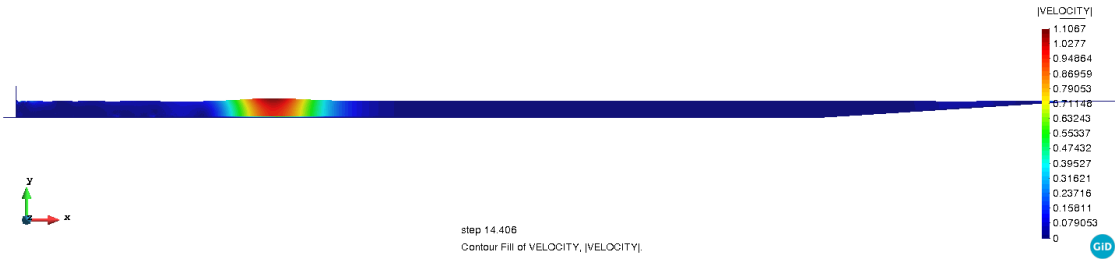

Figure 12. Small-amplitude solitary wave maximum height at x=60 metres pressure distribution.

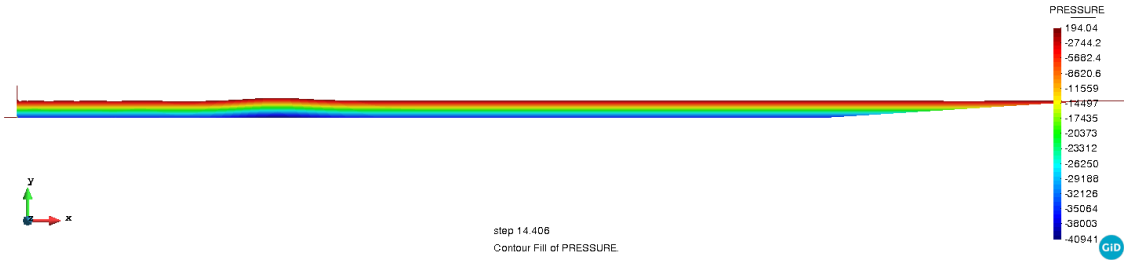

Figure 13. Small-amplitude solitary wave minimum water height at x=60 metres velocity distribution.

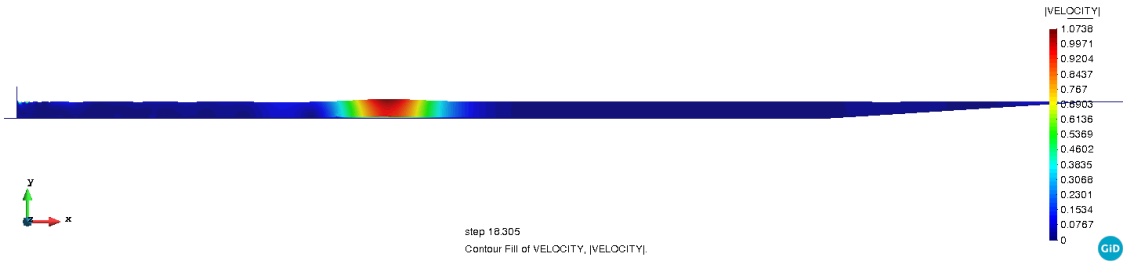

Figure 14. Small-amplitude solitary wave minimum water height at x=60 metres pressure distribution.

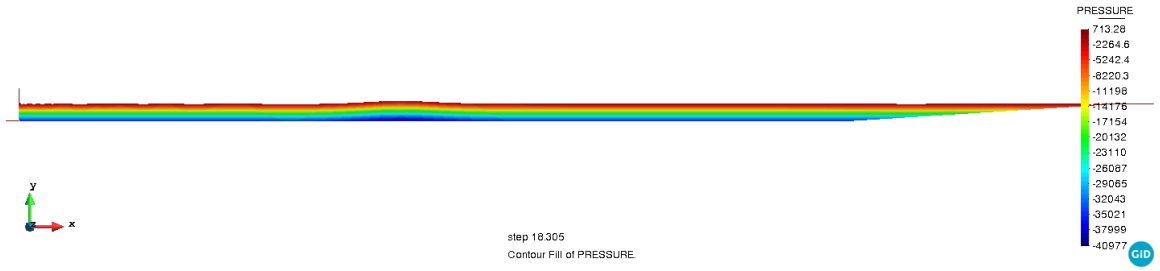

Figure 15 Small-amplitude solitary wave second maximum height at x=60 metres velocity distribution.

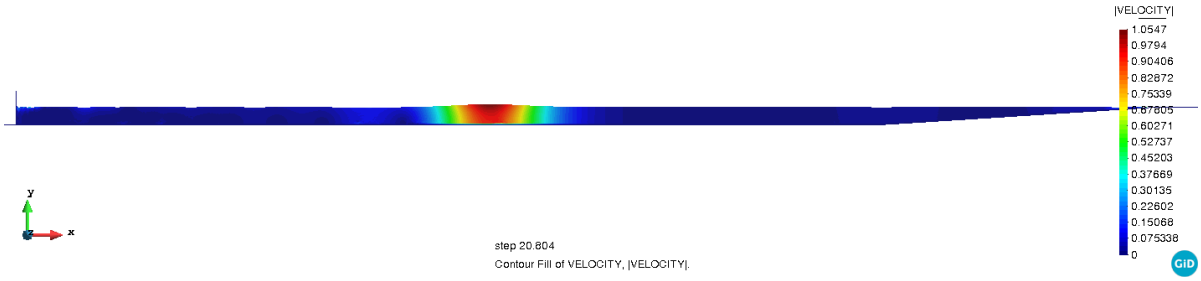

Figure 16. Small-amplitude solitary wave second maximum height at x=60 metres pressure distribution.

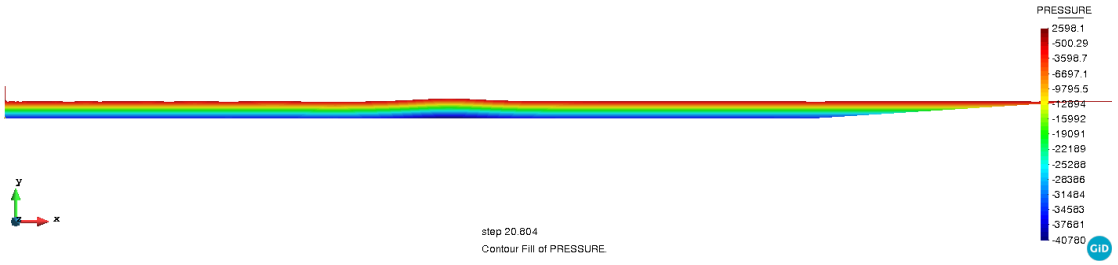

Figure 17. Small-amplitude solitary wave maximum height at x=165.3 metres velocity distribution.

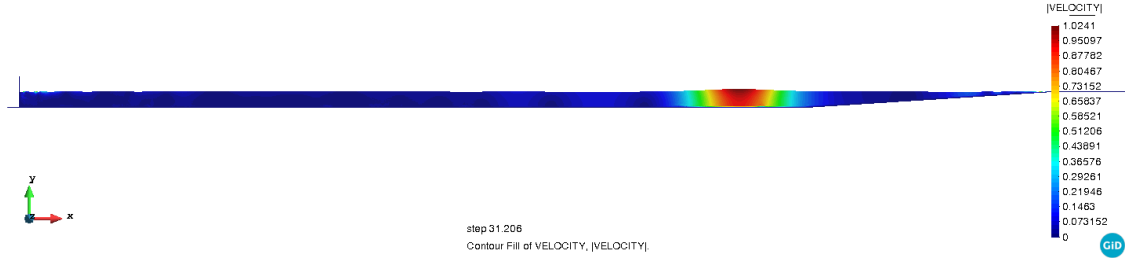

Figure 18. Small-amplitude solitary wave maximum height at x=165.3 metres pressure distribution.

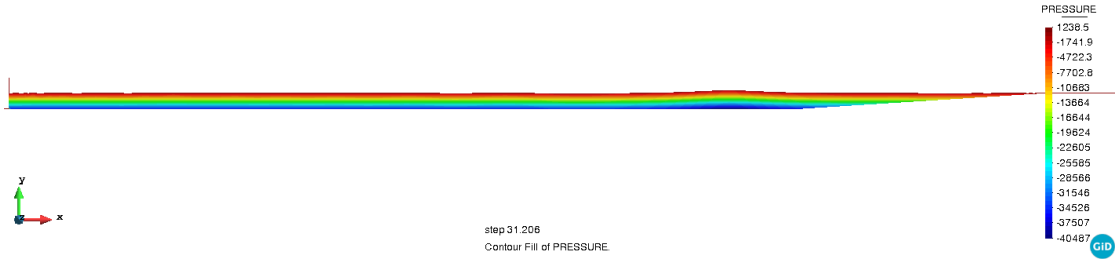

Figure 19. Small-amplitude solitary wave maximum height at x=170 metres velocity distribution.

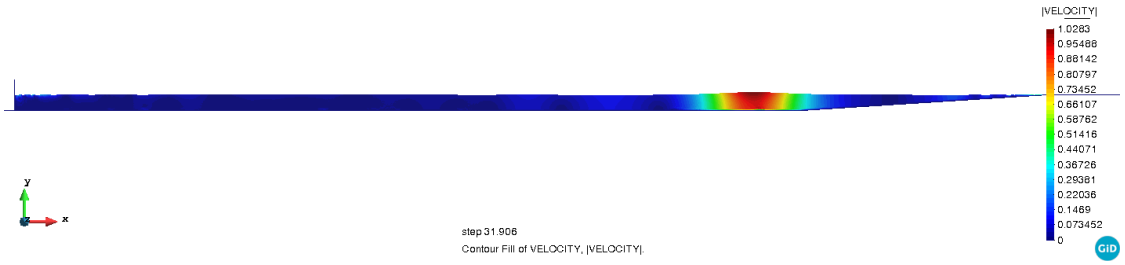

Figure 20. Small-amplitude solitary wave maximum height at x=170 metres pressure distribution.

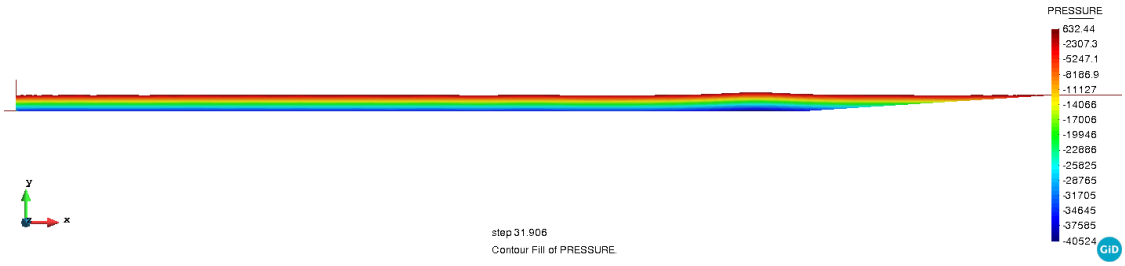

The wave paddle moves so it generates a small-amplitude and long wavelength wave, similar to tsunami ones. The wave reaches the end of the channel slope and flows out of the system boundaries, avoiding a wave reflection

The snapshots show the global behaviour of the wave propagation. They show how the water is at rest until the wave reaches. The pressure on the snapshots has positive values corresponding to traction and negative to compression. As seen, the channel has a practically hydrostatic pressure distribution while the wave propagates.

4.3.1. MESH SIZE CONVERGENCE ANALYSIS

The first analysis to be computed is the observance of the effect of the mesh density on the results of the numerical method. Finer meshes give better results to the problem but have a higher computational cost. However, in PFEM, as in standard FEM, it is expected that the numerical results should be convergent for reducing mesh sizes, this tendency is proved in this study. The different meshes to be used for the analysis are described in (*Table 2*). The time-step is set to be small enough (*ΔT=0.01 seconds*) to give all the alteration effects only dependent on the mesh density.

To do this comparison the wave height measurements of the function will be used. It is important to notice that the outputs of the functions for different mesh densities are highly dependent on the tolerance of the function described in Table 1. Coarse meshes can cause the function to not find any nodes inside the tolerance values given, so it does not print a solution for that time-step. To avoid this, it is appropriate to increase the tolerance. However, too big tolerances can cause errors on the outputs as the function obtain the measurements from nodes that are too far from the point where we want to obtain the solution form. Then, it is needed to set a particular tolerance for the mesh density being used on the problem to have results printed on most of the time-steps iterated but with enough accuracy (*Table 2*). Generally, coarser meshes need higher tolerances.

Table 2. Cases studied for the mesh size convergence of the small-amplitude solitary wave analysis.

Cases	Mesh size (h)	Function Tolerance
Case 1	0.2m	0.4m
Case 2	0.3m	0.4m
Case 3	0.4m	0.4m
Case 4	0.5m	0.4m
Case 5	0.7m	0.5m
Case 6	1m	0.8m

Table 3 and Figure 21 show the exponential relationship between the computational cost and the mesh density, or its more specific value, the number of nodes. It shows the importance to choose an appropriate mesh size to acquire good results with a viable computational cost. The range of tolerances selected for the function gives approximately the same number of printed results so the results have approximately the same accuracy regarding this factor.

Table 3. Computational time – Mesh size dependence of the solitary wave analysis.

Mesh size h (m)	Number of printed results	Computation Time (s)	Number of Nodes
0.2	459	16886.58	22543
0.3	459	6990.46	10470
0.4	459	3157.93	5907
0.5	459	2340.97	3888
0.7	459	1330.09	2171
1	459	714.97	1107
1.5	459	303.57	475

Figure 21. Mesh size – Computational time costs graphical exponential relationship of the small-amplitude solitary wave analysis.

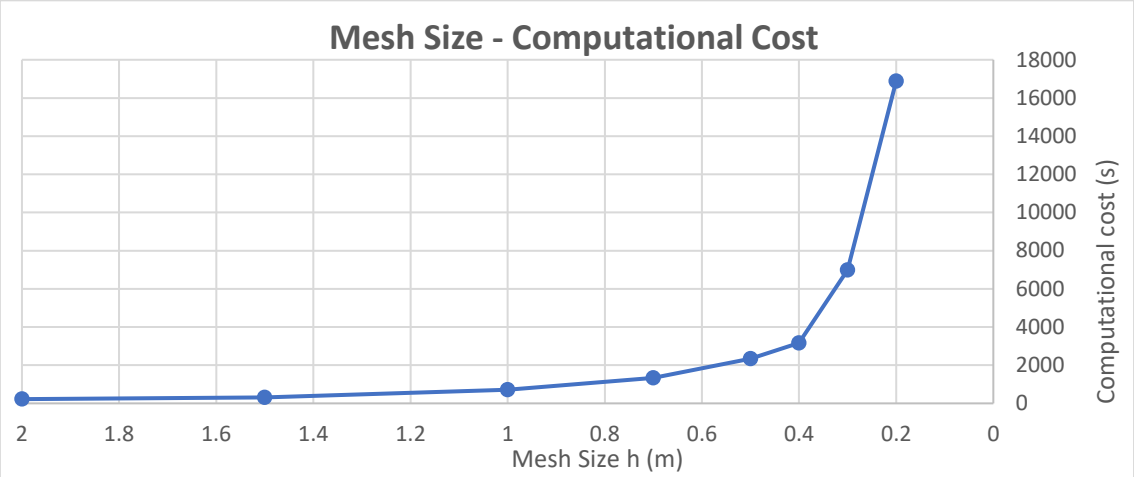

The different cases demonstrated a clear convergence of results in all different wave measurement points (Figure 22, Figure 23 and Figure 24). For the studied problem, it could be considered that convergence is reached after the mesh reaches the value of approximately (h=0.3) (Figure 25, Figure 26 and Figure 27). This proves that by finding an appropriate mesh density the numerical method can provide a good solution to the problem without the necessity to increase the number of elements, which would cause an important increase in the computational cost of the problem.

Figure 22.Mesh density convergence graphic of the small-amplitude solitary wave analysis at 60 metres from wave paddle.

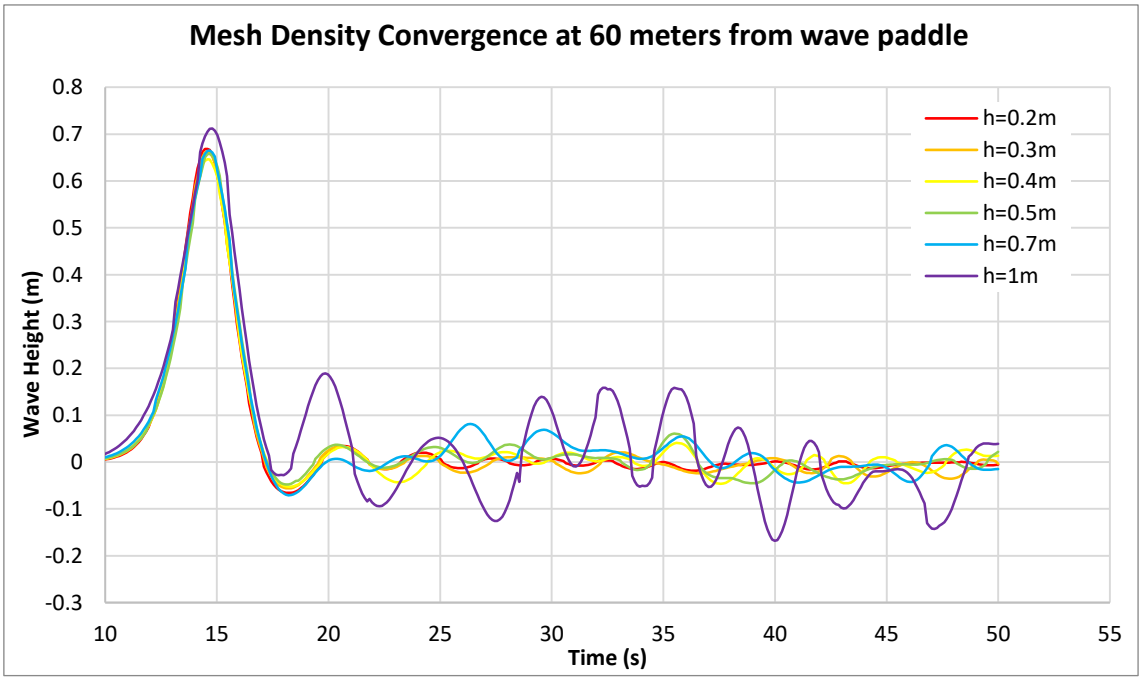

Figure 23. Mesh density convergence graphic of the small-amplitude solitary wave analysis at 165.3 metres from wave paddle.

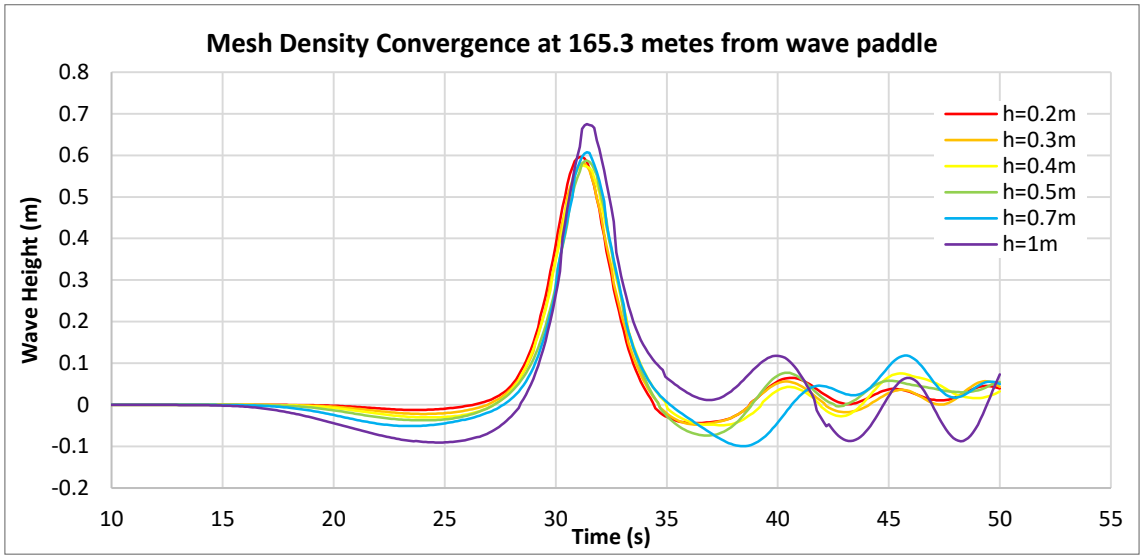

Figure 24. Mesh density convergence graphic of the small-amplitude solitary wave analysis at 170 metres from wave paddle.

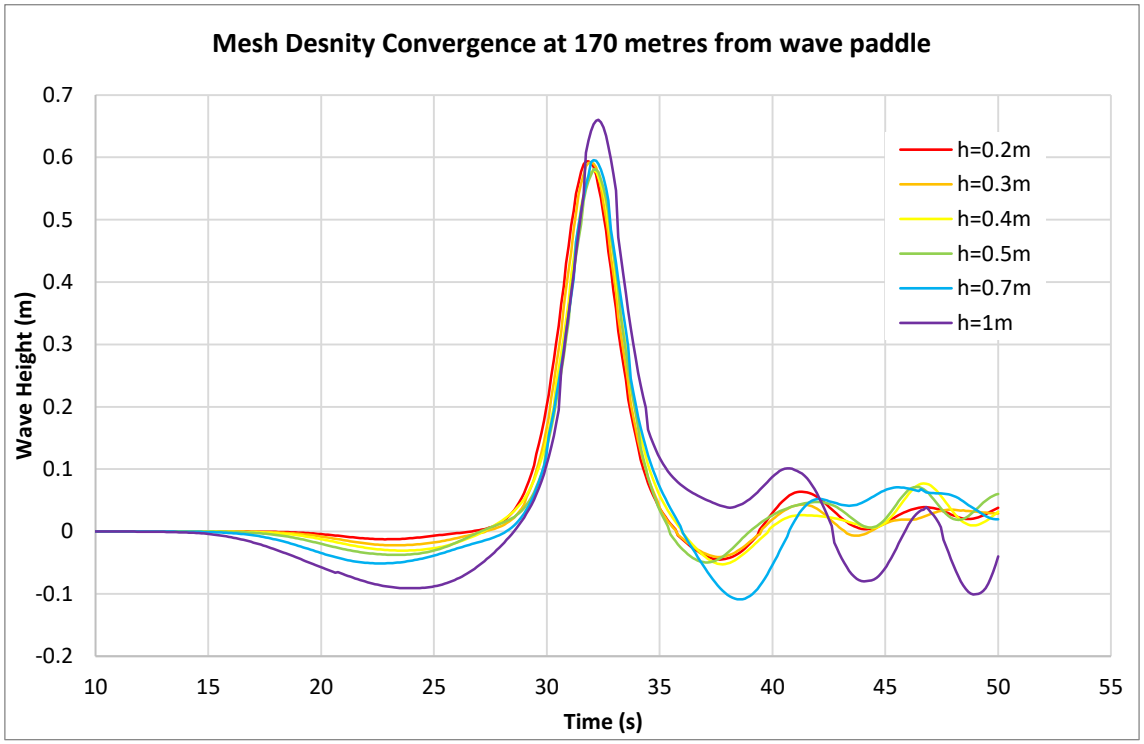

Figure 25. Mesh density convergence of the two finest meshes of the small-amplitude solitary wave analysis at 60 metres from wave paddle.

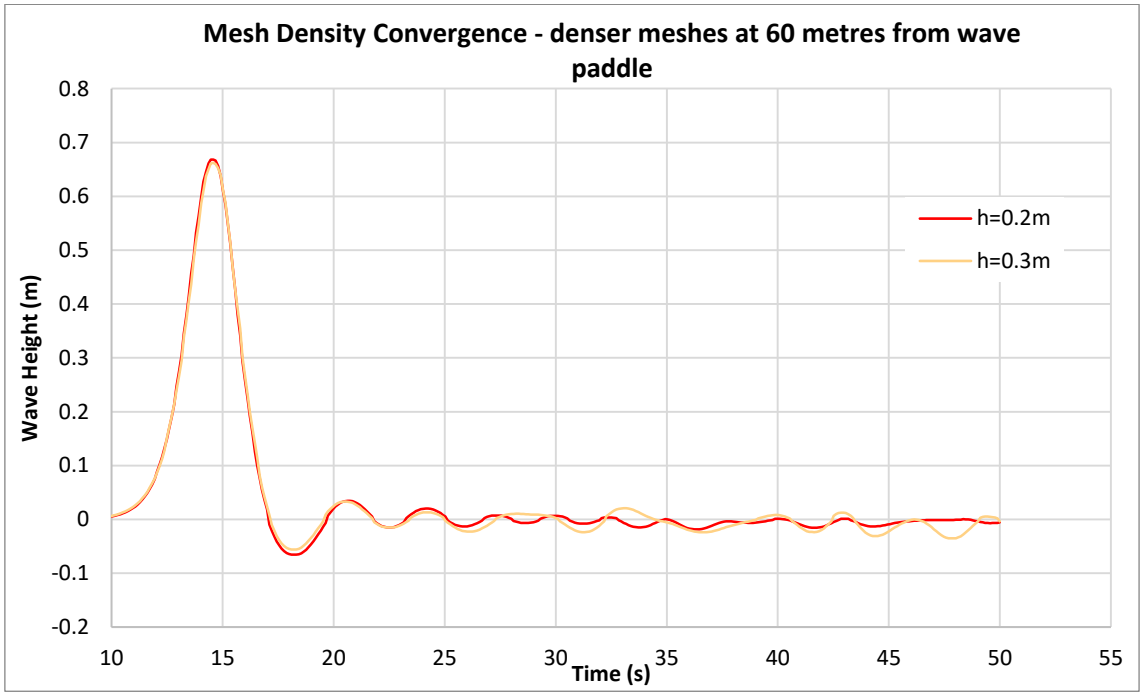

Figure 26. Mesh density convergence of the two finest meshes of the small-amplitude solitary wave analysis at 165.3 metres from wave paddle.

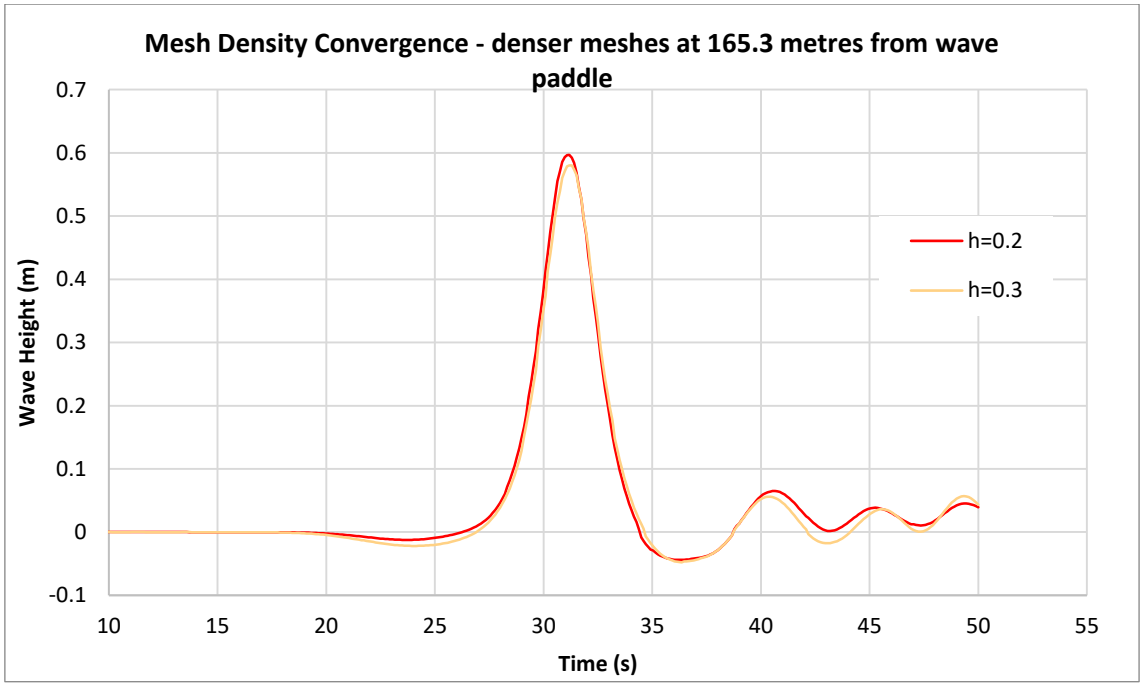

Figure 27. Mesh density convergence of the two finest meshes of the small-amplitude solitary wave analysis at 170 metres from wave paddle.

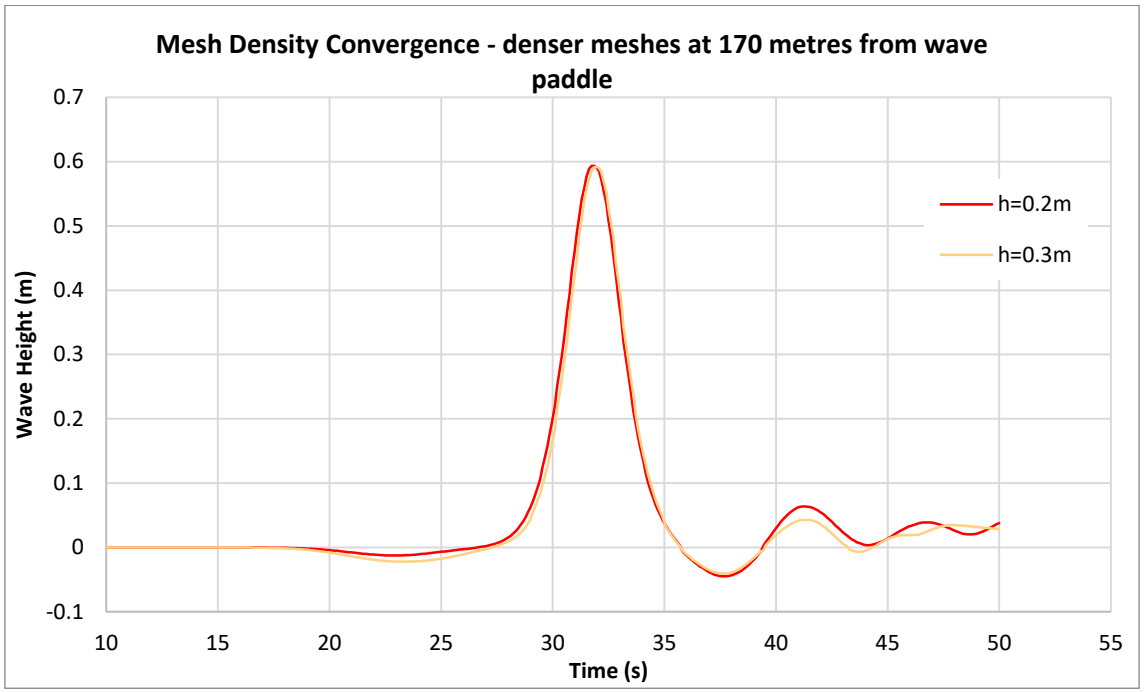

Figure 28, Figure 29 and Figure 30 show how the numerical method results are related to the experimental ones. It shows that the numerical value of the most accurate case has a good agreement with the experimental results. It also displays how the numerical solution gives slightly higher values regarding the first wave height peak. It can also be seen how the discrepancy between the numerical and experimental results increase as time passes, as a consequence of the accumulation of errors consequences.

Figure 28. Comparison of the experimental and numerical results of the small-amplitude solitary wave analysis at 60 metres from wave paddle.

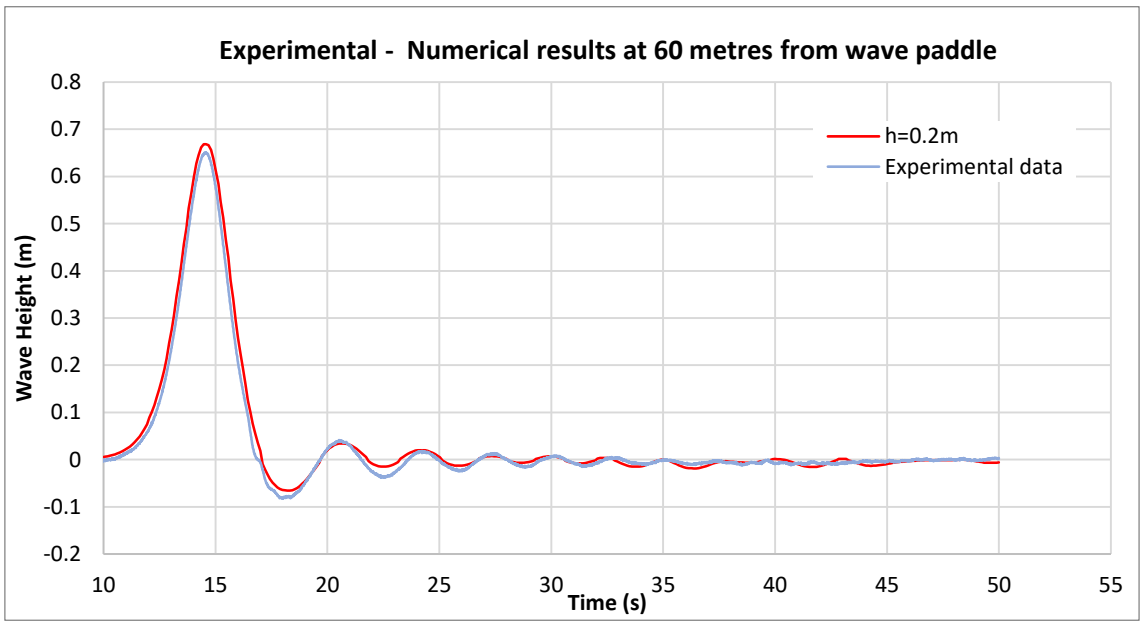

Figure 29. Comparison of the experimental and numerical results of the small-amplitude solitary wave analysis at 165.3 metres from wave paddle.

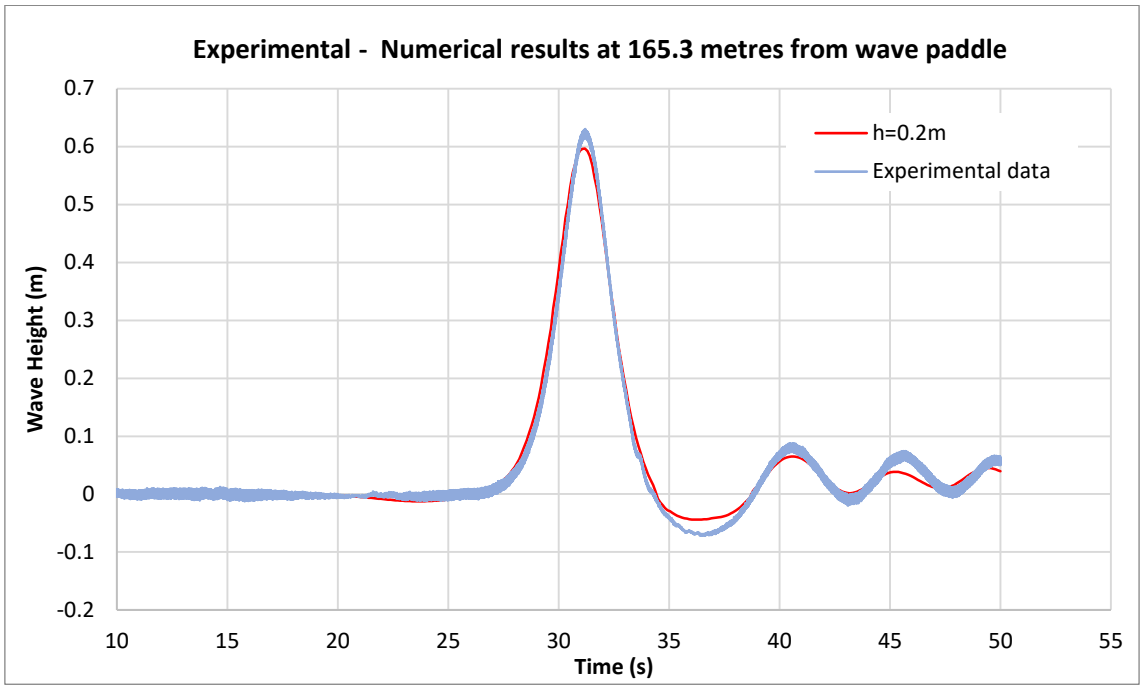

Figure 30. Comparison of the experimental and numerical results of the small-amplitude solitary wave analysis at 170 metres from wave paddle.

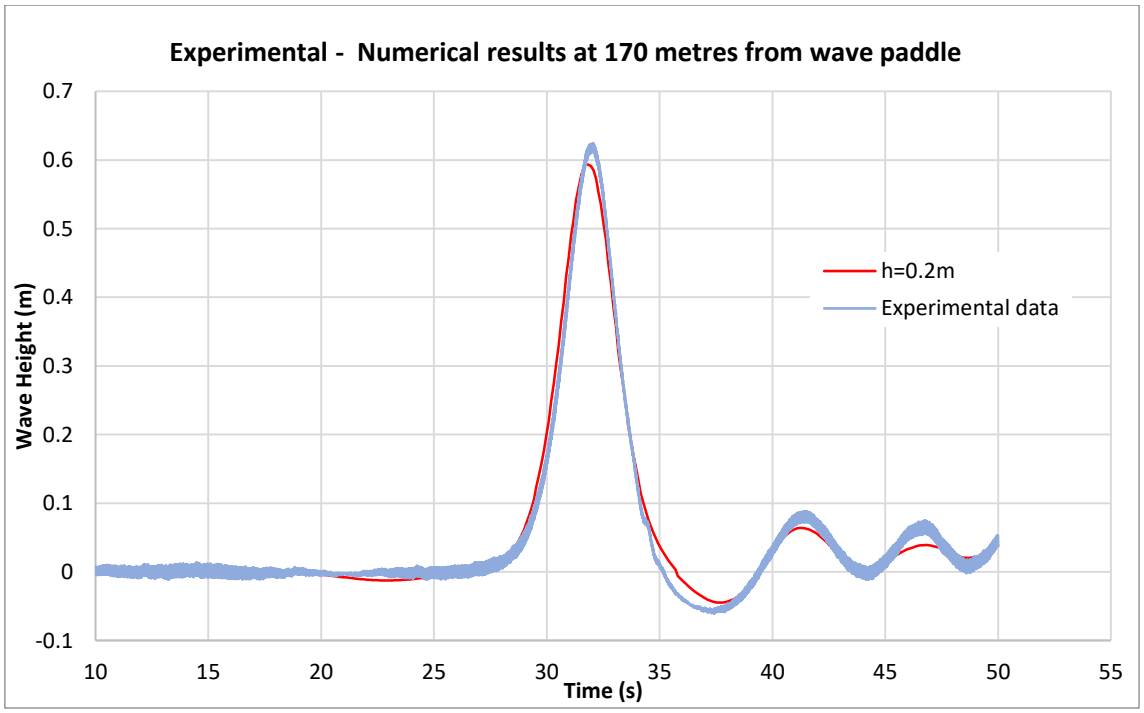

4.3.2. TIME-STEP SIZE CONVERGENCE ANALYSIS

The time-steps used for the computation of the problem also affect the accuracy of the numerical model. Lower time-steps will provide a better solution. However, its computational cost will also increase. As with the mesh density, time-steps size also has convergence on its results. For this analysis different cases of time-steps were studied Table 4.

Table 4. Cases studied for the time-step size convergence of the small-amplitude solitary wave analysis.

Cases	Time-step (ΔT)	Function Tolerance
Case 1	0.007s	0.4m
Case 2	0.01s	0.4m
Case 3	0.02s	0.4m
Case 4	0.05s	0.4m
Case 5	0.1s	0.4m

In this study, the mesh density is set to (*h=0.3m*) in all cases to not alter the time-step analysis. However, it is important to notice that keeping the mesh size constant for different time-steps also has a drawback on its accuracy. Fine meshes with big time-steps may cause that between two iterations the movement of a node is so large it crosses to the next element causing important errors in the computations.

The computational costs of the analyses are compared with their time-step size and the number of nodes as shown in Table 5, there is also in this case high change of the computational time cost values within the different cases Figure 31. The number of printed results also shows an approximately constant value, so results can be considered correct regarding this aspect. The function tolerance is not influenced by the time-step size as the mesh size is constant so it remains as 0.4 (Table 4).

Table 5. Computational time – Time-step size dependence of the solitary wave analysis.

TimeStep Size ΔT (s)	Number of printed results	Computation Time (s)	Number of Nodes
0.007	477	9576.97	10470
0.01	459	4024.13	10470
0.02	430	3865.58	10470
0.05	499	2121.26	10470
0.1	496	1373.09	10470

Figure 31. Time-step size – Computational time costs graphical exponential relationship of the small-amplitude solitary wave analysis.

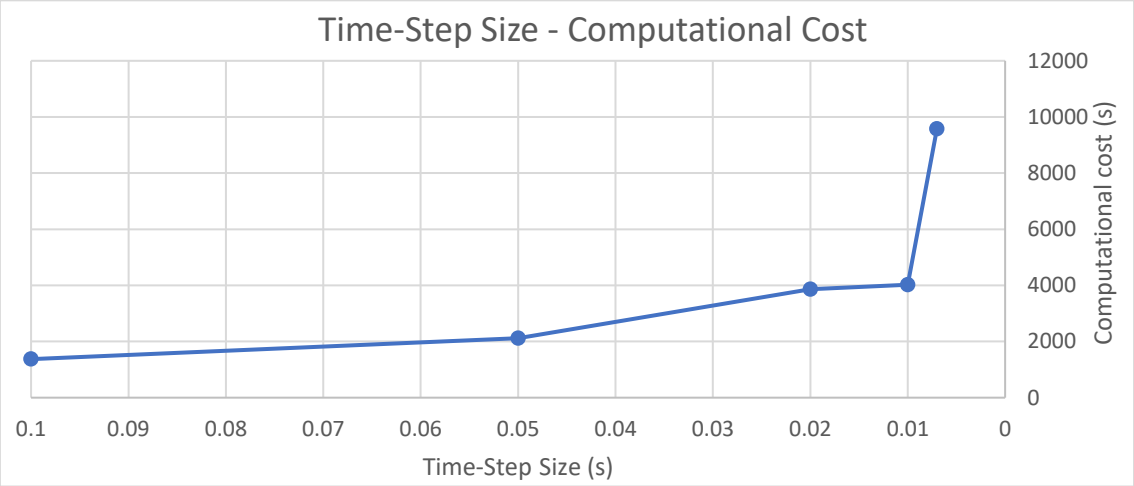

The different cases demonstrated a clear convergence of results for all the wave measurement points (Figure 32, Figure 33 and Figure 34). For the studied problem, it could be considered that convergence is reached after the mesh reaches the value of (ΔT=0.01s) approximately as there is no noticeable difference between this case and the ones with lower time-steps in all the wave measurement points (Figure 35, Figure 36 and Figure 37). This proves that by finding an appropriate mesh density the numerical method can provide a solution to the problem without the necessity to increase the number of elements, which would cause an important increase in the computational cost of the problem.

Figure 32. Time-step size convergence graphic of the small-amplitude solitary wave analysis at 60 metres from wave paddle.

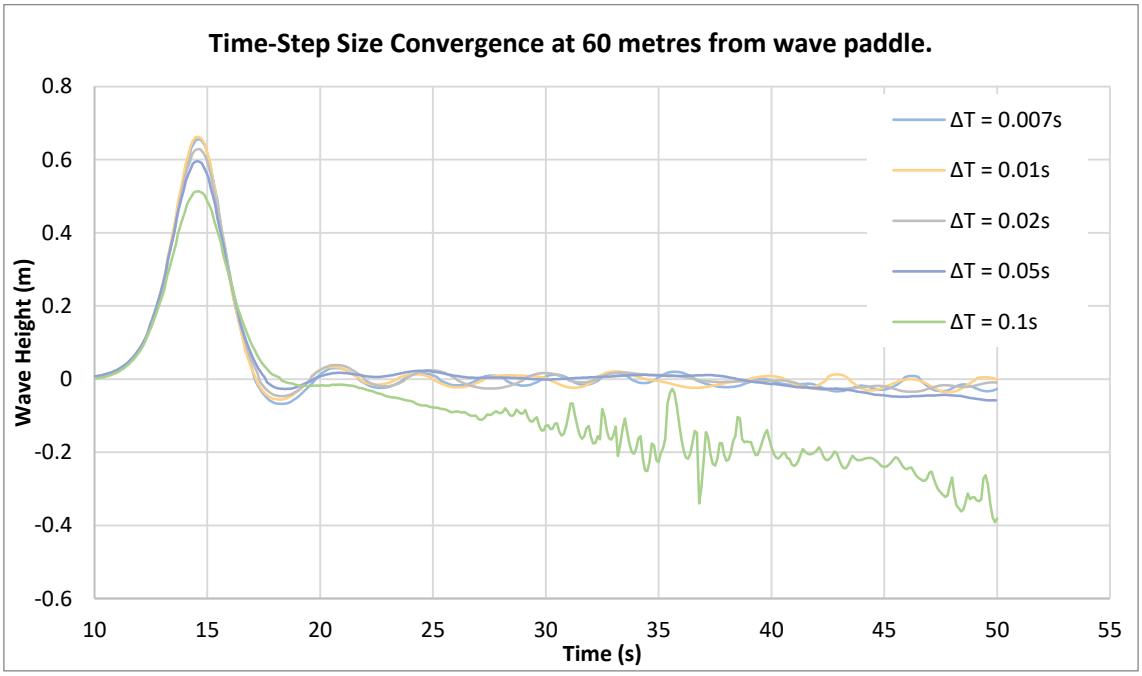

Figure 33. Time-step size convergence graphic of the small-amplitude solitary wave analysis at 165.3 metres from wave paddle.

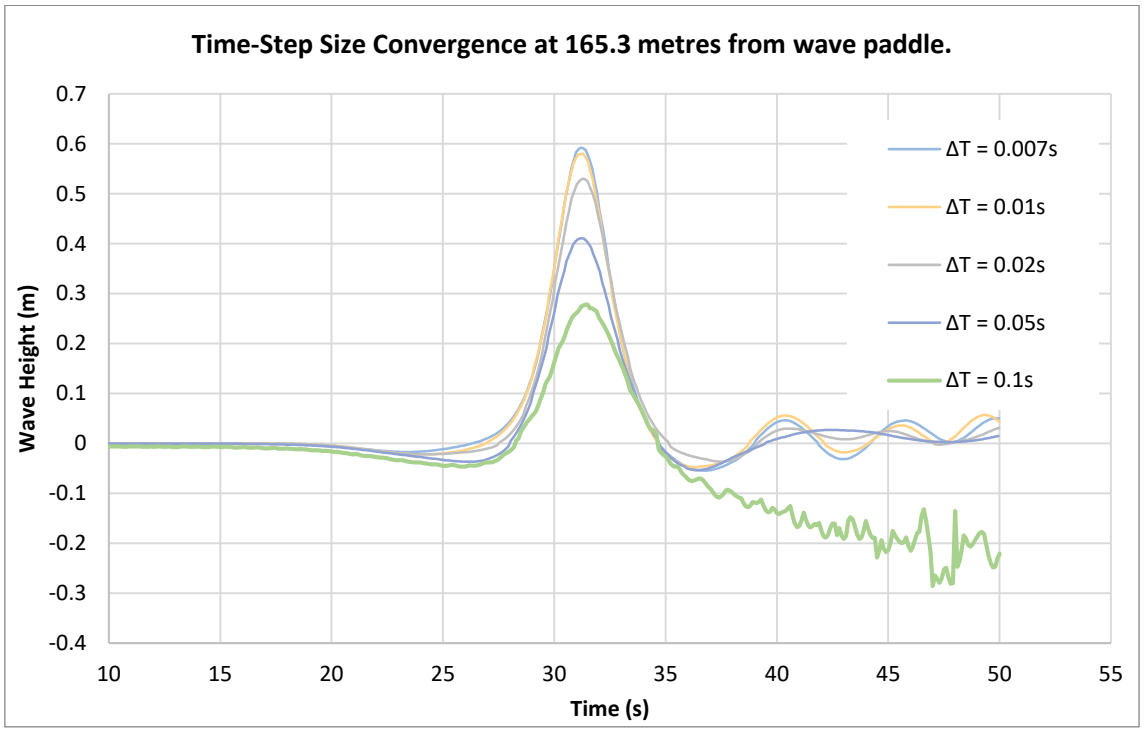

Figure 34. Time-step size convergence graphic of the small-amplitude *solitary wave analysis at 170 metres from wave paddle.*

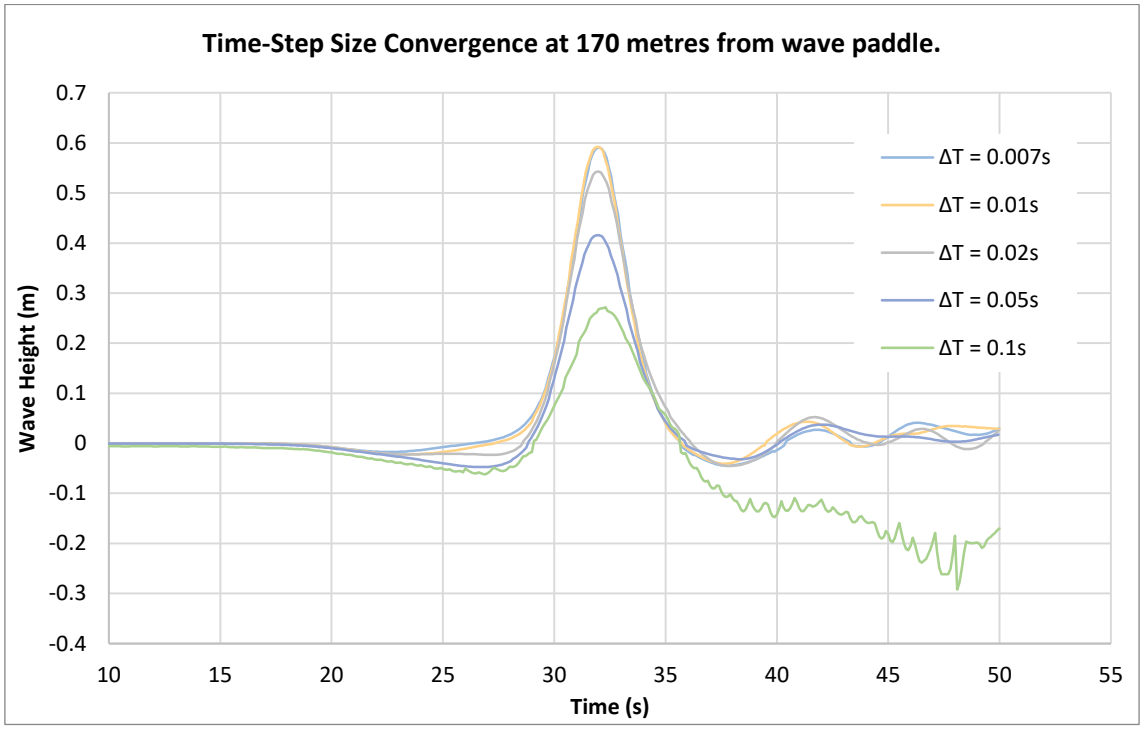

Figure 35. Time-step convergence of the two smaller time-steps of the small-amplitude solitary wave analysis at 60 metres from wave paddle.

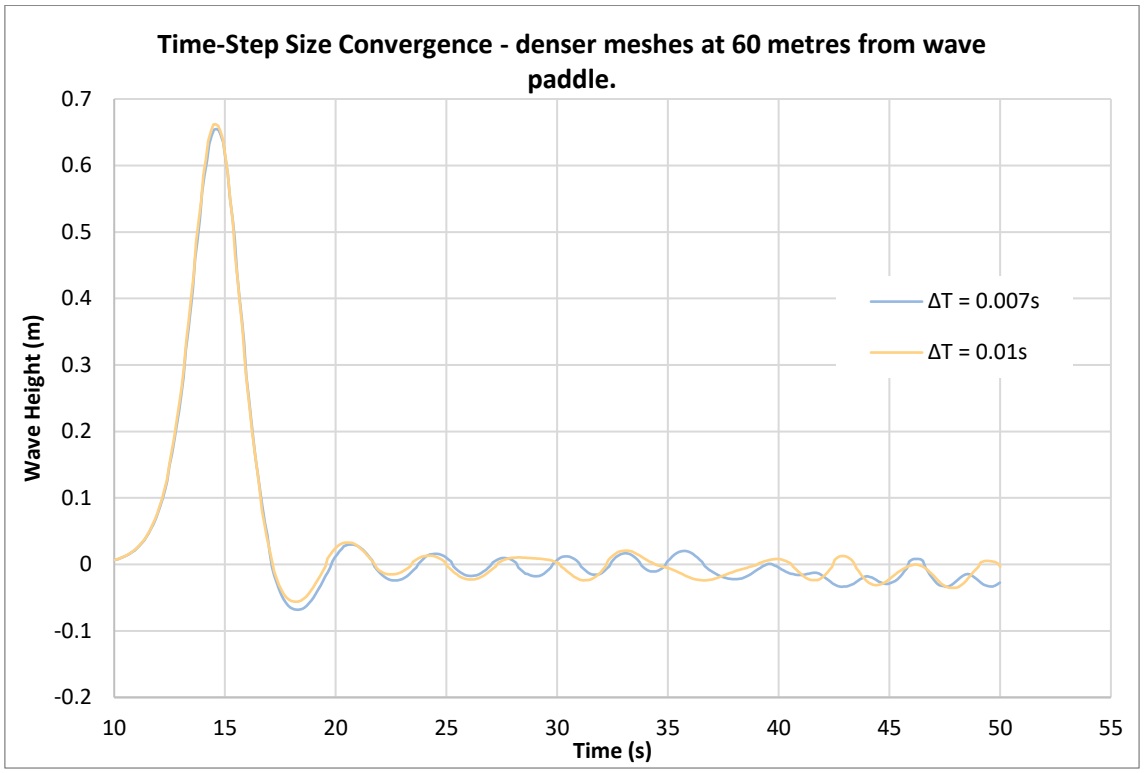

Figure 36. Time-step convergence of the two smaller time-steps of the small-amplitude solitary wave analysis at 165.3 metres from wave paddle.

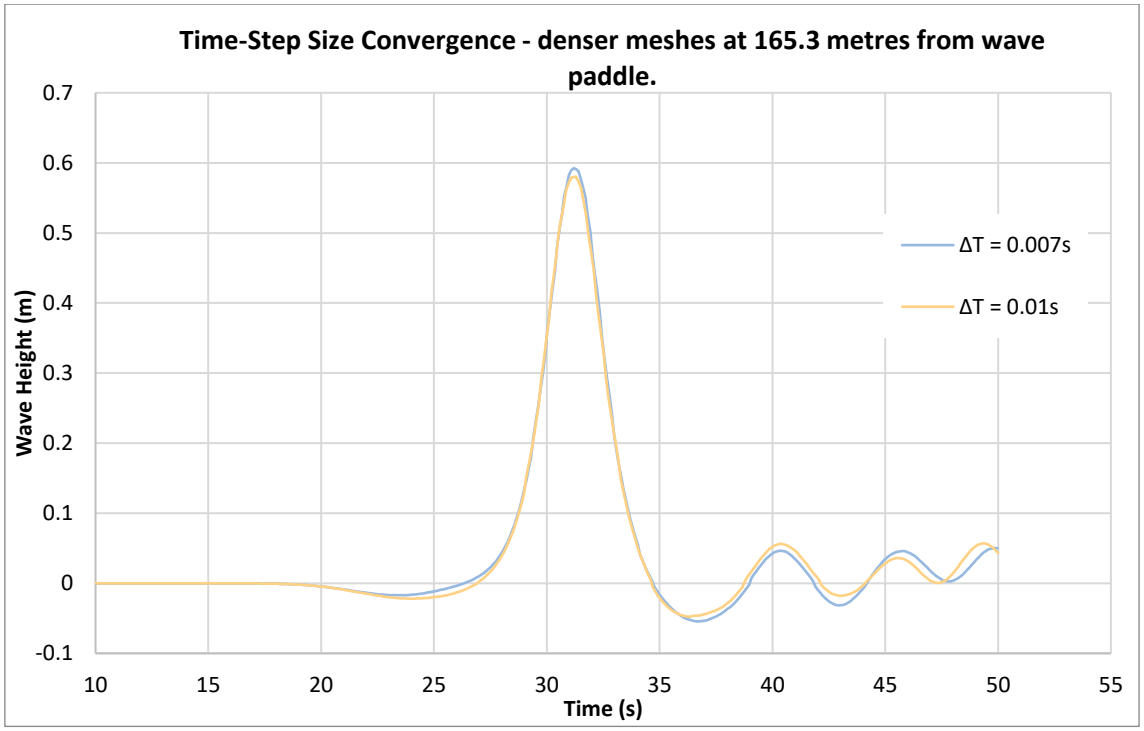

Figure 37. Time-step convergence of the two smaller time-steps of the small-amplitude solitary wave analysis at 170 metres from wave paddle.

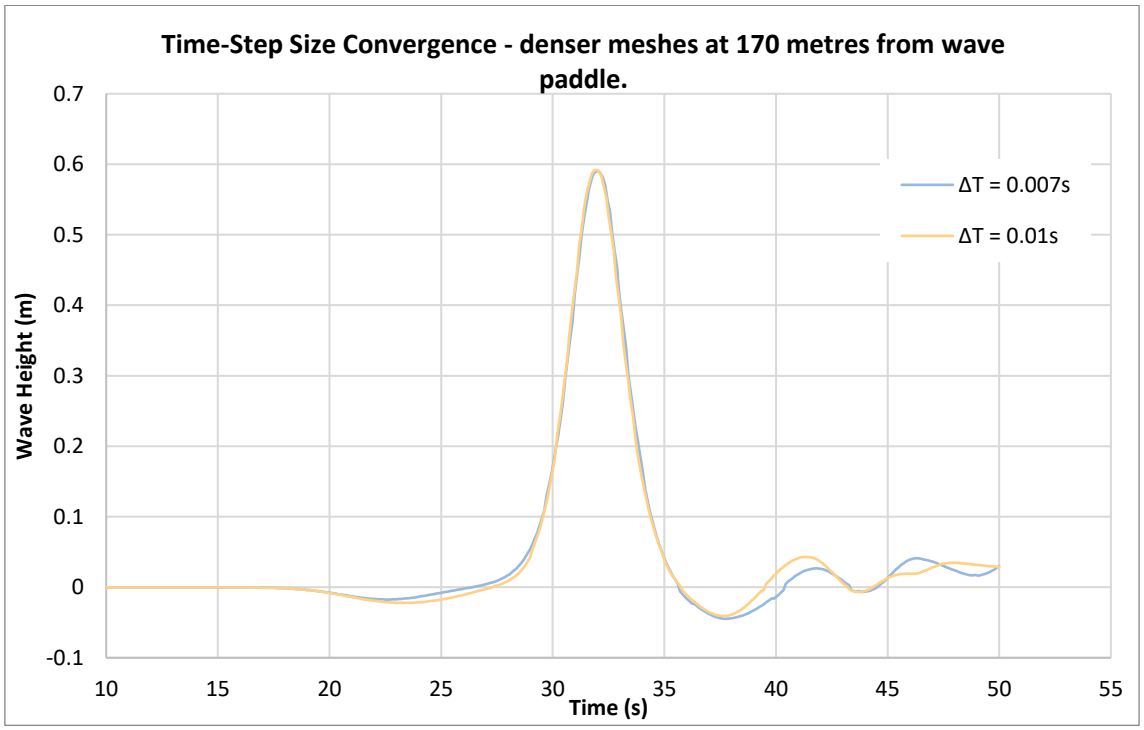

4.4. CONCLUSIONS

In this first study, the PFEM has been applied to the simulation of the propagation of a solitary wave of small amplitude through a 237.5 meters long channel. This test reproduces the experimental test conducted at the tsunami experimental laboratory channel in Braunschweig, Germany (Hitzegrad, 2019).

Although the wave measurement results comparison between the experimental and the finest mesh exhibits an increasing difference as the waves move further from the wave paddle, this error is small and for the long longitude of the study can be considered as acceptable.

For a good analysis of the numerical results, the process of setting the correct tolerance for the wave height function is a crucial operation as the results are highly sensible of the tolerance chosen. On the one hand, the use of high tolerance can cause significant errors in the interpretation of the numerical results, on the other hand, small values may lead to obtaining a reduced number of outputs as no node is found inside the range.

The convergence of the PFEM in terms of mesh size has been clearly proved. It has been shown that for small enough mesh sizes convergent results are obtained. The difference in terms of the computational cost of the analyses for reducing mesh size has been also highlighted. The time-step convergence study also was proved to be successful. The study has shown how for small time-steps values a convergence on the results appears. Time-step size also has high effects on the computational cost of the analysis. It is important to note that, to find a correct value for the

mesh that achieved the convergence, it is necessary to know a good value for the time-step size and vice versa.

The computational cost necessary to perform the analysis has been proved to be highly sensitive to the mesh and time-step sizes. It has been shown that the time duration of the analyses increases exponentially with the number of elements. For computationally expensive problems, it is also important to reduce the memory occupation of the post process files. To decrease the data weight of the outputs, it is possible to print results for a time-step bigger than the one used for the computation

Another option to reduce the computational cost while keeping a good accuracy is the implementation of refinement boxes. This addition will be studied in the next chapter analysing the propagation of a bigger solitary wave.

5. PROPAGATION AND BREAKING OF A BIG-AMPLITUDE WAVE

5.1. INTRODUCTION

The first study validated the numerical method for the propagation of a wave of small amplitude. Nevertheless, waves propagation can have different behaviour depending on their characteristics. Thus, it is necessary to perform further studies on wave propagation analysis of different regimes. To do so, a second analysis is set for the study of a solitary wave on a much smaller channel but with a higher amplitude. In this case, the wave is also breaking at an intermedium point of the channel. PFEM is a good method for solving these cases because it is capable of simulating the behaviour of parts separated from the main fluid body thanks to its Lagrangian formulation.

The analysis is based on the laboratory experiments carried out in Japan by Arikawa in the large Hydro Geo-Flume facility (Arikawa, 2009). The experiments studied the collapse mechanisms of concrete plates under the impact of a wave on scale models.

The numerical analysis is performed by the Lagrangian PFEM method. This computation is performed under the Kratos software and the GID pre and post-processing

5.2. PROBLEM GEOMETRY

The tsunami wave generated by the Large Hydro-Geo Flume was installed at the Port and Airport Research Institute in Japan (Figure 38) (Arikawa, 2009). It consists of a 184 m long, 3.5m wide and 12 metres deep channel, its water SWL is at a height of 5.6 m. It has a wave paddle located at the end of the channel that acts as a piston generating a solitary wave. It has a maximum displacement of 14 m. The channel measures the height of the wave at the wave gauge, at 90 metres from the wave paddle.

Figure 38. Large Hydro-Geo Flume was installed at the Port and Airport Research Institute in Japan geometry from (Oñate, et al., 2022)

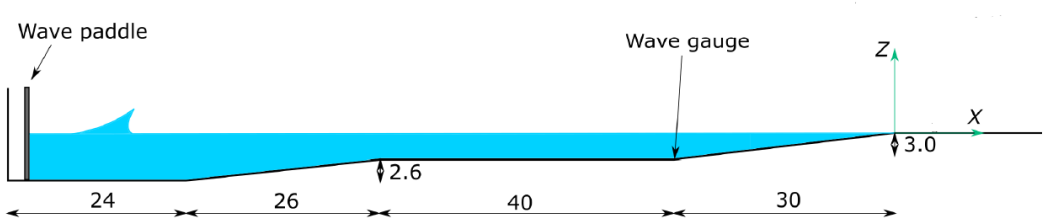

The paddle is a piston that follows a specific time function (Figure 39).

Figure 39. Solitary wave paddle movement in time graphic of the big-amplitude wave analysis, from (Oñate, et al., 2022)

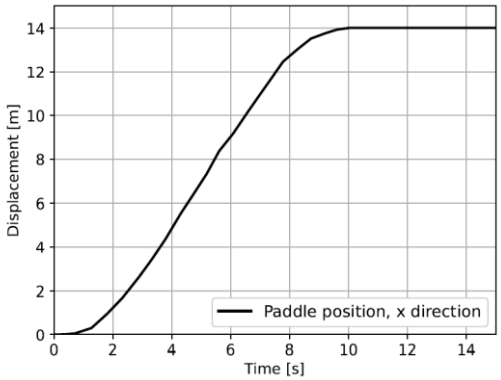

The geometry of the problem is recreated at GID software as shown in Figure 40.

To represent the problem with this software, the water body properties are defined as on the small-amplitude wave propagation analysis. Then, rigid walls are imposed as the boundary on the paddle and the bottom of the problem.

Figure 40. Big-amplitude solitary wave problem geometry on GID software.

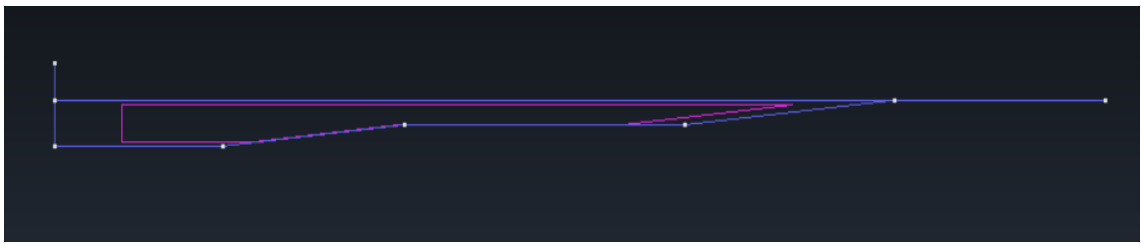

The velocity boundary conditions are determined as follows. The bottom is immobile and the paddle follows the velocity determined in Equation 9 and Figure 39. After the first 10 seconds, the paddle movement is stopped. The system solves the problem for a duration of 30 seconds.

Equation 9. Big-amplitude solitary wave paddle movement in time function

$$V = -5 * 0.0001244279t^4 + 4 * 0.0034774409t^3 - 3 * 0.0658270015t^2 + 2 * 0.6131262459t - 0.3822735836$$

wave height measurements are obtained with the same function used on the first analysis with its appropriate geometry parameters, as described in Figure 10 and Table 1.

During this study, an additional feature is incorporated, the application of refinement boxes to improve the case performance. It consists of applying a denser mesh size to a specific region. First, it is important to establish where the physics of the problem requires a larger definition. For the problem studied this relates to the bottom of the water domain, as its interaction with the wall surface, makes it the more complicated region.

To use this technique on GID it is needed to draw two different surfaces where the two different meshes are going to be set. Then insert the size of the refinement box as an unstructured mesh and assign the same size to the line boundaries as a structured mesh line. This new information is needed to be confirmed in Kratos software. To do so, the existence of the refinement box is set with its appropriate mesh size and its coordinates boundaries.

5.3. NUMERICAL RESULTS WITH PFEM

First of all, it is important to observe the behaviour of the wave on the numerical method approximation. GID software provides the basis to plot figures of the wave parameters at each time-step. To analyse this global result of the wave movement, it is useful to acquire graphic representations of the wave amplitude, pressure and velocity at the most important time-steps of the problem.

Figure 41, Figure 43, Figure 45, and Figure 49 show the velocity distribution of the wave at its most important time-steps, mainly the maximum and minimums wave height measurements on the wave gauge. Figure 42, Figure 44, Figure 46, Figure 48 and Figure 50 show the pressure distribution at these same time-steps.

Figure 41. Big-amplitude solitary wave development velocity distribution.

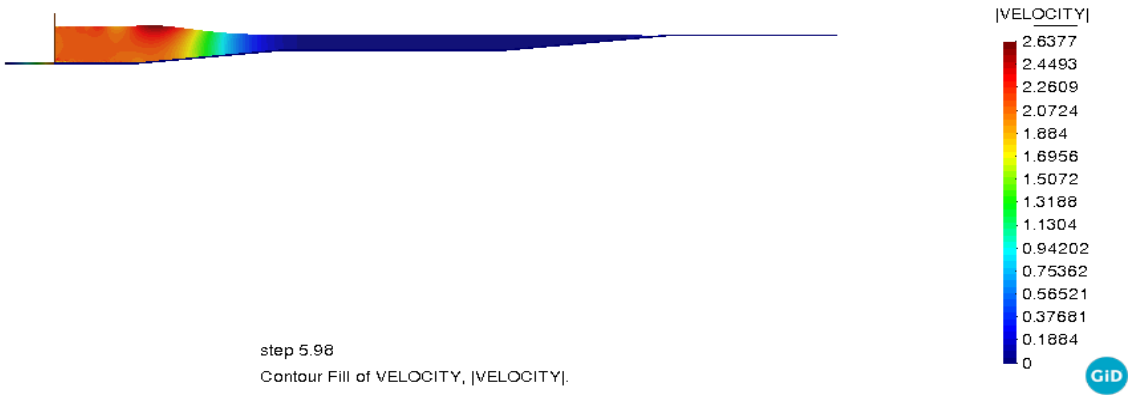

Figure 42. Big-amplitude solitary wave development pressure distribution.

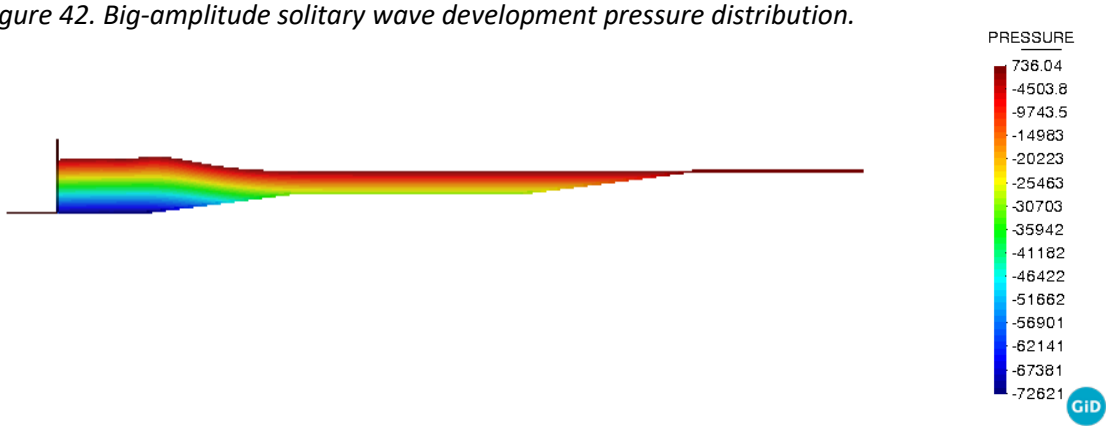

Figure 43. Big-amplitude solitary wave maximum height velocity distribution.

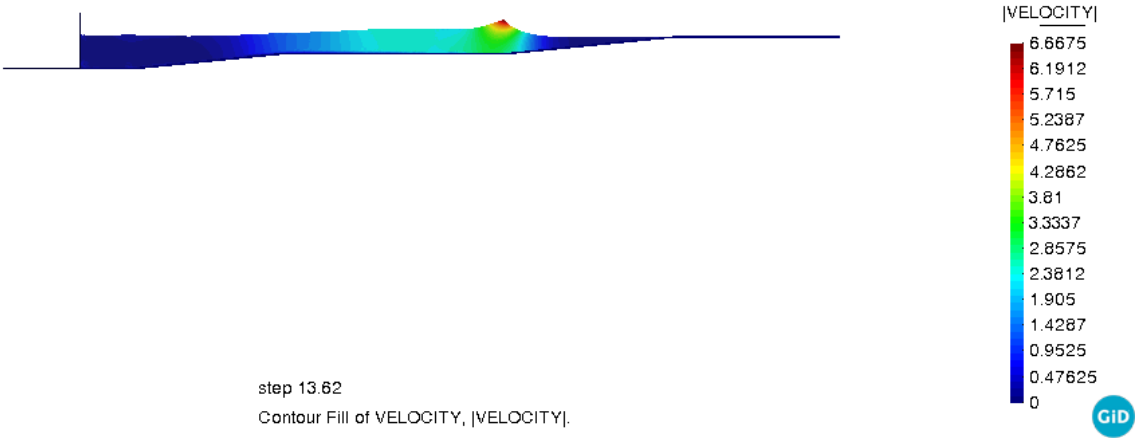

Figure 44. Big-amplitude solitary wave maximum height pressure distribution.

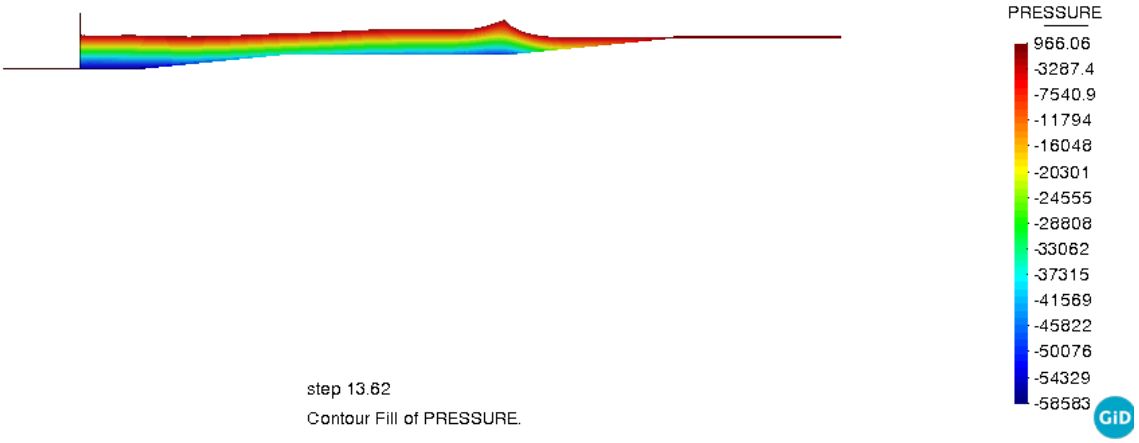

Figure 45. Big-amplitude solitary wave second maximum height velocity distribution.

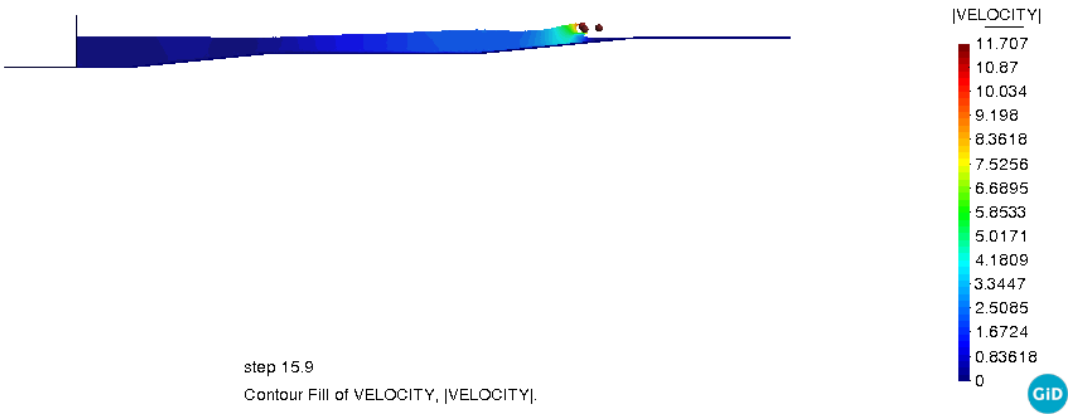

Figure 46. Big-amplitude solitary wave second maximum height pressure distribution.

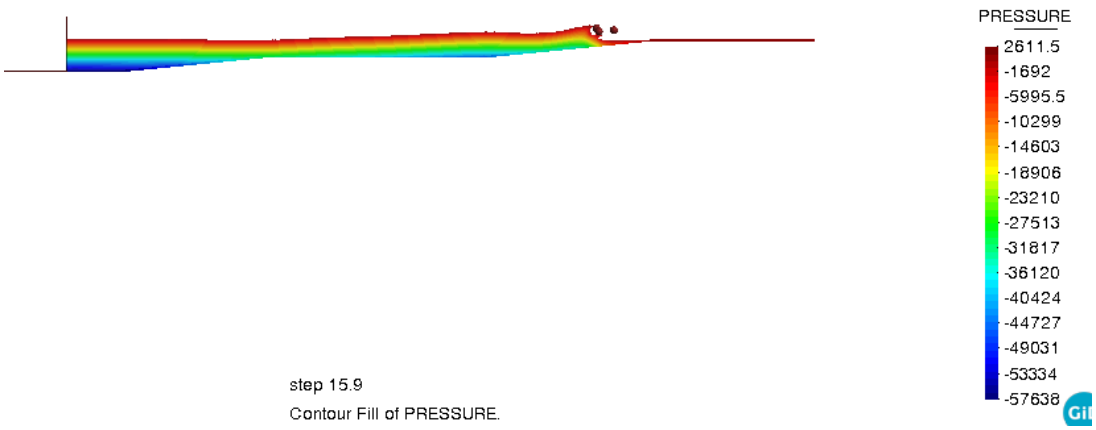

Figure 47. Big-amplitude solitary wave minimum water height velocity distribution.

Figure 48. Big-amplitude solitary wave minimum water height pressure distribution.

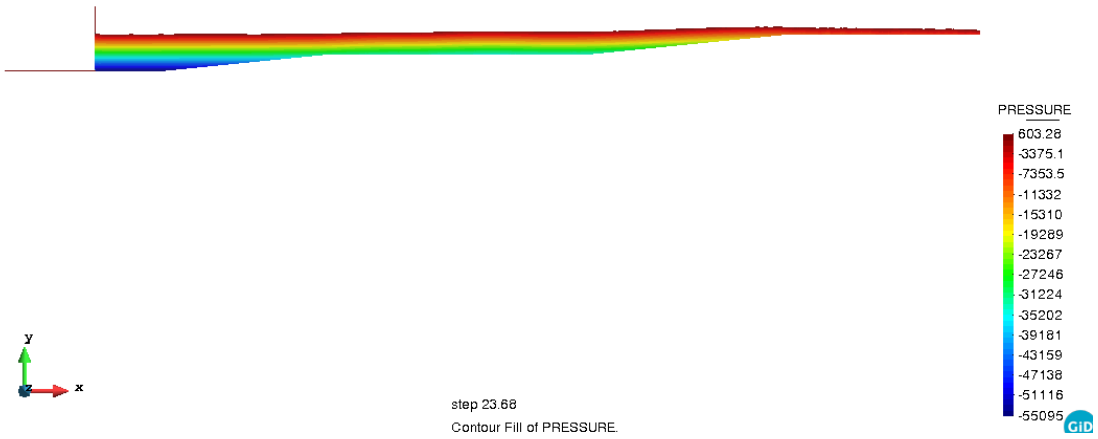

Figure 49. Big-amplitude solitary wave third maximum height velocity distribution.

Figure 50. Big-amplitude solitary wave third maximum height pressure distribution.

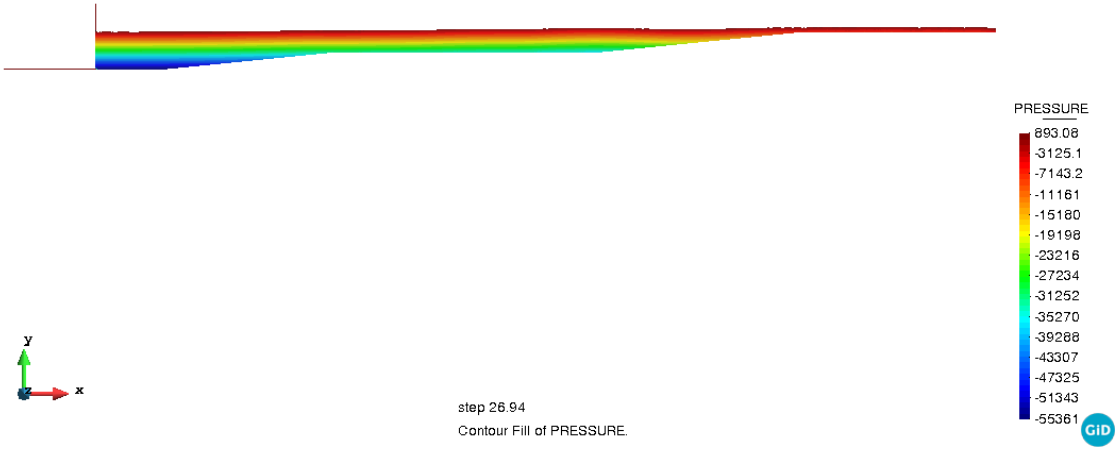

The previous snapshots show how the water propagates inside the channel leaving the system boundaries when reaching the beach end. They show how the velocity peaks are created at the moment of the breaking wave formation. It also describes a hydrostatic pressure field distribution of the water body far from the breaking zone.

Figure 45 and Figure 46 show the wave behaviour on its breaking phase. The snapshots demonstrate how PFEM is capable of analysing fluid dynamics with free surfaces where the wave breaks and splashes generating separated parts outside the domain. When the wave breaks, the velocity of the separated water parts is much higher than on the rest of the water body.

5.3.1. MESH SIZE CONVERGENCE ANALYSIS

As in the first case, the initial analysis to be done is the observance of the impact of the mesh density on the results of the numerical method. The different meshes to be used for the analysis are described in Table 6. The time-step is set to be small enough (*ΔT=0.02 seconds*).

Again, to do this comparison the wave height measurements of the function will be used. The different tolerance values are set for the different cases as described in Table 6.

Table 6. Cases studied for the mesh size convergence of the big-amplitude big-amplitude solitary wave analysis.

Cases	Mesh size (h)	Function Tolerance	Number of Nodes
Case 1	0.2m	0.4m	12371
Case 2	0.3m	0.4m	5604
Case 3	0.5m	0.4m	2182
Case 4	0.7m	0.5m	1107
Case 5	1m	0.8m	1107
Case 6	1.5m	1m	300
Case 7	2m	3m	202

After computing all the cases it is seen that as shown in Table 7 there is a high difference in the computational time needed to perform the simulation for the different mesh densities, its relation is exponential (Figure 51) so it is crucial to choose an appropriate time-step to obtain good results with a viable computational cost. The range of tolerances selected for the function gives approximately the same number of printed results so the results have similar accuracy regarding this factor.

Table 7. Computational time – Mesh size dependence of the big-amplitude solitary wave analysis.

Mesh size (h)	Number of printed results	Computation Time (s)
0.2 m	263	3776.93
0.3 m	263	1476.31
0.5 m	261	606.4
0.7 m	256	247.47
1 m	254	236.74
1.5 m	254	72.46
2 m	263	75.29

Figure 51. Mesh size – Computational time costs graphical exponential relationship of the big-amplitude solitary wave analysis.

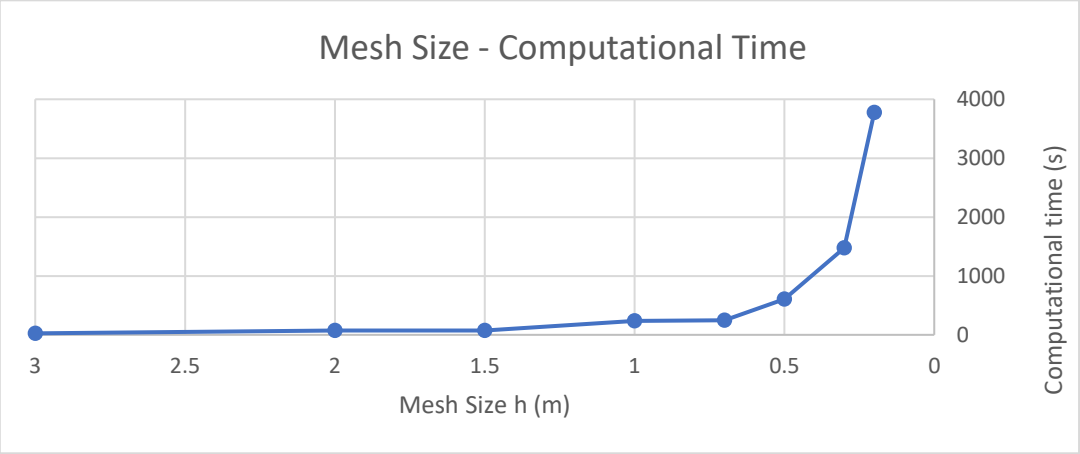

The different cases studied demonstrated a convergence of the results for low enough values of mesh size (Figure 52). For the studied problem, it could be considered that convergence is reached after the mesh reaches the approximate value of (*h=0.3m*) (Figure 53).

The computational-time difference between the mesh of (*h=0.3m*) and (*h=0.2m*) is around 155% of the first. This difference proves the importance of defining a correct value for the mesh size. Moreover, the analysis performed was in 2D, for analysis of 3D, the order of the exponential relationship between computational-time and mesh size would increase even more.

The results demonstrate that by finding an appropriate mesh density the numerical method can provide a solution to the problem without the necessity to increase the number of elements, which would cause an important increase in the computational cost of the problem.

Figure 52.Mesh density convergence graphic of the big-amplitude solitary wave analysis.

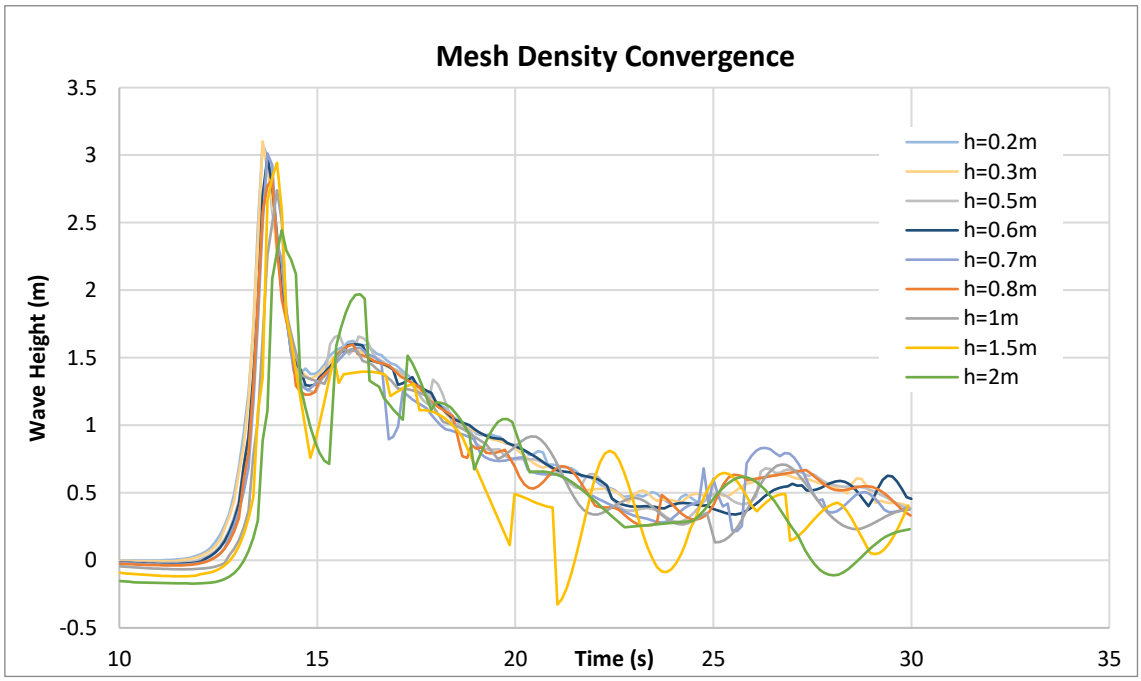

Figure 53. Mesh density convergence of the two finest meshes of the big-amplitude solitary wave analysis.

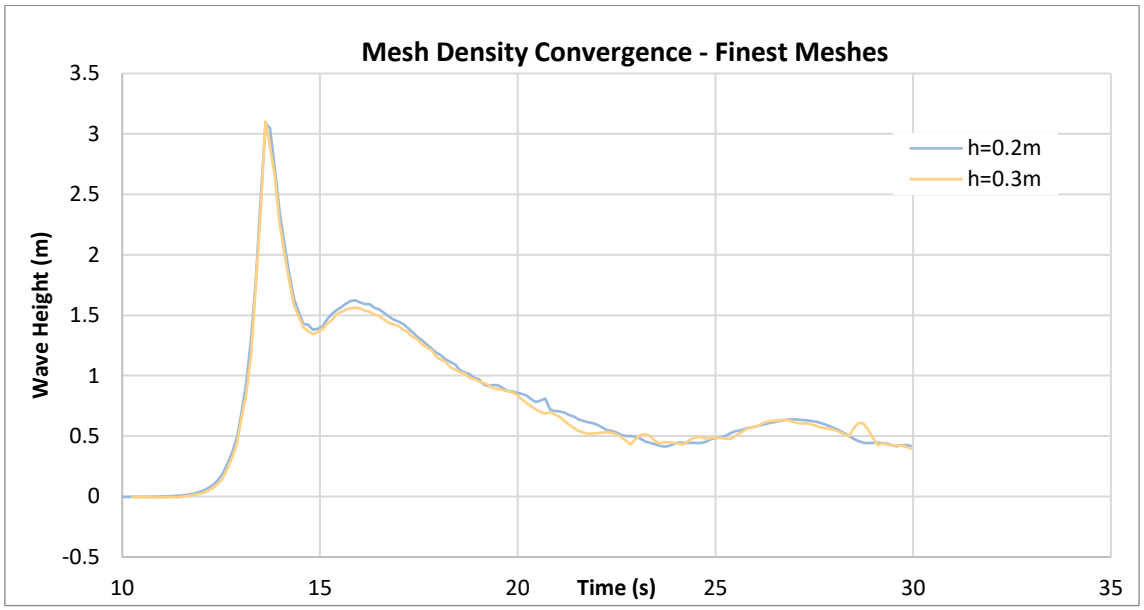

Figure 54 shows the comparison of the numerical results with the experimental cones carried out. It shows that the numerical values of the most accurate case did a good approximation of the wave behaviour. We note that the numerical solution gives higher values regarding the first wave height peak. This may be influenced by the friction caused in the laboratory experiment by the lateral walls which cannot be captured by the 2D numerical analysis where the wave is considered to have an infinite width.

Figure 54. Comparison of the experimental and numerical results of the big-amplitude solitary wave analysis.

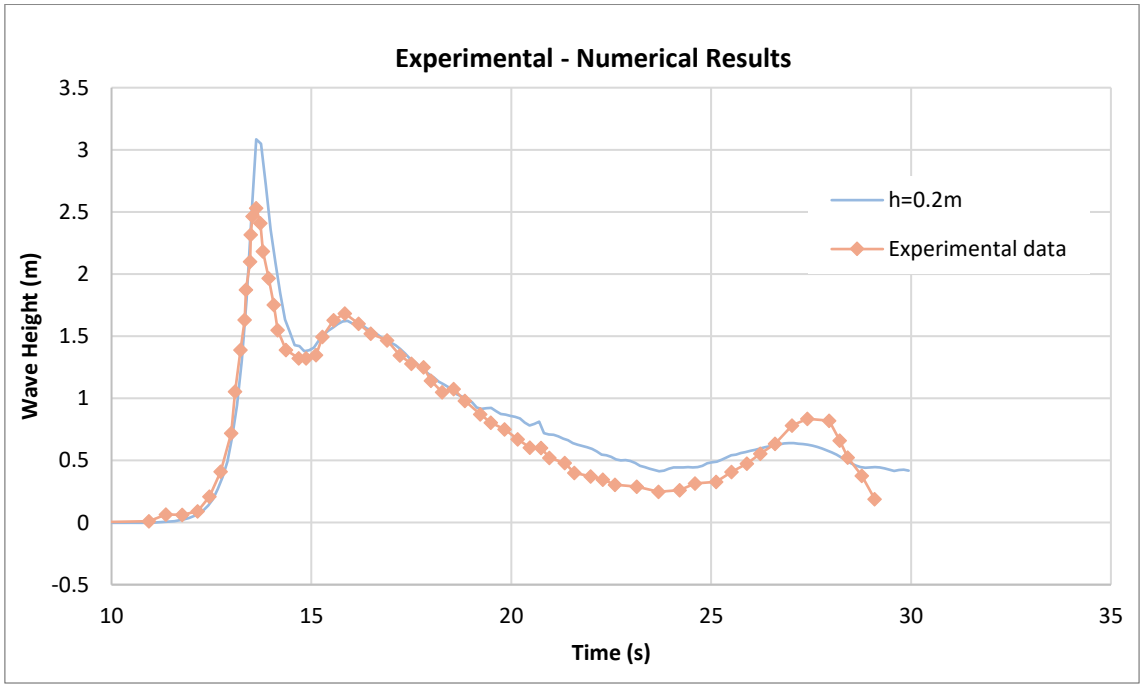

Another important phenomenon to consider in the results is the difference of boundaries between the numerical and experimental analysis. The experimental analysis contemplated the existence of a concrete wall at the end of the channel which causes a reflection wave that affects the solitary wave propagation. This is one of the factors that cause big differences in the experimental and numerical results at the end of the analysis. For this reason, it is fairer to compare the numerical and experimental results during only the first 18 seconds, as shown in Figure 55.

Figure 55. Comparison of experimental and numerical results adapted to the correct time range of the big-amplitude solitary wave analysis.

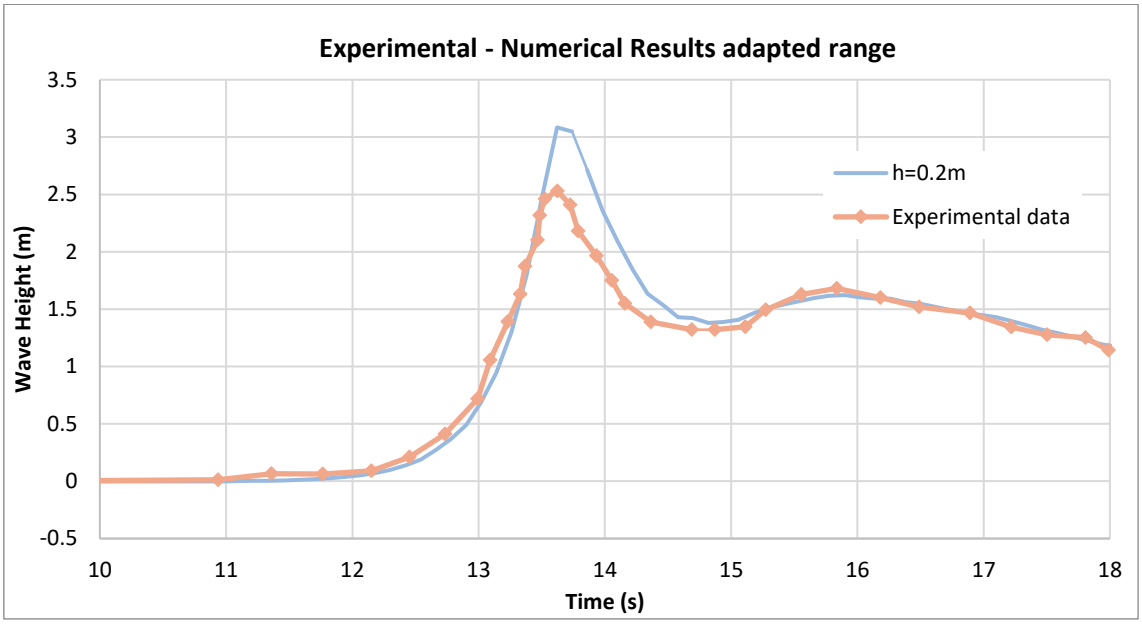

5.3.2. TIME-STEP SIZE CONVERGENCE ANALYSIS

As on the first analysis, it is appropriate to do a time-step convergence study to prove its importance on the accuracy of the problem. For this analysis different cases of time-steps were studied (Table 8). The mesh density is set to (*h=0.5 m*) for all cases to not alter the time-step study.

Table 8 Cases studied for the time-step size convergence of the big-amplitude solitary wave analysis.

Cases	Time-step (ΔT)	Function Tolerance	Number of Nodes
Case 1	0.005 s	0.4m	2182
Case 2	0.007 s	0.4m	2182
Case 3	0.01 s	0.4m	2182
Case 4	0.05 s	0.4m	2182
Case 5	0.1 s	0.4m	2182

The cases are computed and as shown in Table 9, there is also in this case high change of the computation time values within the cases Figure 56.

Table 9. Computational time – Time-step size dependence of the big-amplitude solitary wave analysis.

Time Step (ΔT)	Number of printed results	Computation Time (s)
0.005 s	283	1831.22
0.007 s	281	1452.71
0.01 s	276	1238.11
0.05 s	297	281.7
0.1 s	293	120.85
0.2 s	149	69.41

Figure 56. Time-step size – Computational time costs graphical exponential relationship of the big-amplitude solitary wave analysis.

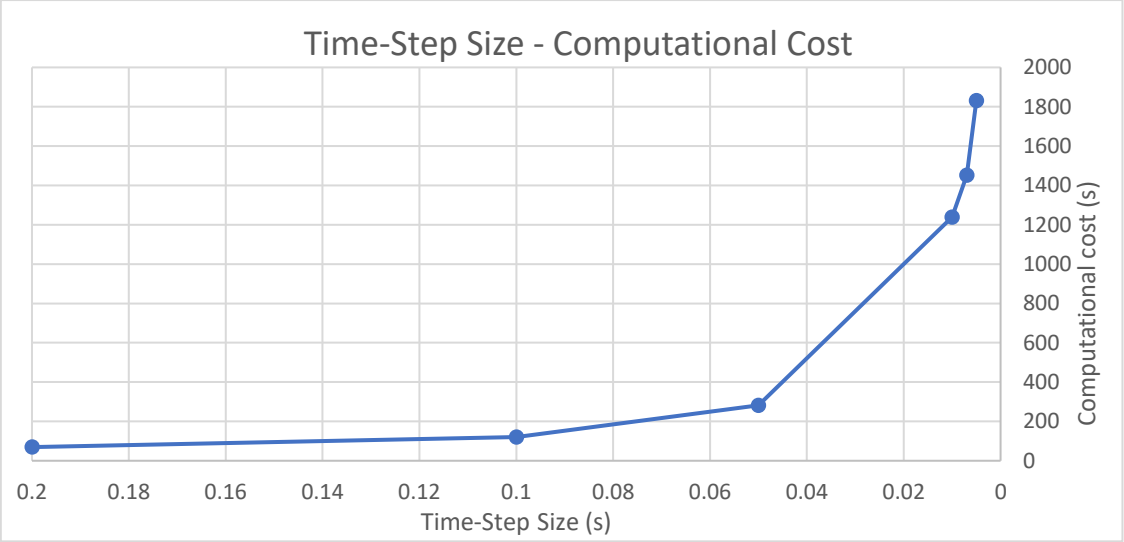

The different cases demonstrated a clear convergence of results (Figure 57). For this problem, it could be considered that convergence is reached after the time-step reaches the approximate size of (*ΔT=0.7s*) (Figure 58). This proves that by finding an appropriate mesh density the numerical method can provide a solution to the problem without the necessity to increase the number of elements, which would cause an important increase in the computational cost of the problem.

Figure 57. Time-step size convergence graphic of the big-amplitude solitary wave analysis.

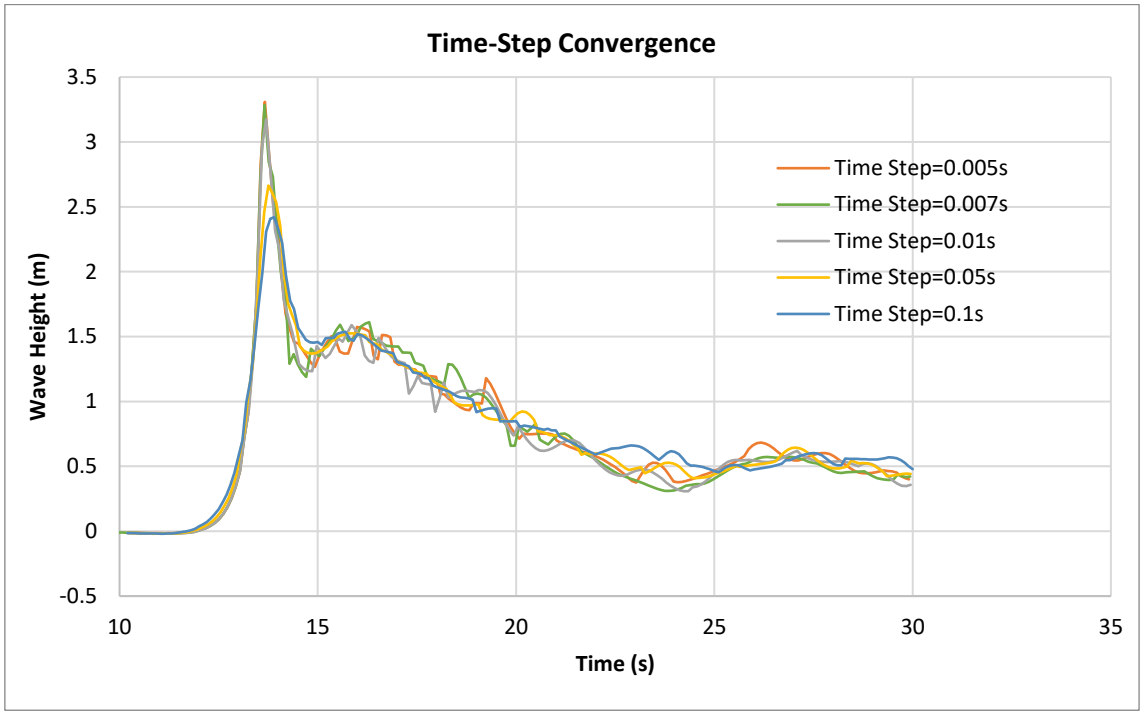

Figure 58. Time-step convergence of the two smaller time-steps of the big-amplitude solitary wave analysis.

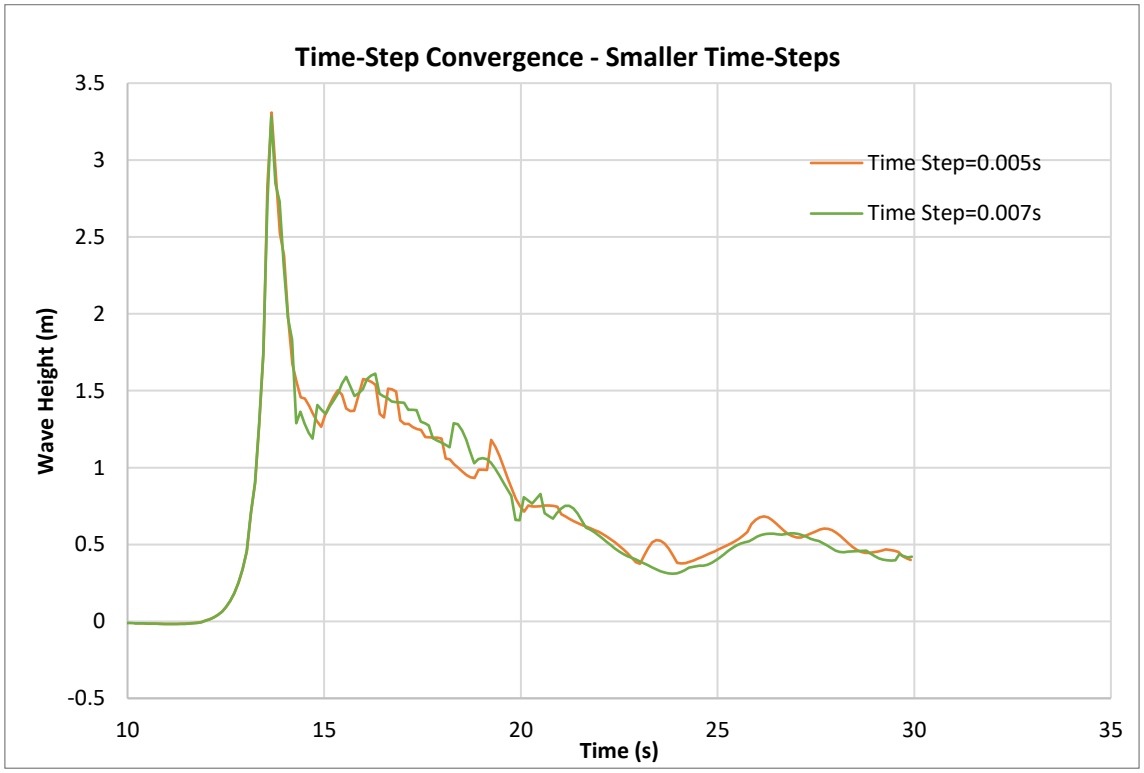

5.3.3. REFINEMENT BOXES ANALYSIS

To study the possibility of obtaining good results with lower computational cost, the technique of refinement boxes of different mesh sizes is used. As highlighted in the mesh density analysis, making the mesh denser cause a big increase in the computational cost of the analysis.

Then, using denser meshes only on lower parts of the domain problem bottom could improve the efficiency of the mesh, being the interaction with the walls the key factor for good modelling of the fluid flow.

To study the impact of the refinement meshes three initial cases are performed. They all have a refinement box of mesh size (*h=0.3m*) on a global mesh of (*h=0.7m*). but with different heights of the refinement box. On a total water body height of 5,6 metres, the refinement box is set to reach 5, 3 and 1 metres for each of the three cases (Figure 59, Figure 60 and Figure 61).

Figure 59. Mesh distribution for refinement box of h=0.3m at 5 metres height and global mesh of h=0.7m of the big-amplitude solitary wave analysis.

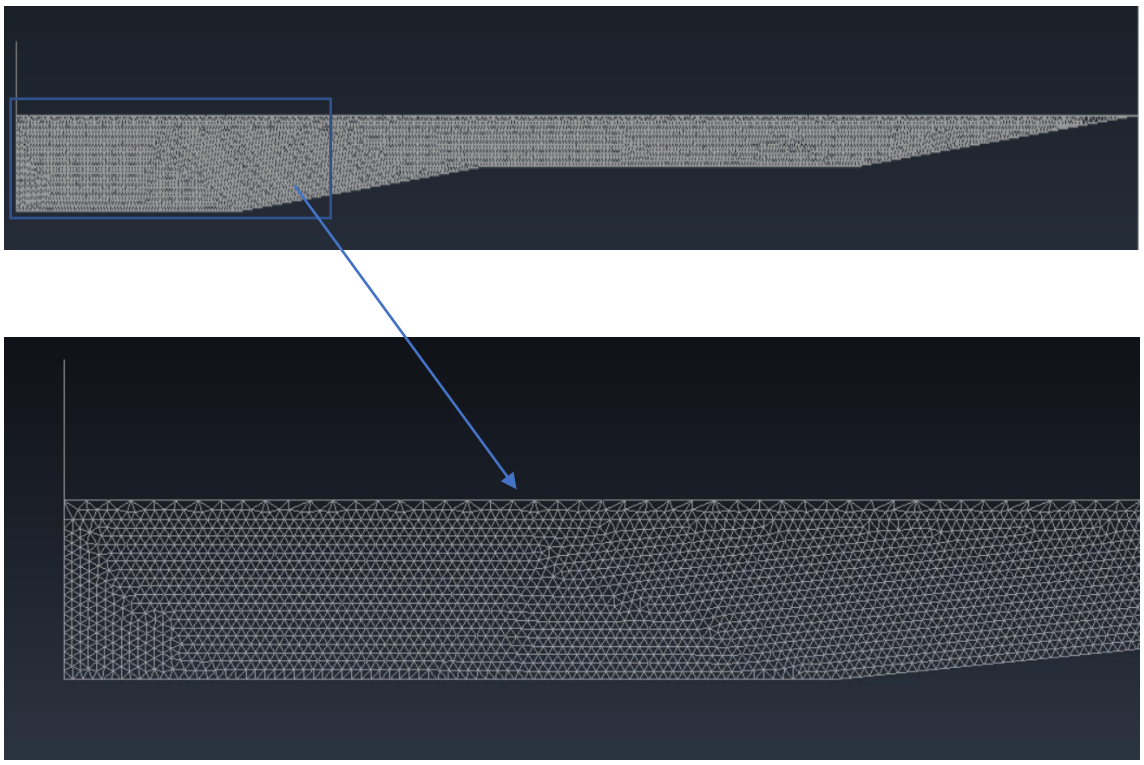

Figure 60. Mesh distribution for refinement box of h=0.3m at 3-metre height and global mesh of h=0.7m of the big-amplitude solitary wave analysis.

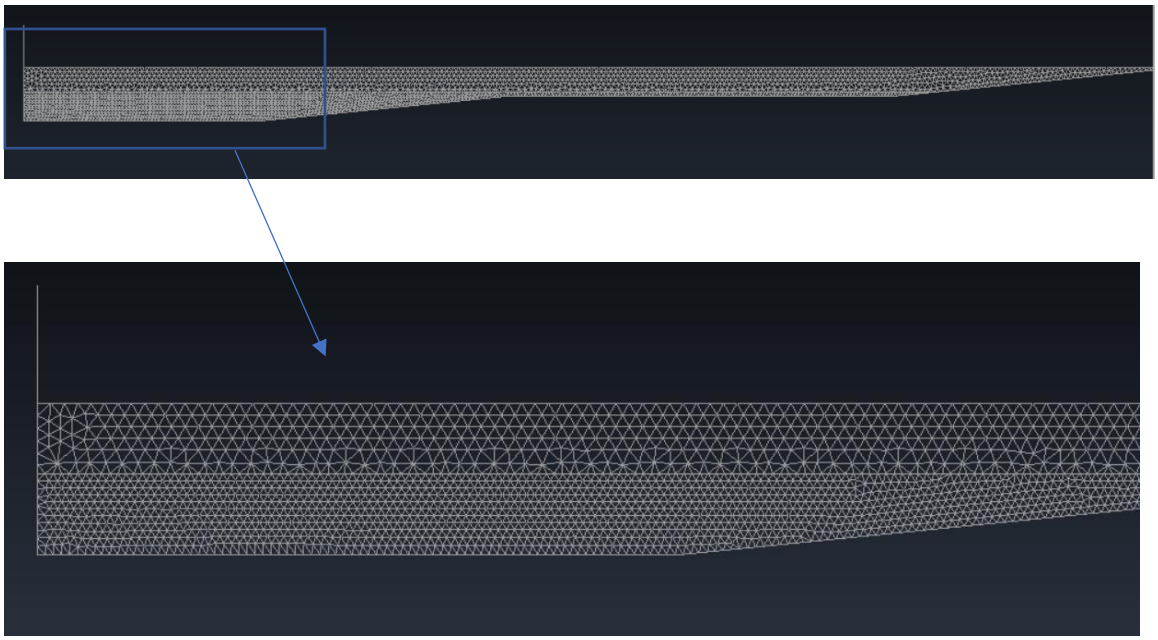

Figure 61. Mesh distribution for refinement box of h=0.3m at 1-metre height and global mesh of h=0.7m of the big-amplitude solitary wave analysis.

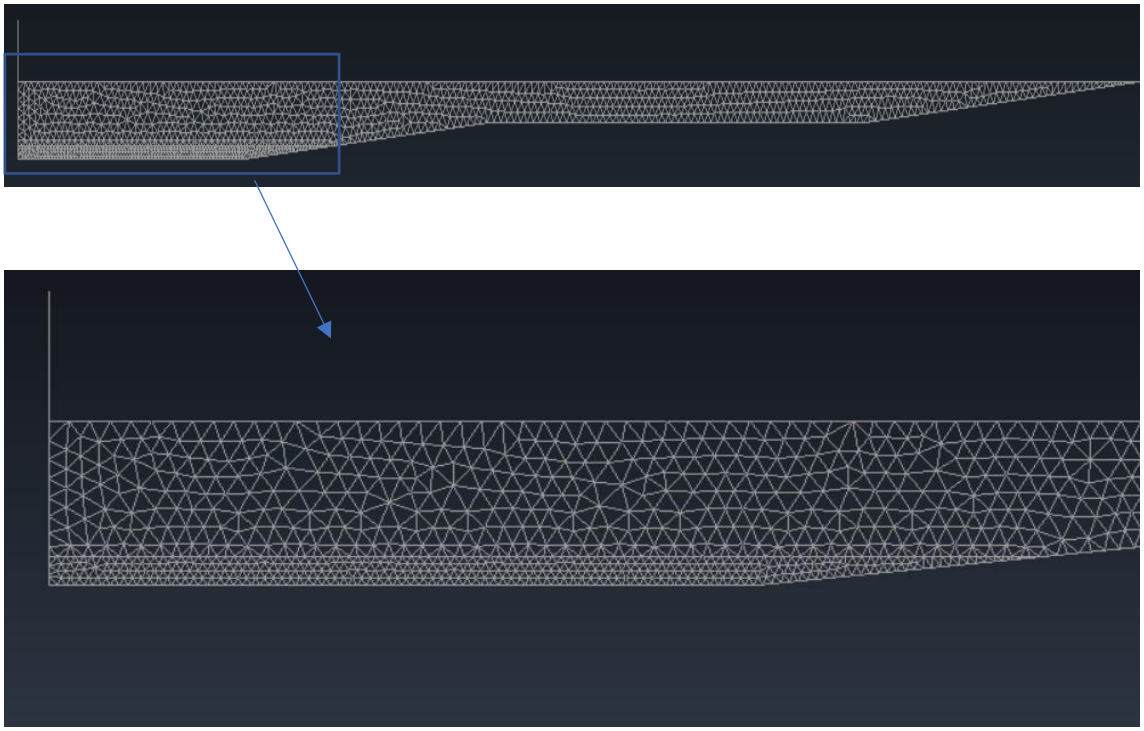

The three cases used the data shown in Table 10.

Table 10. Data used for the mesh refinement analysis of the big-amplitude solitary wave analysis.

DATA	
Time Steps (s)	0.02
Wave Height Measurement (m)	90
Mesh size (m)	0.5
Refinemnet box mesh size (m)	0.1

Table 11 shows the results obtained from the different cases. It demonstrates the relationship between the mesh size distribution, the computation time and the number of nodes compared to the ones of homogenous mesh distribution. The computational cost is much lower when using the refinement boxes compared to the homogenous one of (*h=0.7m*). Then, Figure 62 shows the comparison of the wave height measurements on the three refinement exercises. As seen, there is almost no difference between the refinement types. This proves that the refinement at height (*y=1 metre*) should be enough to improve considerably the analysis accuracy.

Table 11. Computational time – Mesh size with a refinement of (h=0.3m) and uniform mesh of (h=0.7m) dependence of the solitary wave analysis.

Mesh type	Number of printed resutls	Tolerance	Computation Time (s)	Number of Nodes
Uniform Mesh h=0.3m	263	0.4	1476.31	5604
Refinement y<5m	263	0.4	1460.83	4976
Refinement y<3m	243	0.4	923.78	2637
Refinement y<1m	253	0.4	391.49	1546
Uniform Mesh h=0.7m	256	0.5	247.47	1107

Figure 62. Wave height measurements of the refinement cases of refinement boxes of h=0.3m and global meshes of h=0.7m at y=3m of the big-amplitude solitary wave analysis.

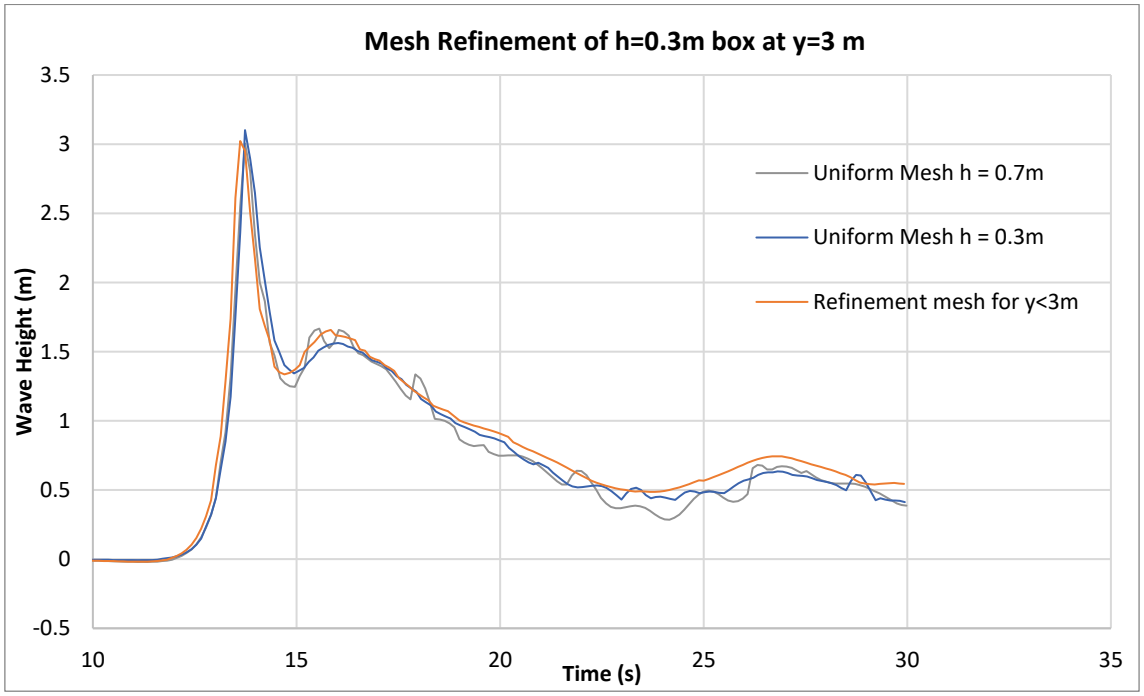

Figure 63. Wave height measurements of the refinement cases of refinement boxes of h=0.3m and global meshes of h=0.7m at the different heights of the big-amplitude solitary wave analysis.

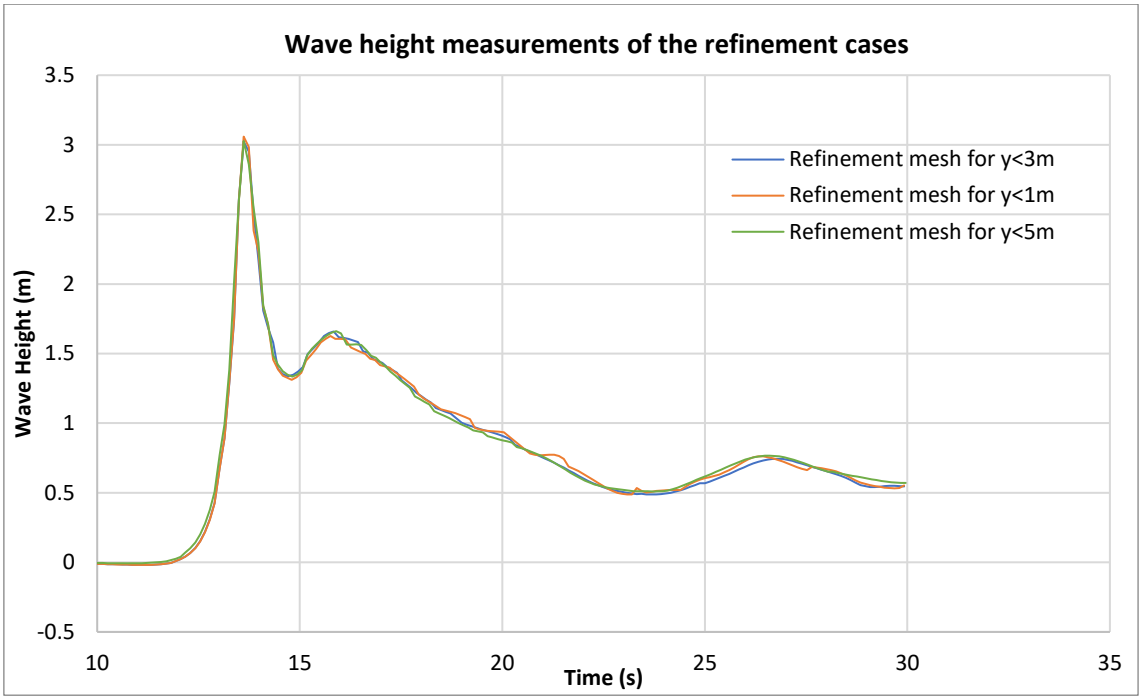

Table 12 and Figure 64 show the same analysis procedure of refinement analysis but with a denser general mesh of (*h=0.5m*). Comparing the results (Figure 65), it can be seen that outputs are sufficiently similar to assume a convergence of the ones with the general mesh of (*h=0.7m*). Then, the convergence of the system is proved and we can deduce that refinement at height (*y=1 m*) is enough to improve the analysis accuracy.

Table 12. Computational time – Mesh size with a refinement of (h=0.3m) and uniform mesh of (h=0.5m) dependence of the big-amplitude solitary wave analysis.

Mesh type	Number of printed resutls	Tolerance	Computation Time (s)	Number of Nodes
Uniform Mesh h=0.3m	263	0.4	1476.31	5604
Refinement y<5m	263	0.4	1427.01	5008
Refinement y<3m	257	0.4	858.56	3248
Refinement y<1m	261	0.4	697.52	2448
Uniform Mesh h=0.5m	261	0.4	606.4	2182

Figure 64. Wave height measurements of the refinement cases of refinement boxes of h=0.3m and global meshes of h=0.5m of the big-amplitude solitary wave analysis.

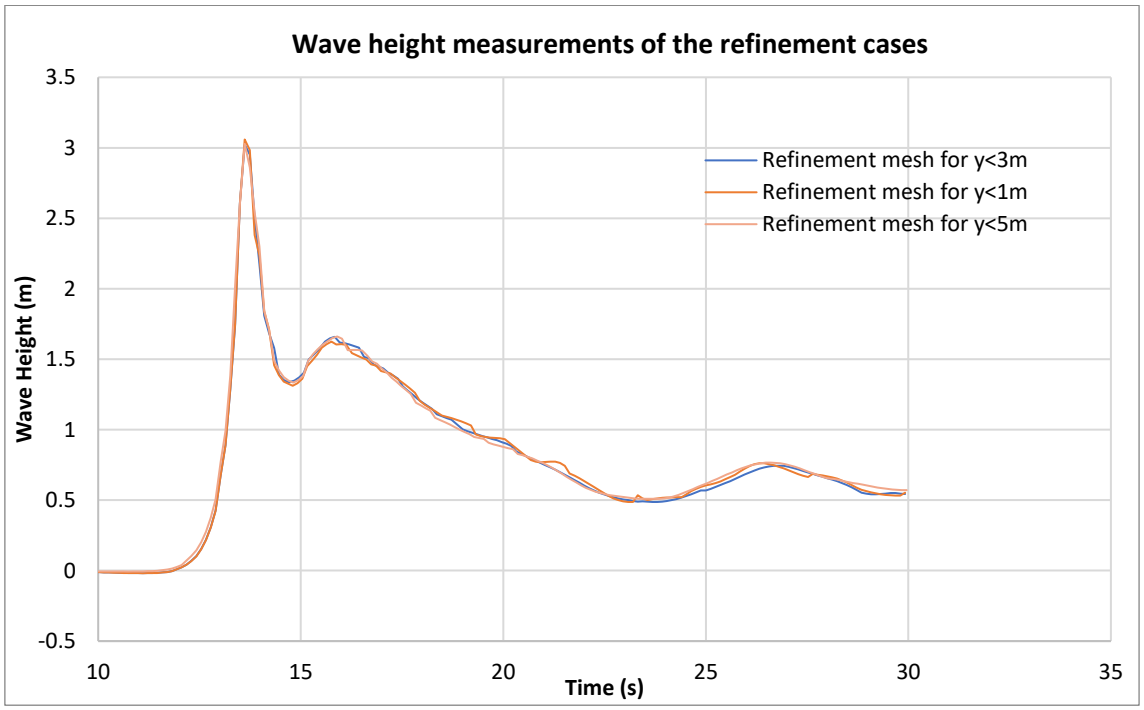

Figure 65. Wave height measurements of the refinement cases of global mesh size of h=0.7m and h=0.5m for refining box at y=3m of the big-amplitude solitary wave analysis.

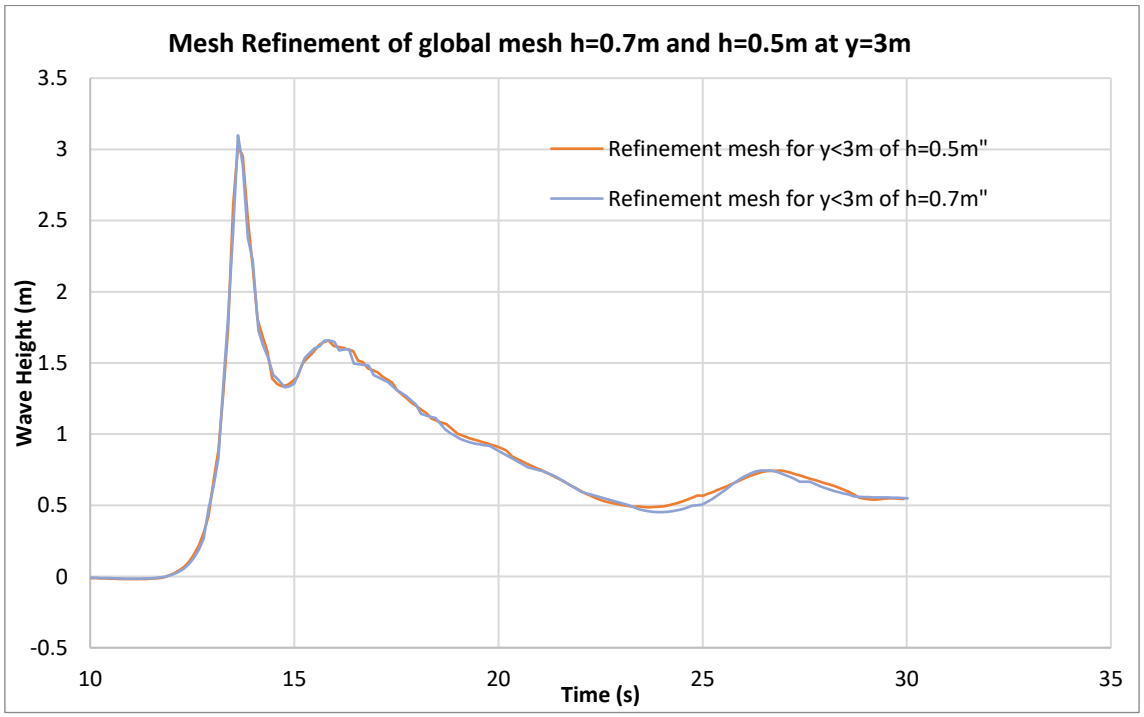

In the next analysis, we consider the box refinement technique using a bigger difference between the mesh size of the fine mesh and that of the coarse mesh. In particular, as shown in Figure 66, we conformed a mesh size of (*h=0.1m*) on the bottom height of (*y=1 m*) on a global mesh of (*h=0.5m*).

Figure 67 exposes how this mesh distribution correctly approximate the wave behaviour and Table 13 shows the computational cost of the analysis.

Figure 66. Mesh distribution for refinement box of h=0.1m at 1-metre height and global mesh of h=0.7m of the big-amplitude solitary wave analysis.

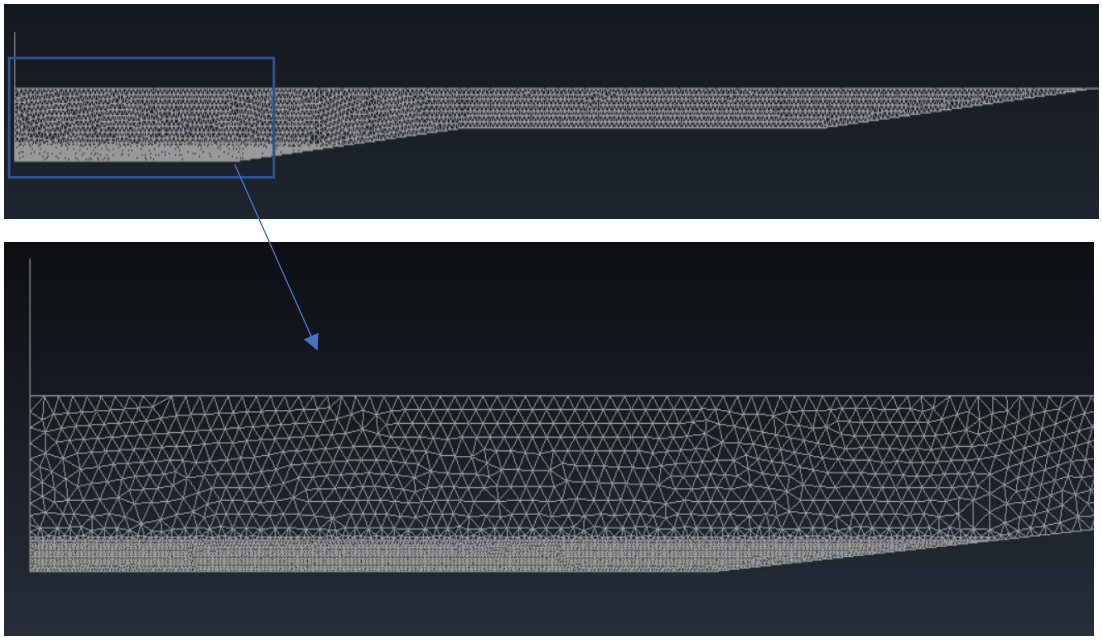

Table 13 Computational time – Mesh size with the refinement of (h=0.1m) and uniform mesh of (h=0.5) dependence of the big-amplitude solitary wave analysis.

Mesh type	Number of printed resutls	Tolerance	Computation Time (s)
Uniform Mesh h=0.5m	263	0.4	606.4
Refinement y<1m	251	0.4	1452.69
Uniform Mesh h=0.3m	256	0.4	1476.31

Figure 67. Wave height measurements of the refinement case of refinement boxes of h=0.1m and global meshes of h=0.5m. compared to the continuous meshes of h=0.3m and h=0.5m. of the big-amplitude solitary wave analysis.

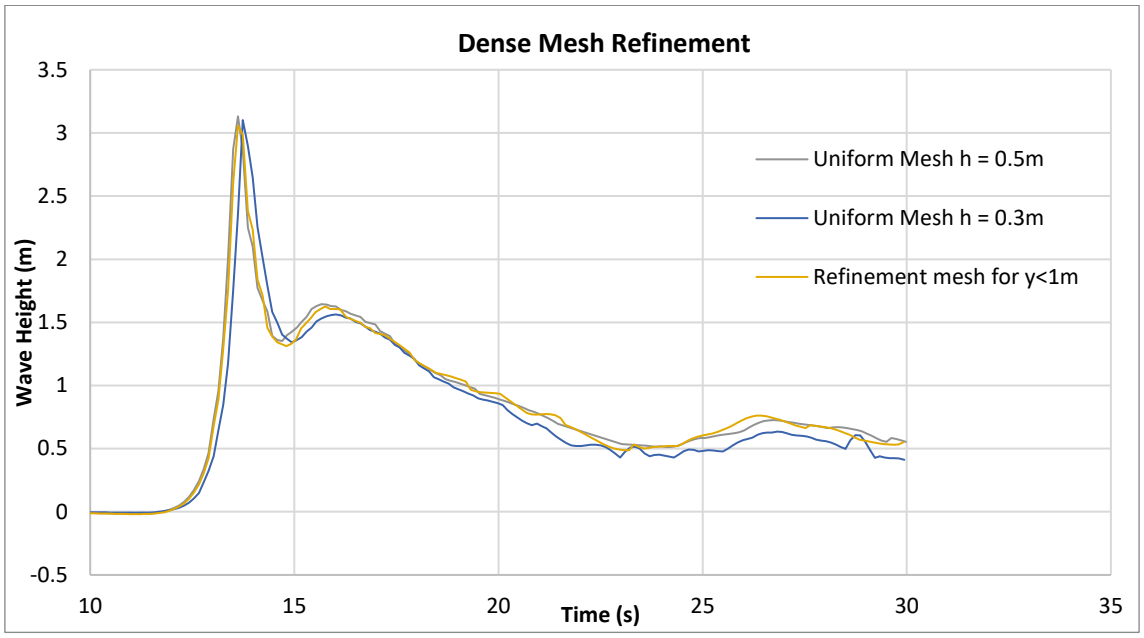

5.4. CONCLUSIONS

In this analysis, the validation of the numerical method PFEM was performed for a more complex case of breaking waves. The numerical results have shown a good agreement concerning the experimental results conducted on the Large Hydro-Geo Flume was installed at the Port and Airport Research Institute in Japan.

Nevertheless, it is important to highlight some notes regarding the issues and limits of the analysis. The wave height measurements compared to the experimental ones (Figure 55) shows how the experimental wave height measurements are slightly smaller than the numerical ones. This factor may be influenced by the infinite width of the study set on the numerical method while on the experimental one, the lateral width is limited and cause resistance to the motion. These errors increase as time goes on. This analysis was carried out for a short period and the important focus of the study was the first water height peak. However, longer studies with more complex situations could magnify the errors obtained and decrease notoriously the accuracy of the system.

Furthermore, it is necessary to highlight that the experimental analysis channel had an additional concrete wall on the beach where the waves impacted not considered on the numerical study. This is the reason why it is appropriate to only focus on the first part of the analysis before the reflected wave of the concrete wall alters the results of the experimental analysis.

As in the first analysis, the process of finding the correct tolerance for the wave height function is a complicated procedure as the results are highly sensible of the tolerance chosen. High

tolerance causes big errors in the results but short ones cause the number of outputs to decrease as no node is found inside the range, then losing the precision of the results.

As noted in the first case, to find a correct value for the mesh that achieved the convergence, it is necessary to know a good value for the time-step size, and otherwise. Then, it is needed to do iterations between both inputs to obtain correct values. It is recommendable to iterate first with a range of values for the mesh size as it is more important to have an approximate correct value for the mesh density before doing the time-step size convergence analysis than the other way around.

The process of refinement provided the opportunity of decreasing the computational cost maintaining good accuracy. However, the results show a small difference in the wave height measurements, the wave peak happens slightly before when using a mesh refinement than in the uniform mesh cases. This error may happen because of the contact between the two different meshes that can cause some irregularities on the mesh development and the cause errors in the results This factor should be studied to find alternatives or corrections that could avoid it.

6. WAVE TRAIN ANALYSIS

6.1. INTRODUCTION

During the previous analyses, the behaviour of a numerical method was studied for the case of a single wave. However, in reality, sea and coastal structures regularly suffer the impacts of a set of waves over large time spans. Then, to recreate reality in such cases, it is necessary to study also the behaviour of *wave trains*.

To do so, this study will analyse a wave train in the vicinity of a beach. The method used for the numerical study will be the PFEM as in the previous analysis. The results will be compared to the ones obtained using Eulerian FEM software previously conducted and validated (Ryzhakov & Oñate, 2017).

6.2. PROBLEM GEOMETRY

The geometry of the channel consists of a long beach with a small slope. It has a length of 1000 meters and a maximum height of 20 meters at the wave paddle., located at the right end of the channel (Figure 70).

There is a set of four wave gauges that measure the height of the created waves. They are located at 500, 550, 700 and 900 metres from the shoreline.

The paddle is a piston that causes the wave to follow a specific movement in time (Equation 10 and Equation 11) where the maximum velocity of the paddle was set to 1.6 m/s and the period to 10 seconds. The functions follow a sinusoidal movement of the wave paddle that is supposed to create identical waves (Figure 68 and Figure 69). This paddle is expected to create waves with a height of around 5 meters.

Equation 10. Paddle velocity in time of the wave train problem

$$V = -VMax * Sin\left(\frac{2\pi * t}{T}\right) = \ V = -1{,}6 * Sin(\frac{2\pi * t}{10})$$

Equation 11 Paddle movement in time of the wave train problem

$$X = \frac{2\pi}{T} VMax * Cos\left(\frac{2\pi * t}{T}\right) = X = \frac{10}{2\pi} 1{,}6 * Cos\left(\frac{2\pi * t}{10}\right) - \frac{10}{2\pi} 1{,}6$$

Figure 68. Sinusoidal paddle movement in time of the wave train problem

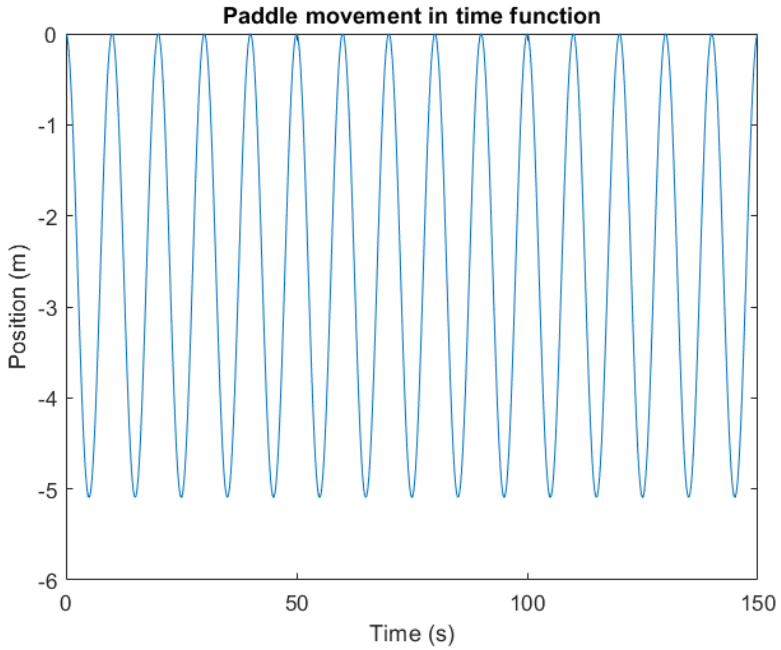

Figure 69. Sinusoidal paddle velocity in time of the wave train problem

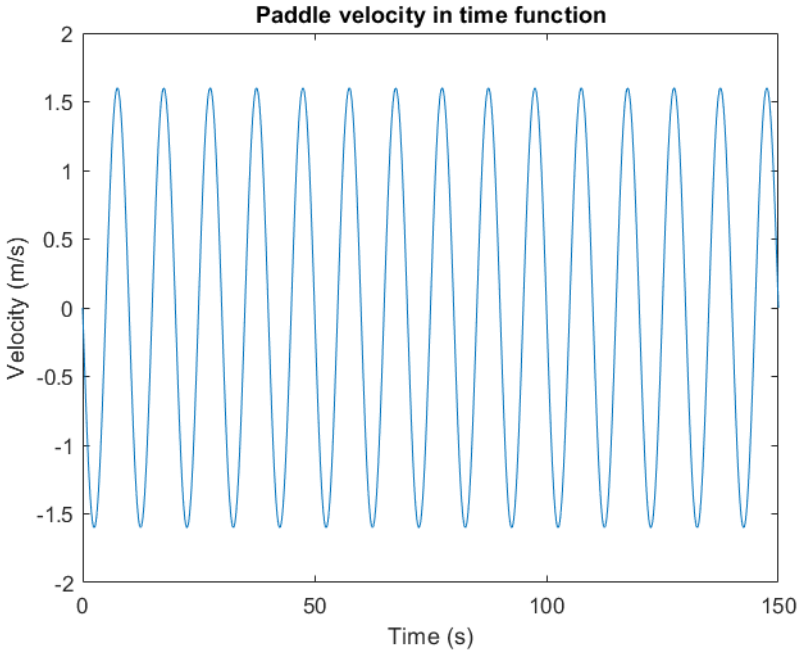

This paddle motion will be applied during the entire simulation of the problem, which is set to last 150 seconds. This time measure should be sufficiently large to study a representative set of the nearly identical waves.

To recreate this experiment in a numerical method, as in the previous studies, Kratos software is used with the support of GID pre-processing and post-processing. The geometry of the problem is created in GID software (Figure 70). The fluid and boundaries properties are defined identically as on the previous analysis of the solitary wave propagation.

Figure 70. Wave train problem geometry on GID software.

For this case, there are some features to be modified from the original geometry to make the PFEM analysis work. First of all, the movement of the paddle passes through the channel floor with a non-zero slope. This can create problems for the re-meshing mechanism of PFEM. Then, the bottom slope is set to terminate 10 metres away from the paddle, facilitating its horizontal motion (Figure 71). With this modification, the wave paddle never intersects the sea-bed.

Figure 71. Slope modification on GID software of the wave train analysis.

Secondly, to avoid water "flowing out" at the boundaries (*leakage*), the wave paddle is set to stop slightly above the sea bed, but with a lower distance than the ones of the mesh size of the finest study (*h=0.4 m*). For this case, this distance is set to 0.2 metres (Figure 72). This is needed to be applied because otherwise the movement of the paddle "grabs" a node of the wall creating an empty space on the floor wall where the water can flow out.

Figure 72. Geometry of the wave paddle – floor link on GID software of the wave train analysis.

The FEM study was conducted with a specific mesh refinement box along the channel of (*h=0.325m*). However due to the high computational cost, for the PFEM study, the mesh is kept homogenous for the value of (*h=0.4m*). On the other hand, the time-step size is set to (ΔS=0.005s)

Figure 73. Wave train analysis mesh distribution on GID.

To obtain numerical results comparable with the ones obtained using Eulerian FEM, the same additional function is added to the Kratos scripts to measure the wave height at the four different wave gauges, setting its inputs to the channel geometry.

6.3. NUMERICAL RESULTS

To understand the behaviour of the wave, GID post-processor software plotting is used to analyse the global wave movement and acquire a graphic representation of the wave amplitude, pressure and velocity distribution at a representative time-step of the problem using FEM and PFEM. Figure 74 and Figure 75 shows the PFEM snapshots of the velocity and pressure distribution respectively at a specific time-step. Figure 76 and Figure 77 shows the Eulerian FEM snapshots of the velocity and pressure distribution this same time-step.

The snapshots display a good wave train development. The behaviour of the wave on both numerical methods, PFEM and Eulerian FEM are similar. It is important to notice that the pressure positive values are referred to traction of PFEM while on Eulerian FEM they correspond to compression. Moreover, while PFEM only displays data on the fluid body, the computation

mechanism of the Eulerian FEM computes the parameters at all the nodes inside the study boundaries, then, it also displays the velocity and pressure values of the parts outside the fluid domain.

The wave propagation creates the velocity peaks to be situated on the wave crests, increasing as the closer they are to the beach shoreline. The pressure follows a hydrostatic distribution increasing when closer to the beach shoreline

Figure 74. Velocity distribution of the wave train analysis on PFEM

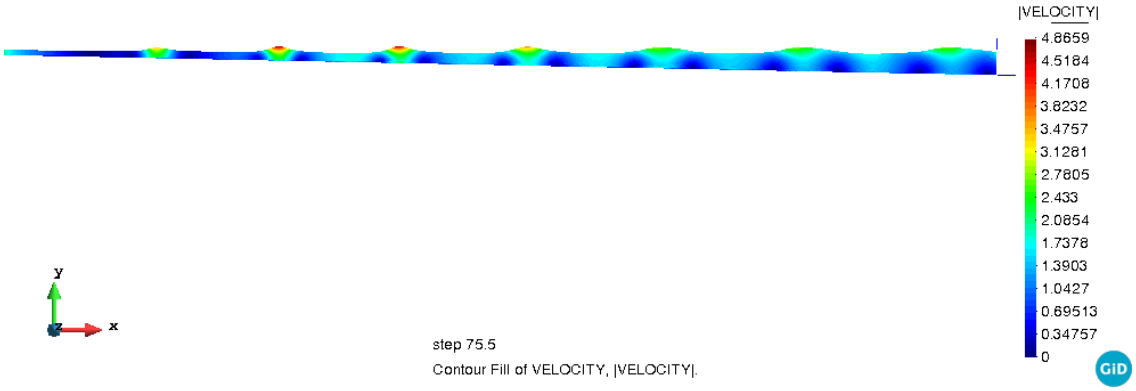

Figure 75. Pressure distribution of the wave train analysis on PFEM

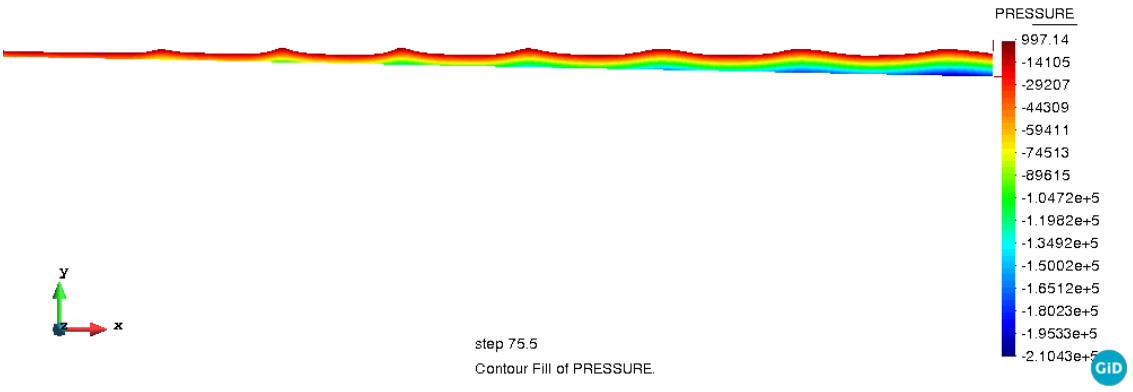

Figure 76. Velocity distribution of the wave train analysis on Eulerian FEM

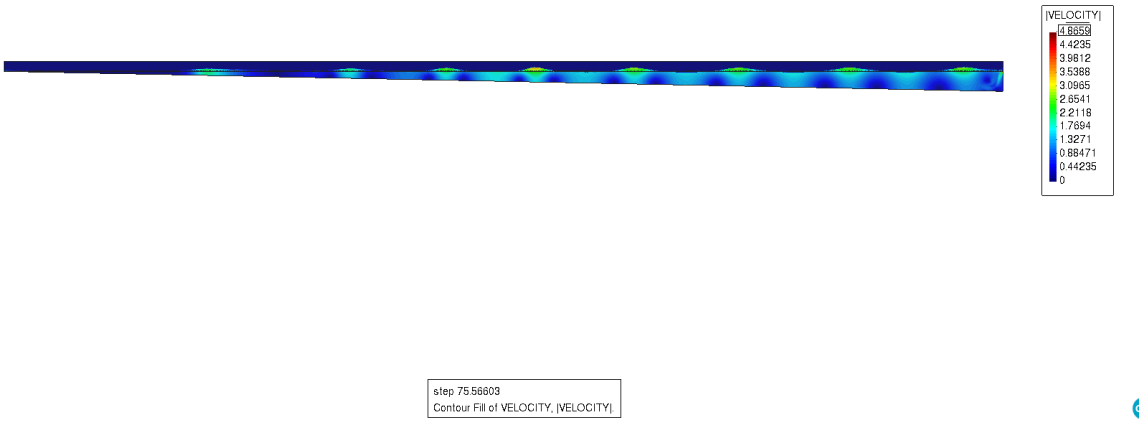

Figure 77. Pressure distribution of the wave train analysis on Eulerian FEM

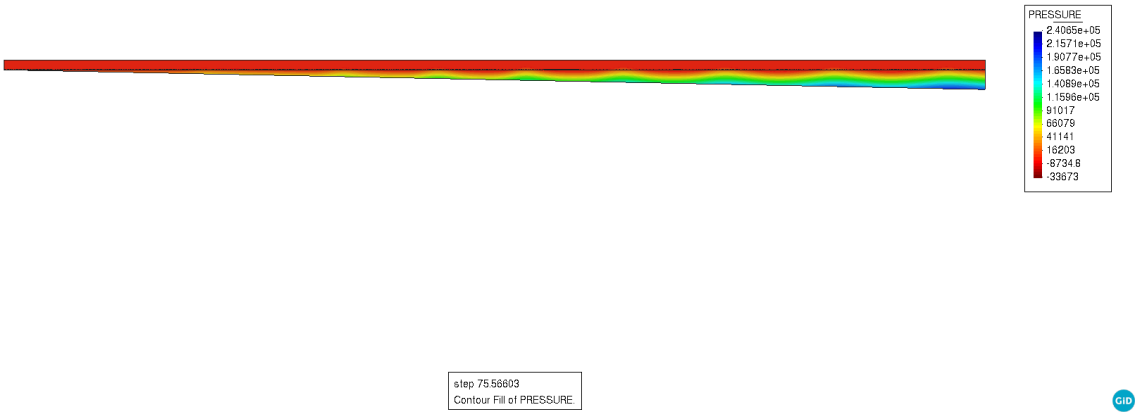

6.3.1. FEM SLIP AND FEM NO-SLIP BOUNDARY CONDITIONS COMPARISON

There are two possibilities of modelling the boundary effects between fluid and solid walls that can be applied in a numerical method, namely, slip and no-slip. The slip boundary condition suggests that water that touches the walls flows through it freely, without any friction in the longitudinal direction. The no-slip boundary condition, on the other hand, suggests that the mesh node in touch with the wall remains immobile during all the analysis.

In reality, there is friction between the walls and the fluid on them that cause the very first particle in touch with the wall is always immobile, so it would mean that it has a no-slip behaviour. However, this occurs in the direct proximity of the wall, a very small distance much lower than the employed mesh resolution, so to use this method accurately, the mesh size would have to be of a sub-millimetric scale, which is practically impossible. Then, applying a no-slip method exaggerates this friction effect reducing the velocity of the wave while applying a slip method also cause errors regarding the absence of friction on the system. This factor has a particular impact on the places close to the wall.

As explained in the theoretical framework, in PFEM it is not convenient to apply a slip method on the boundary walls of the system. That is because the nodes of the wall are also nodes of the water system on the edge, so they have to remain still to avoid water passing through it and to keep the outer boundaries constant. So, generically, it works with a no-slip method.

On the other hand, the static behaviour of the Eulerian FEM mesh allows the numerical method to apply both types of boundary conditions, slip and no-slip. The analyses performed using Eulerian FEM allow to do a comparison of both methods for the cases studied on the different points where the wave height was measured (Figure 78, Figure 79, Figure 80 and Figure 81).

Figure 78. FEM no-slip – FEM slip comparison at 500 metres from shoreline of the wave train analysis

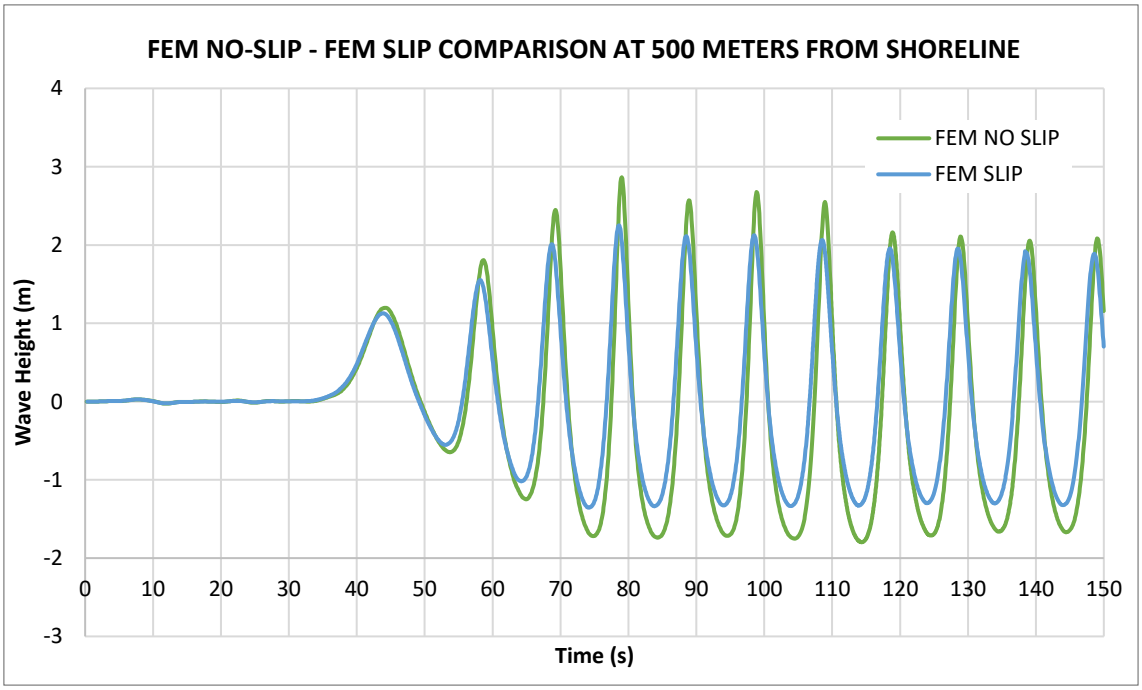

Figure 79. FEM no-slip – FEM slip comparison at 550 metres from shoreline of the wave train analysis

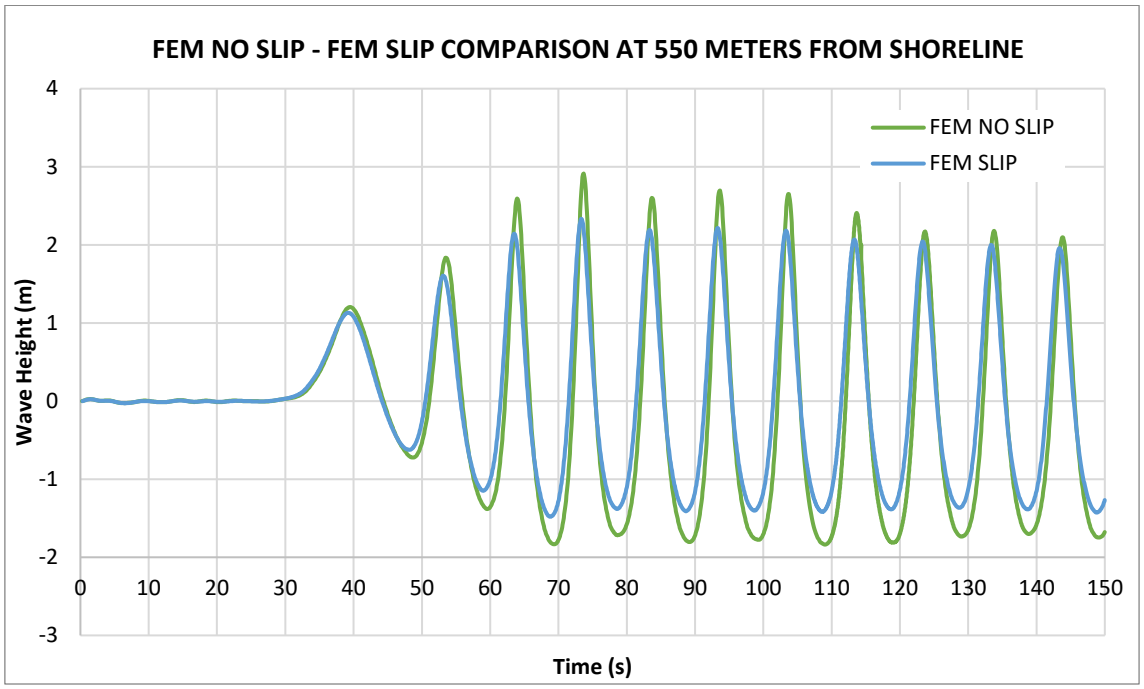

Figure 80. FEM no-slip – FEM slip comparison at 700 metres from shoreline of the wave train analysis

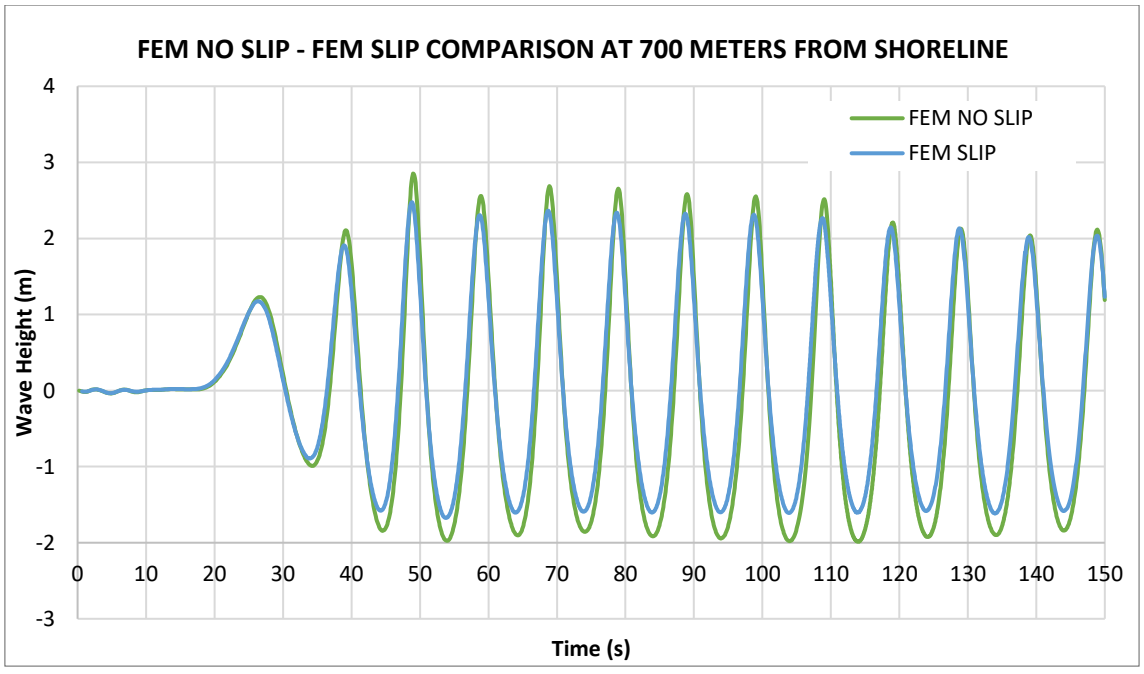

Figure 81. FEM no-slip – FEM slip comparison at 900 metres from shoreline of the wave train analysis

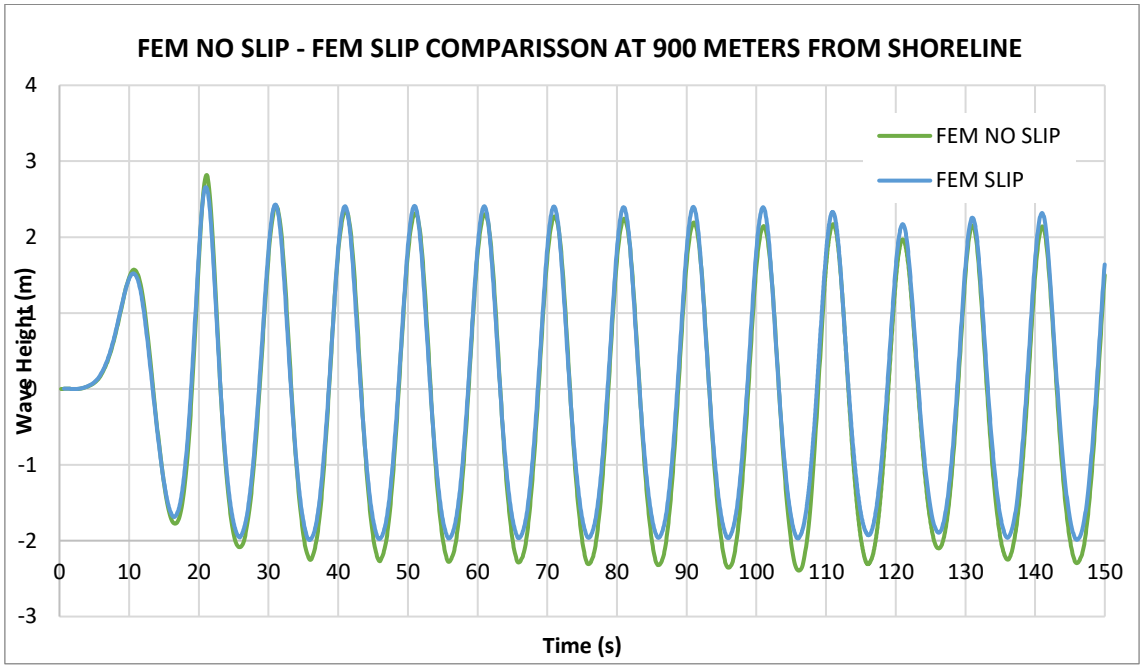

The graphical results (Figure 78, Figure 79, Figure 80 and Figure 81) show two important factors to be pointed out. First, it is noticeable how the results of the FEM no-slip method experiment bigger wave amplitudes than the ones of the FEM slip. Secondly, the difference increases as the waves move away from the wave paddle, so errors are accumulated as waves propagate. This can be explained by the fact that the water depth becomes smaller as the wave approaches the shore and then this boundary effect has a greater effect on the wave propagation.

6.3.2. PFEM AND FEM NO-SLIP COMPARISON

As explained, the PFEM analysis conducted during this study, like the ones before, follows a no-slip boundary condition as it is not straightforward to use slip boundaries on PFEM. The results obtained are compared to the FEM ones, both the no-slip and slip on the different wave height measurement points considered (Figure 82, Figure 83, Figure 84 and Figure 85).

Figure 82. PFEM – FEM comparison of the wave train analysis at 500 metres from beach shoreline.

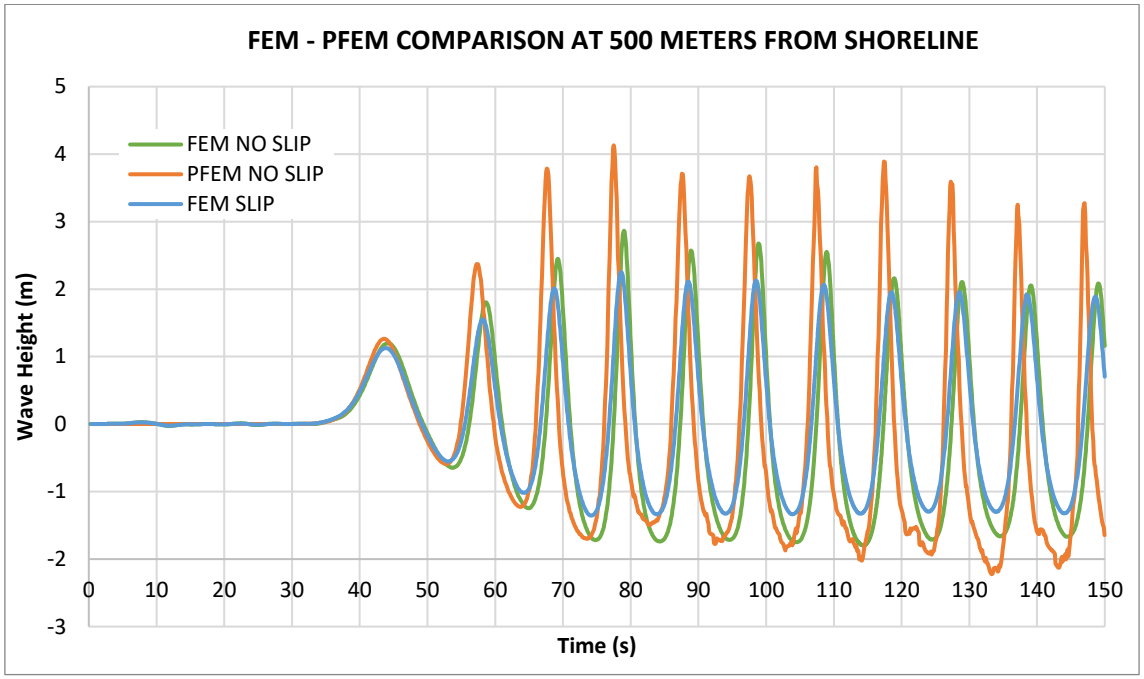

Figure 83. PFEM – FEM comparison of the wave train analysis at 550 metres from beach shoreline.

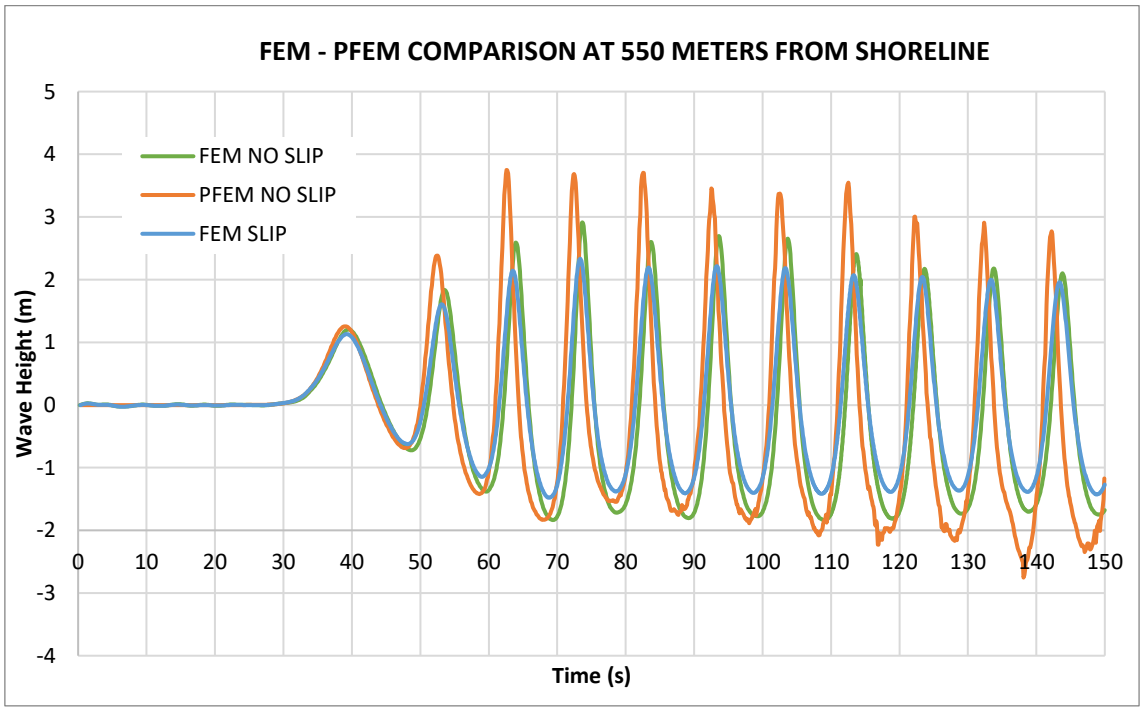

Figure 84. PFEM – FEM comparison of the wave train analysis at 700 metres from beach shoreline.

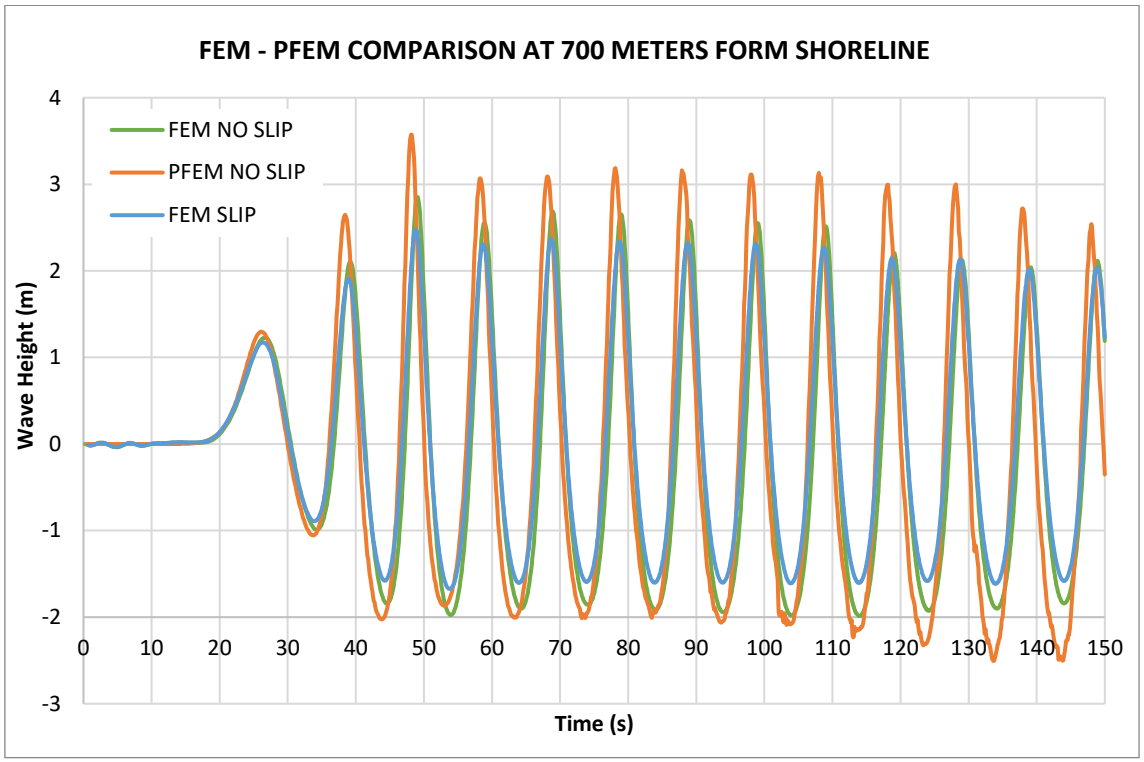

Figure 85. PFEM – FEM comparison of the wave train analysis at 900 metres from beach shoreline.

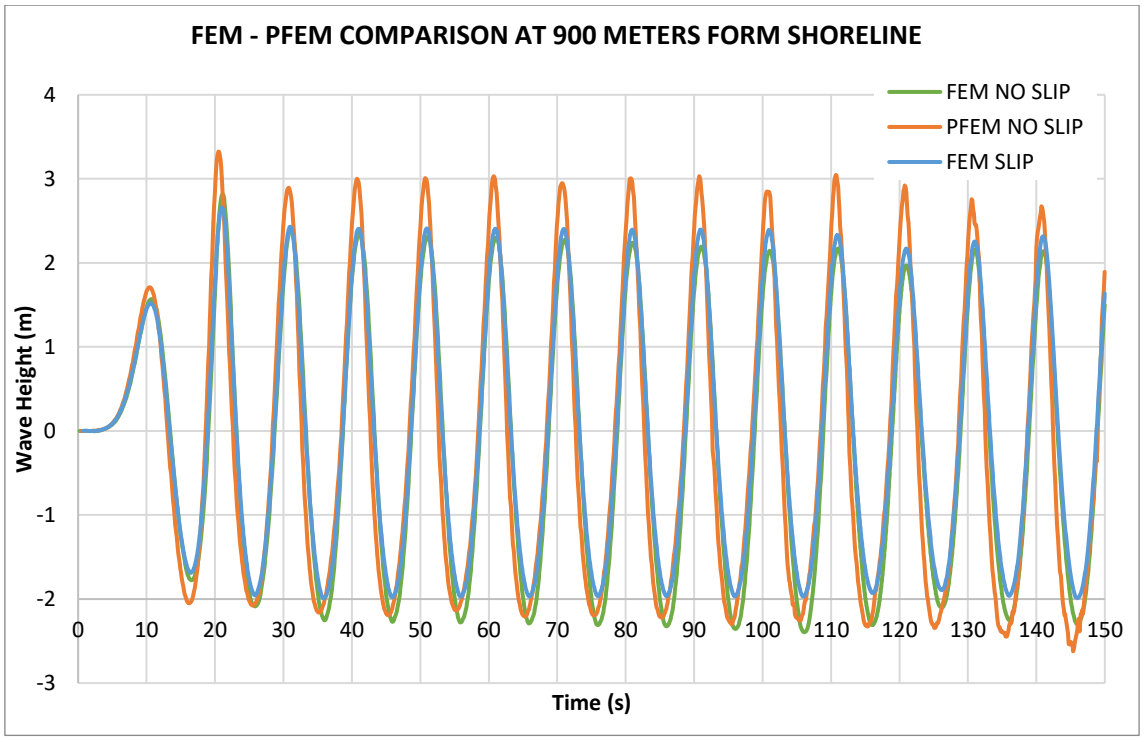

The results show a visible difference (10-20%) regarding wave height between the Eulerian FEM and PFEM results independently of the slip or no-slip study method of Eulerian FEM. The PFEM results have higher wave height measurements than on the Eulerian FEM. Precisely, this difference is bigger on the maximum wave measurements while on the minimum measurements the results of PFEM and Eulerian FEM are more similar. The difference between PFEM and Eulerian FEM becomes more pronounced as the wave approaches the shore. The observed difference may be caused by a different numerical dissipation and require further study.

As the difference between PFEM and FEM is bigger than the ones of FEM slip and FEM no-slip, it is not appropriate to abstract conclusions of the comparison between PFEM no-slip and FEM no-slip or FEM slip independently.

6.3.3. MESH SIZE CONVERGENCE STUDY

The mesh applied for the PFEM study was set to be similar to the Eulerian FEM one. Nevertheless, PFEM and Eulerian FEM convergence mesh sizes do not always coincide. Then, it is appropriate to do a homogenous mesh convergence study to see if the mesh used for the previous study was correct.

The different homogenous meshes to be used for the analysis are described in Table 14 and its time-step is set to be constant to a value of ($\Delta T=0.005\ s$). The time of analysis is set to last 150 seconds.

To do this comparison the wave height measurements of the function will be used. As in the previous analyses, the outputs of the functions for different mesh densities are highly dependent on the tolerance of the function. Then, the cases use different tolerance values to have a representative number of printed results with an appropriate accuracy (Table 14).

Table 14. Cases studied for the mesh size convergence of the wave train analysis.

Cases	Mesh size (h)	Function Tolerance	Number of Nodes
Case 1	0.4m	0.4m	74869
Case 2	0.5m	0.4m	48173
Case 3	0.75m	0.4m	21662
Case 4	1m	0.5m	12543

After computing all the cases it is seen that as shown in Table 15, there is a high difference in the computational time needed to perform the simulation for the different mesh resolutions, its relation, as in the previous studies, is exponential (Figure 86), so it is crucial to choose an appropriate time-step to acquire good results with a viable computational cost. The range of tolerances selected for the function gives approximately the same number of printed results so

the results have approximately the same accuracy regarding this factor. The big dimensions of the considered computational domain and time of study of this analysis make the computational cost very large, of the order of 4 days on the denser mesh.

Table 15. Computational time – Mesh size dependence of the wave train analysis.

Mesh size h (m)	Number of printed results	Computation Time (s)	Number of Nodes
0.4	1430	363354.29	74869
0.5	1417	225399.89	48173
0.75	1388	69913.86	21662
1	1409	49205.67	12543

Figure 86. Mesh size – Computational time costs graphical exponential relationship of the wave train analysis.

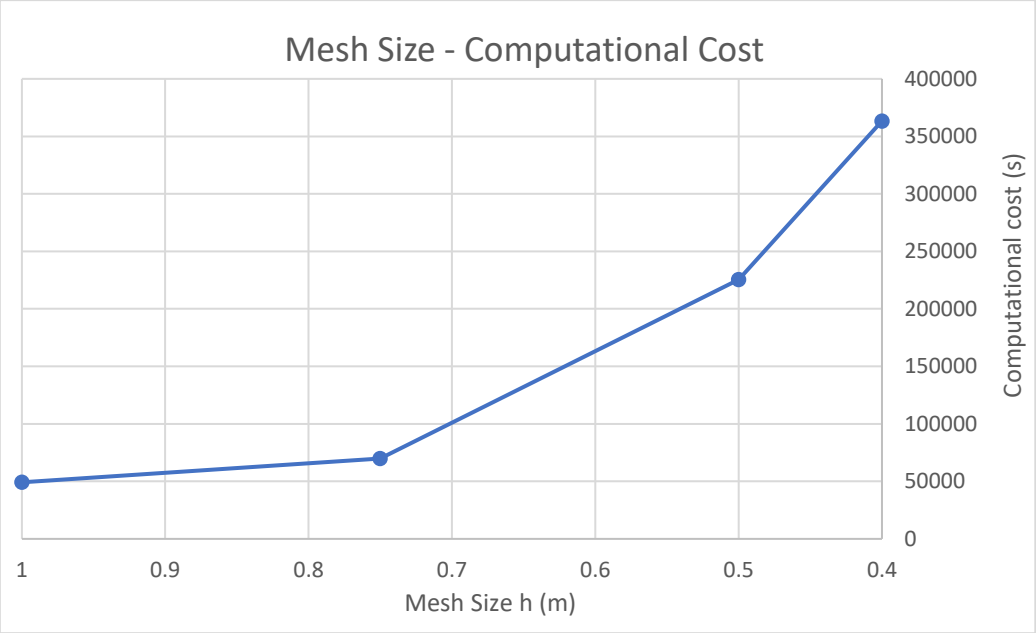

The different cases demonstrated that the convergence is reached early, on the first cases (Figure 87, Figure 88,Figure 89 and Figure 90). However, it can be seen how errors on the results increase notoriously with time and with distance from the paddle, especially on the wave trough. These irregularities are present but smaller on denser meshes. For this reason, a mesh of (*h=0.5m*), could be considered as the adequate one for this analysis.

Figure 87.Mesh density convergence graphic of the wave train analysis at 500 metres from beach shoreline.

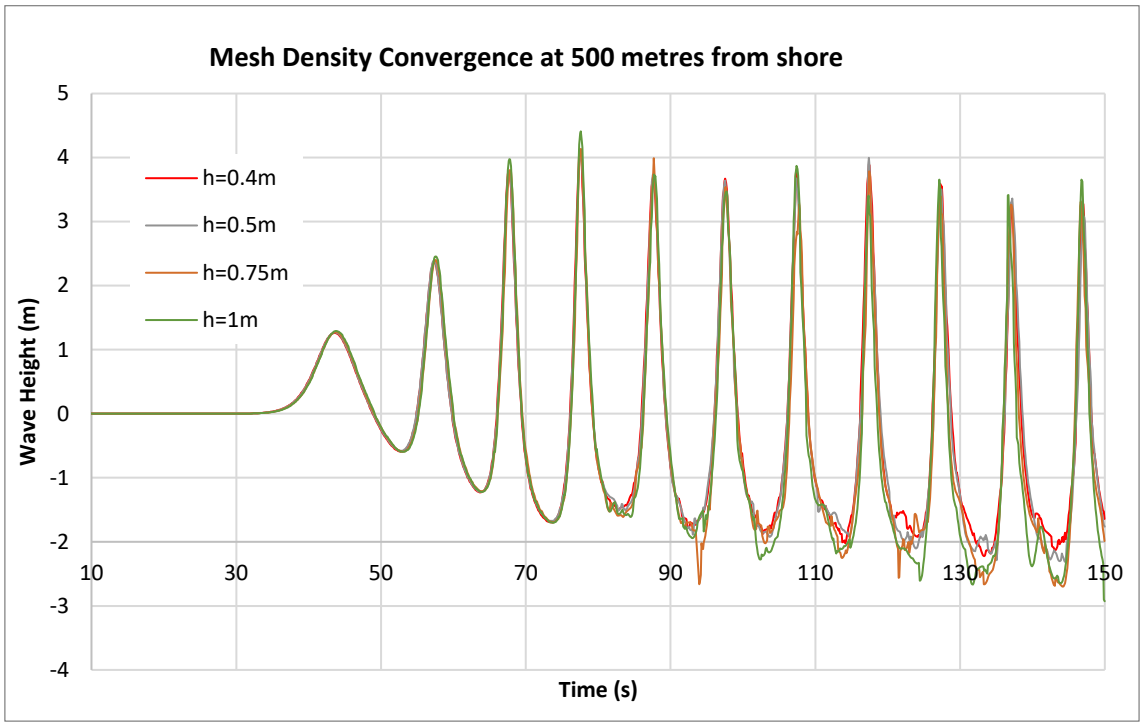

Figure 88. Mesh density convergence graphic of the wave train analysis at 550 metres from beach shoreline

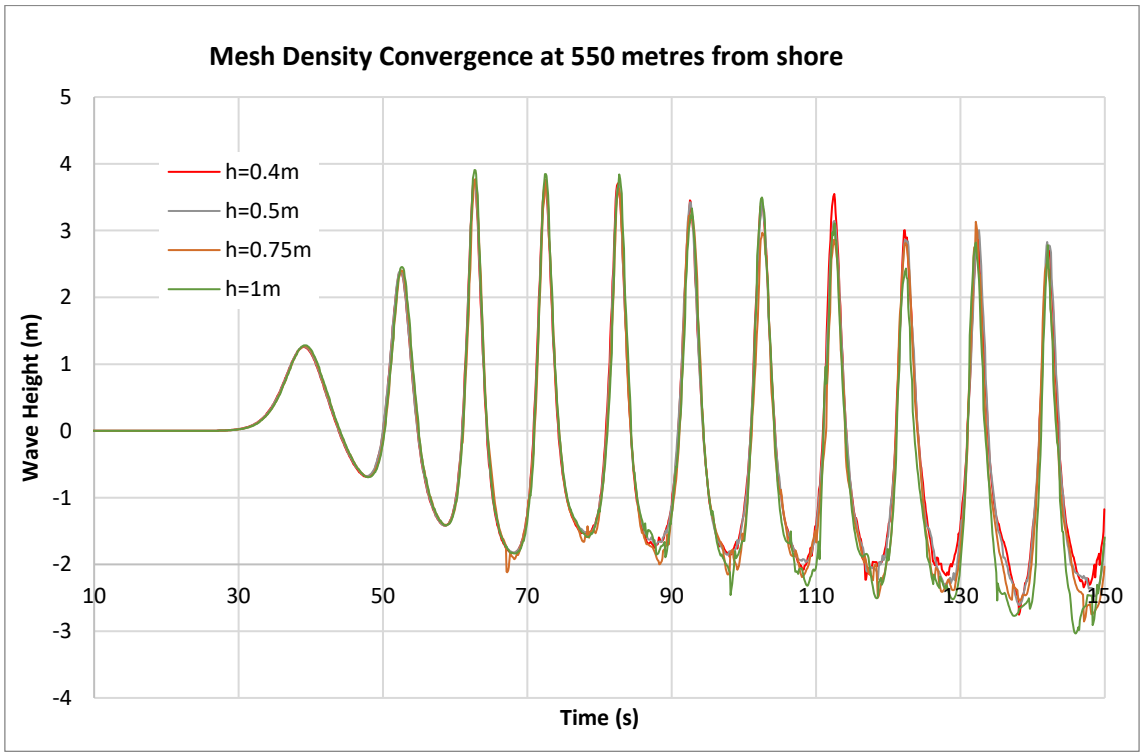

Figure 89. Mesh density convergence graphic of the wave train analysis at 700 metres from beach shoreline

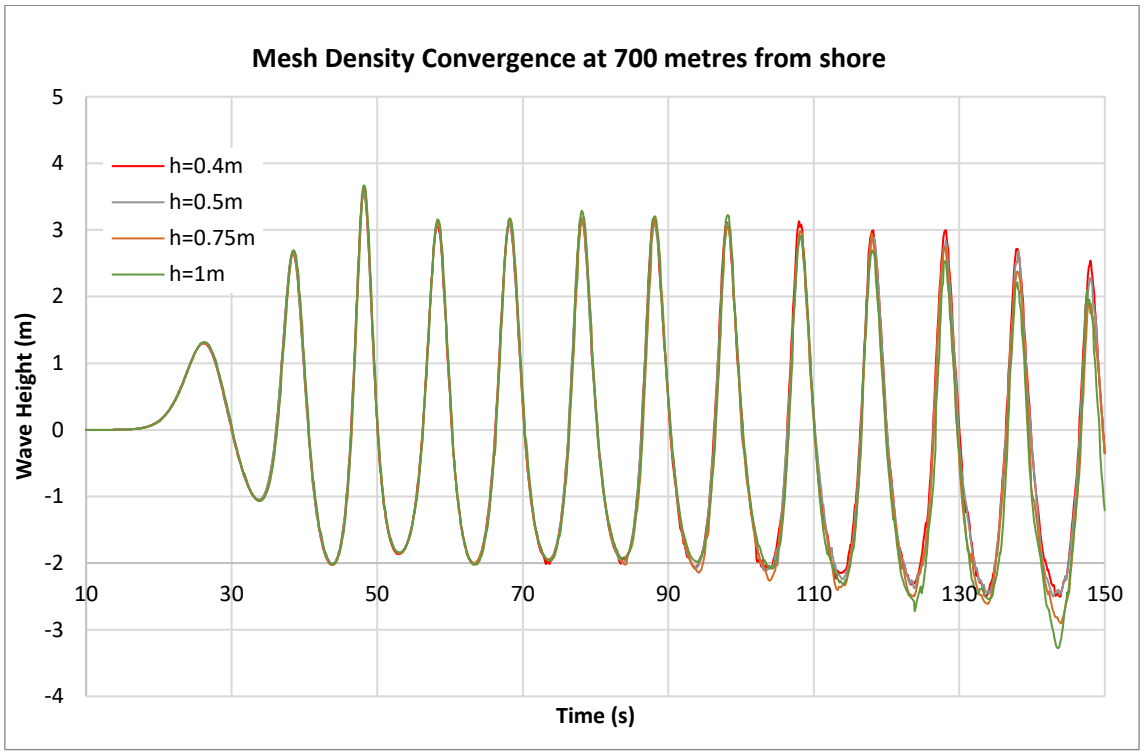

Figure 90. Mesh density convergence graphic of the wave train analysis at 900 metres from beach shoreline

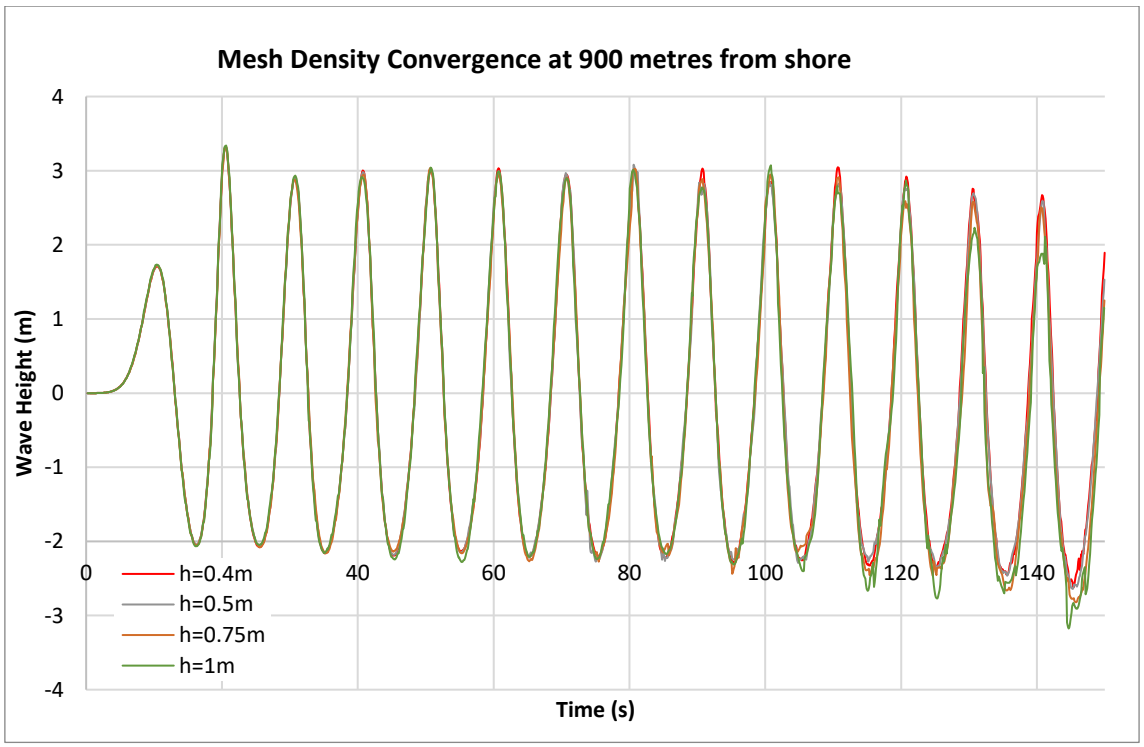

It is important to note how the wave height decrease with time in the PFEM simulation. This tendency appears due to the spurious "leakage" of water outside of the problem boundaries. The water flows out of the system after passing the beach shore, when, theoretically it should return while losing its kinetical energy. Then, as the system loses water the SWL decreases as the study goes on. Another reason for the loss of water on the system could be the re-meshing mechanism on PFEM as the process substitution of elements can cause water to disappear.

It is also noticeable how the wave amplitude increases the closer it is to the shoreline. This may be attributed to the shoaling effect which causes the wave amplitude of a wave to increase as the water depth decreases. However, this issue requires further study to be able to make adequate conclusions.

6.3.4. REFINEMENT STUDY

Due to the strong distortion of the water free-surface on the paddle location, a case is studied where the location of the refinement box is placed on the first 100 metres from the paddle.

To choose the meshes to be used, the results from the mesh convergence study are looked at. Then an additional case is run for a uniform mesh of (*h=0.75m*) and a refined mesh of (*h=0.4m*) with the properties described in Table 16.

Table 16. Properties of the refinement case of the wave train analysis

DATA	
Mesh Size Global zone (h)	0.75
Mesh Size Refined Zone (h)	0.4
Wave Height Measurement	500
Time step size (ΔT)	0.005
Compuational cost (s)	161272.46
Number of printed elements PFEM	1336
Number of Nodes	32513

The case computed showed good performance of results with an adequate computational cost for this specific problem compared with the cases of the homogenous study (Table 14). The accuracy of the results is described in Figure 91, Figure 92, Figure 93 and Figure 94. They show how the refinement study has fewer irregularities and the computational cost is around 70% of the homogenous mesh one (*h=0.5m*). Then, this option would be more optimum for this case. It is also important to notice how the refinement results have higher values of wave heights in general, especially on the wave trough. However, overall, one can conclude that the differences are negligible.

Figure 91. Mesh refinement study of the wave train analysis at 500 metres from shore.

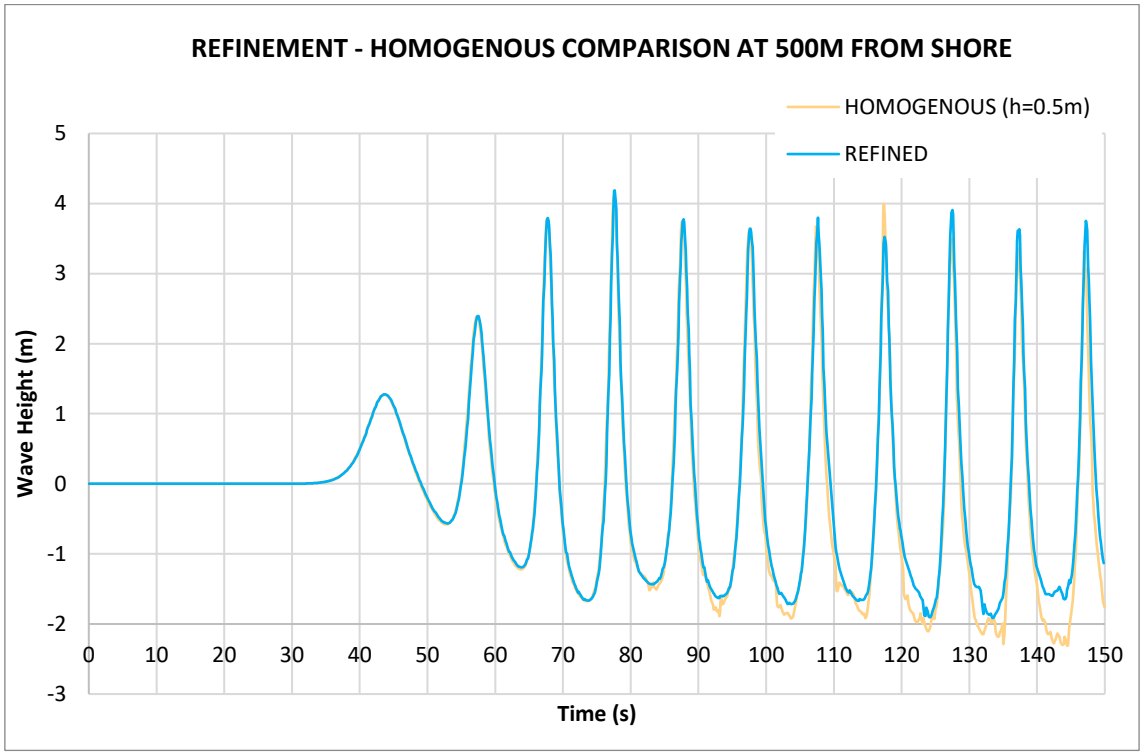

Figure 92. Mesh refinement study of the wave train analysis at 550 metres from shore.

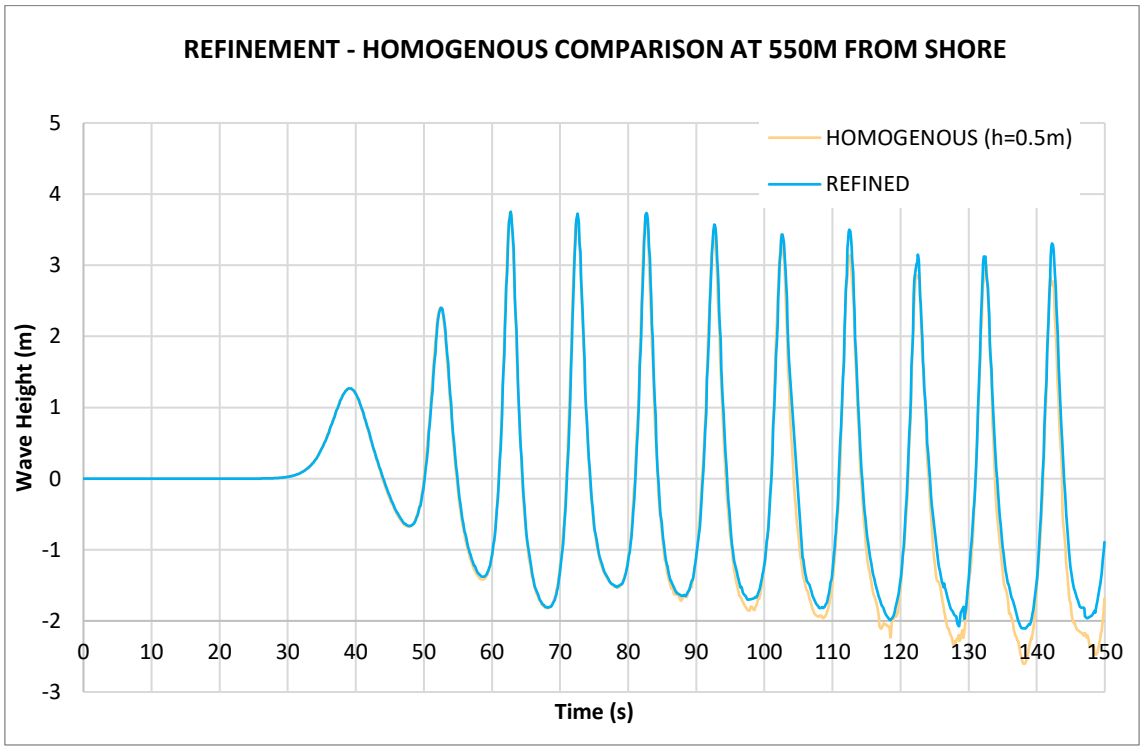

Figure 93. Mesh refinement study of the wave train analysis at 700 metres from shore.

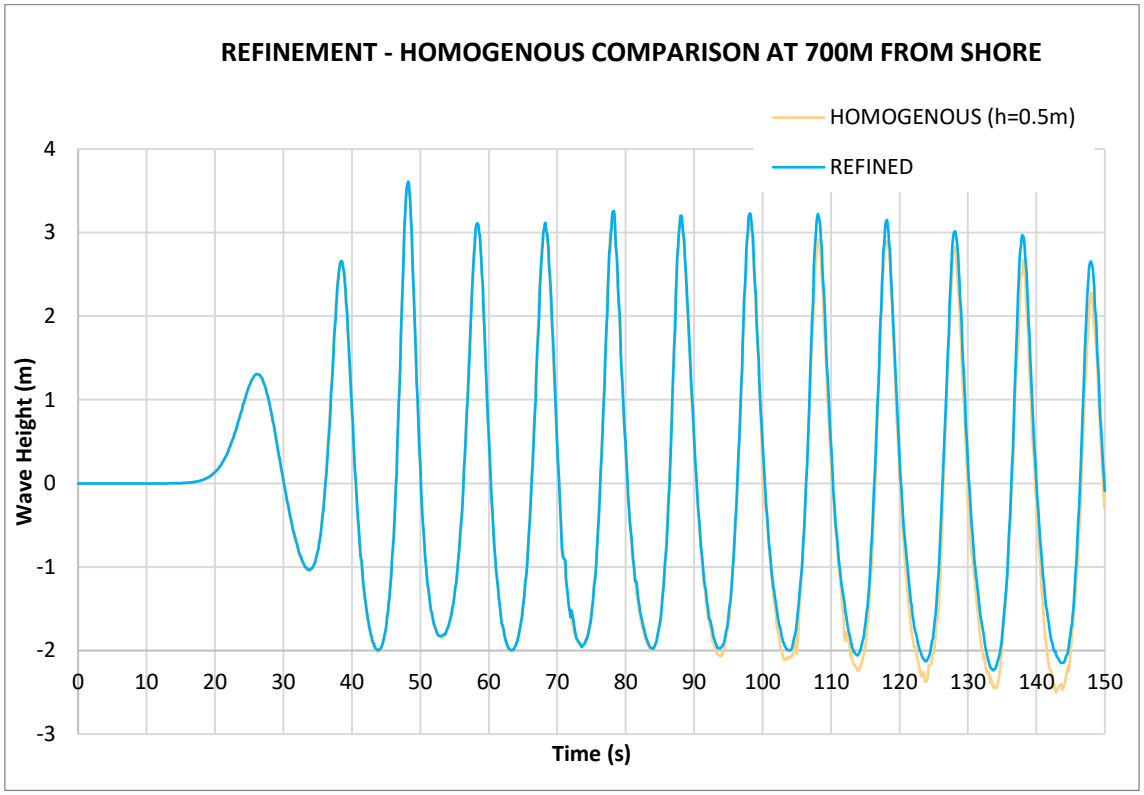

Figure 94. Mesh refinement study of the wave train analysis at 900 metres from shore.

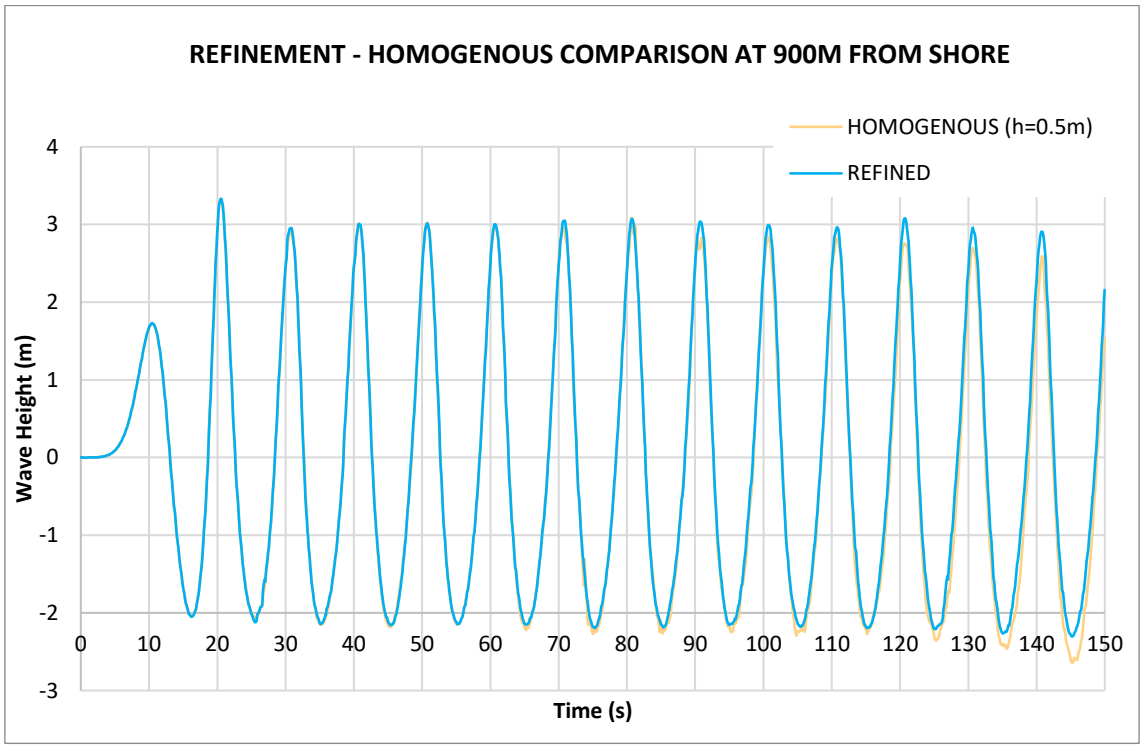

6.4. CONCLUSIONS

The study validated PFEM for the cases of wave trains and overall ¡ the results were physically meaningful. Nevertheless, they presented some imperfections. PFEM system has important geometry conditions and limitations that need to be taken care of to run the problem correctly as explained while defining the geometry of the problem. This may cause a difference in geometry with the Eulerian FEM analysis reducing the precision of the comparison. However, for this case, the big dimensions of the study and the small mesh size allow to reduce this error notoriously, so the results may be considered accurate regarding this factor.

The Eulerian FEM slip and Eulerian FEM no-slip study showed an originally unforeseen behaviour in its results, as the wave height of no-slip boundary conditions is bigger than the ones of the slip method. One hypothesis that could explain this behaviour is a node elevation creation on the no-slip method. In this method, the linkage of the wall with the first node in contact may cause it to get the water body elevated then causing an overall increase in the wave amplitude of the system as a consequence of the depth decrease. Nevertheless, the difference between these two boundary condition types is more visible in the case where the wave propagates in shallow waters as these boundary effects are more considerable near the walls of the boundaries. That is why in the case of studies with structures like breakwater in contact with the waves the importance of the boundary condition employed is higher.

Regarding the comparison between the PFEM and Eulerian FEM methods: the PFEM results have considerably higher wave height measurements than on the FEM, especially on the maximums. Then, as the difference between PFEM and FEM is bigger than the ones of FEM slip and FEM no-slip, it is not appropriate to abstract conclusions of the comparison between PFEM no-slip and FEM no-slip or FEM slip independently.

The mesh density convergence study was satisfactory and proved that the mesh used to imitate the FEM study was not optimum for the case. However, it clearly shows the loss of accuracy of the numerical method on long analyses due to the accumulation of results and the loss of optimum mesh regeneration. The decrease of wave height due to the loss of water mass on the numerical channel also incentive the creation of these errors on the system meshes. An option to avoid this imperfection to happen could be to increase the mesh density although it is not optimum to do so as the computational cost of the problem would exponentially increase. Then, another option could be to modify the system geometry to avoid water flowing out of the domain by introducing some slope on a long beach shore or by introducing water to the system at the same rate it flows out.

The refinement study was optimum for this case as increased the accuracy of the problem with lower computational costs. It would be interesting to analyse the system with different refinement structures to know if there may be a better option. The refinement performed showed lower values of wave height measurement, especially on the wave trough. The reason for this to happen is not defined and could be several, within them the possibility of it to be an implicit error of the refinement process as noted on the big-amplitude solitary wave analysis.

7. WAVE TRAIN BREAKWATER ANALYSIS

7.1. INTRODUCTION

The previous analysis conducted numerical methods for waves on beaches. An interesting addition to the analyses would be to look at how the system reacts to the contact of waves with a solid structure. To do so, a study is set to analyse the same beach geometry as the one used in the wave train analysis but with the addition of a breakwater that allows waves overtopping. This analysis supposes a much more complex situation for the numerical method since the introduced obstacle leads to wave breaking.

The method used for the numerical study will be the PFEM as in the previous analysis. The results will be compared to the ones of an Eulerian FEM analysis already conducted and validated with the appropriate numerical results.

7.2. PROBLEM GEOMETRY

The geometry of the channel is identical to the one of the wave train analysis (*Section 6*) with the addition of the breakwater. It consists of a long beach with a small slope. It has a length of 1000 metres and a maximum height of 20 metres on the wave paddle., located at the end of the channel. The breakwater is located 620 metres from the beach shoreline and allows no permeability (Figure 95).

Figure 95. Breakwater analysis geometry on GID software.

There is a set of four wave gauges that measure the height of the created waves on 500, 550, 700 and 900 metres from the shoreline.

The settings used are equivalent to the ones of the wave train analysis (*Section 6*).

As for the mesh, two different resolutions are analysed. The first one with a homogenous mesh o (*h=0.5m*) and the second with a homogenous mesh of (*h=0.75m*) and a refinement box between 550 and 700 metres from the shoreline where the mesh is of (*h=0.4m*).

7.3. NUMERICAL RESULTS

The wave propagation and impact with the breakwater is displayed by GID software plotting Snapshots of the wave amplitude, pressure and velocity distribution at representative time steps are obtained. Figure 96 and Figure 97 shows the velocity and pressure distribution of the wave train before it impacts the breakwater. Figure 98 and Figure 99 shows the velocity and pressure distribution of the wave train after it does several impacts with the breakwater. The snapshots display how the velocity peaks on the wave crests and the hydrostatic pressure distribution. It is notorious how the wave impact with the breakwater causes a visible disturbance of the wave velocity, pressure and free surface on both sides of the breakwater. On the left side due to the complex impact and overtopping of the breakwater and on the right side because of the reflected wave created when impacting the solid structure.

Figure 96. Velocity distribution of the breakwater analysis on PFEM before wave impacts breakwater.

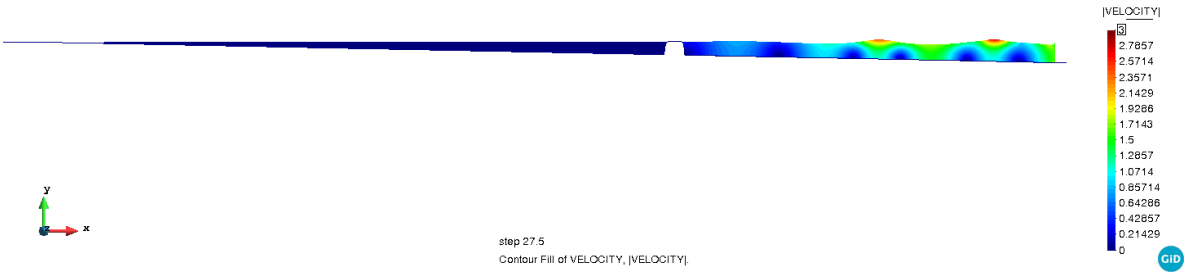

Figure 97. Pressure distribution of the breakwater analysis on PFEM before wave impacts breakwater.

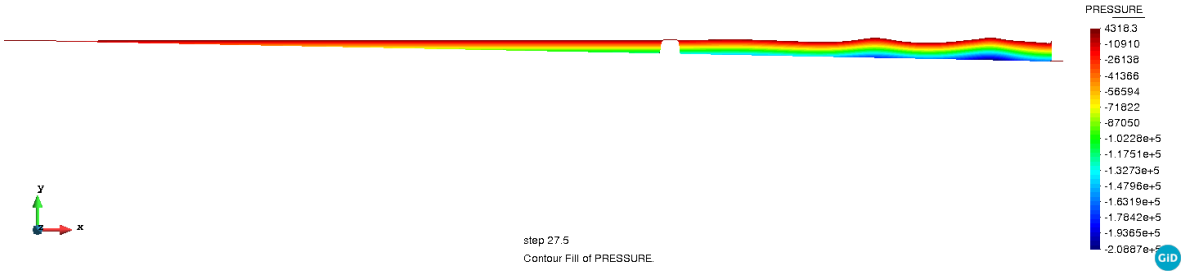

Figure 98. Velocity distribution of the breakwater analysis on PFEM after wave impacts breakwater.

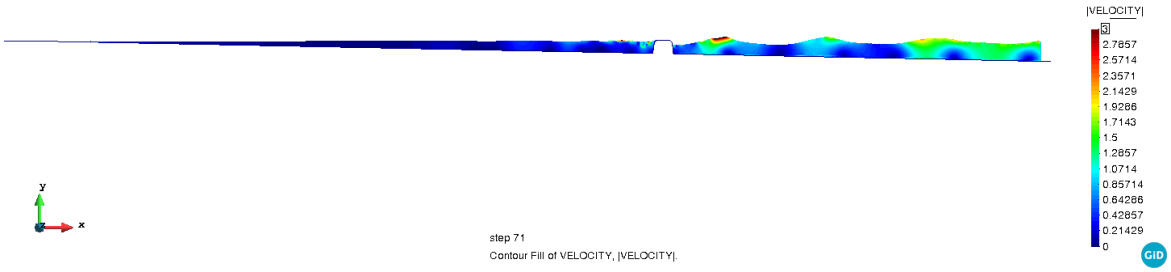

Figure 99. Pressure distribution of the breakwater analysis on PFEM after wave impacts breakwater.

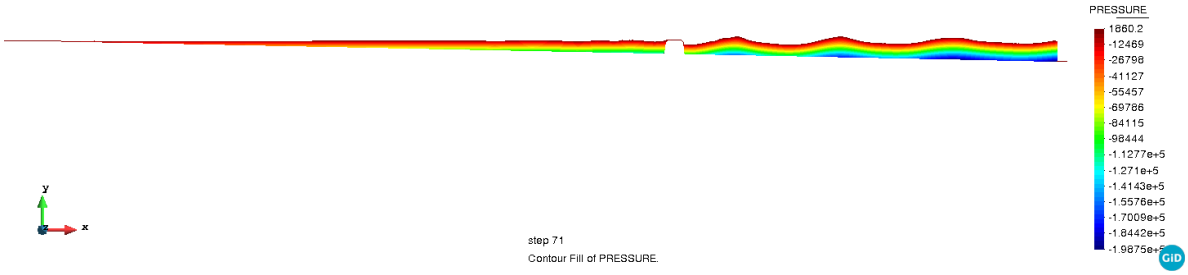

Then, the results are compared with the ones of the Eulerian FEM method using the no-slip boundary on two different wave gauges to look at the wave behaviour of the numerical method before and after the wave reaches the breakwater (Figure 100 and Figure 101). The data used and obtained for the different cases are shown in Table 17 and Table 18.

Table 17. Data used and obtained for the homogenous mesh case of the breakwater analysis

DATA HOMOGENOUS	
Mesh Size Global zone (h)	0.5
Time step size (ΔT)	0.005
Compuational cost (s)	161272.46
Number of printed elements PFEM	1393
Number of Nodes	32513
Tolerance	0.4

Table 18. Data used and obtained for the refined mesh case of the breakwater analysis

DATA REFINED	
Mesh Size Global zone (h)	0.75
Mesh Size Refined Zone (h)	0.4
Time step size (ΔT)	0.005
Compuational cost (s)	161272.46
Number of printed elements PFEM	1370
Number of Nodes	32513
Tolerance	0.4

Figure 100. Breakwater wave height measurement of PFEM and FEM at 550 metres from the shoreline

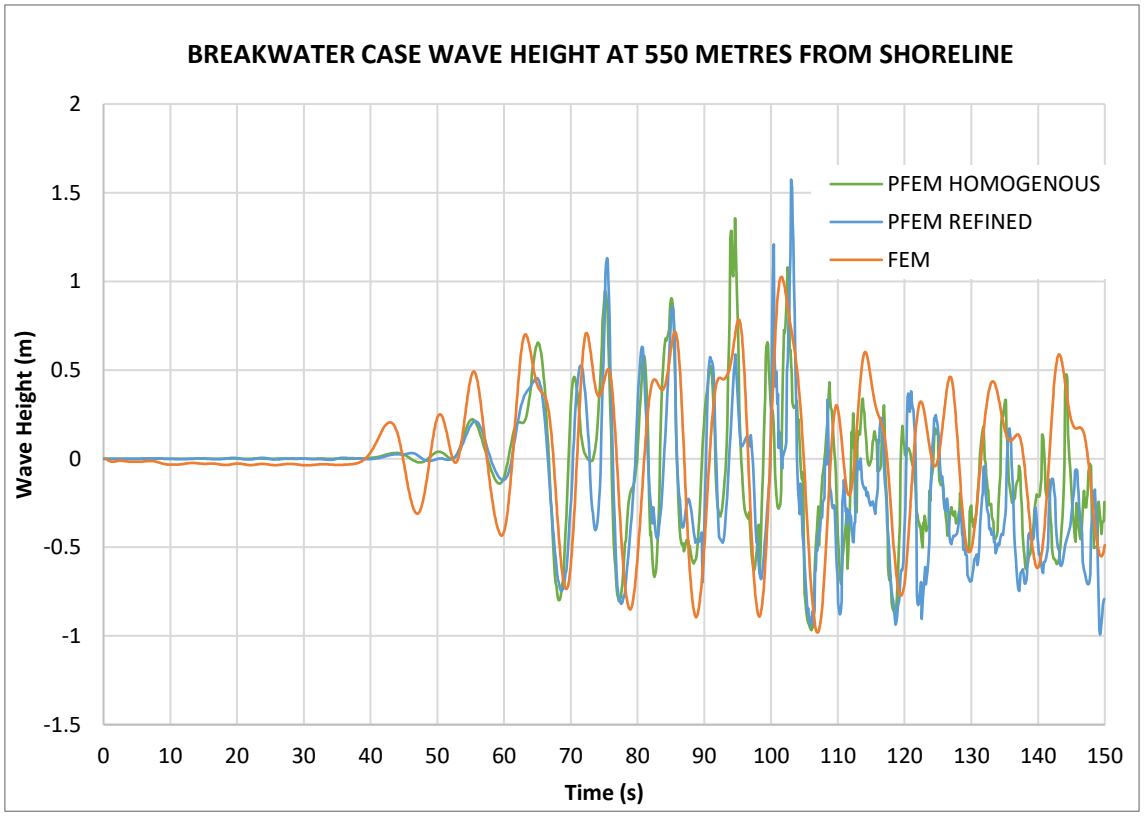

Figure 101. Breakwater wave height measurement of PFEM and FEM at 700 metres from the shoreline

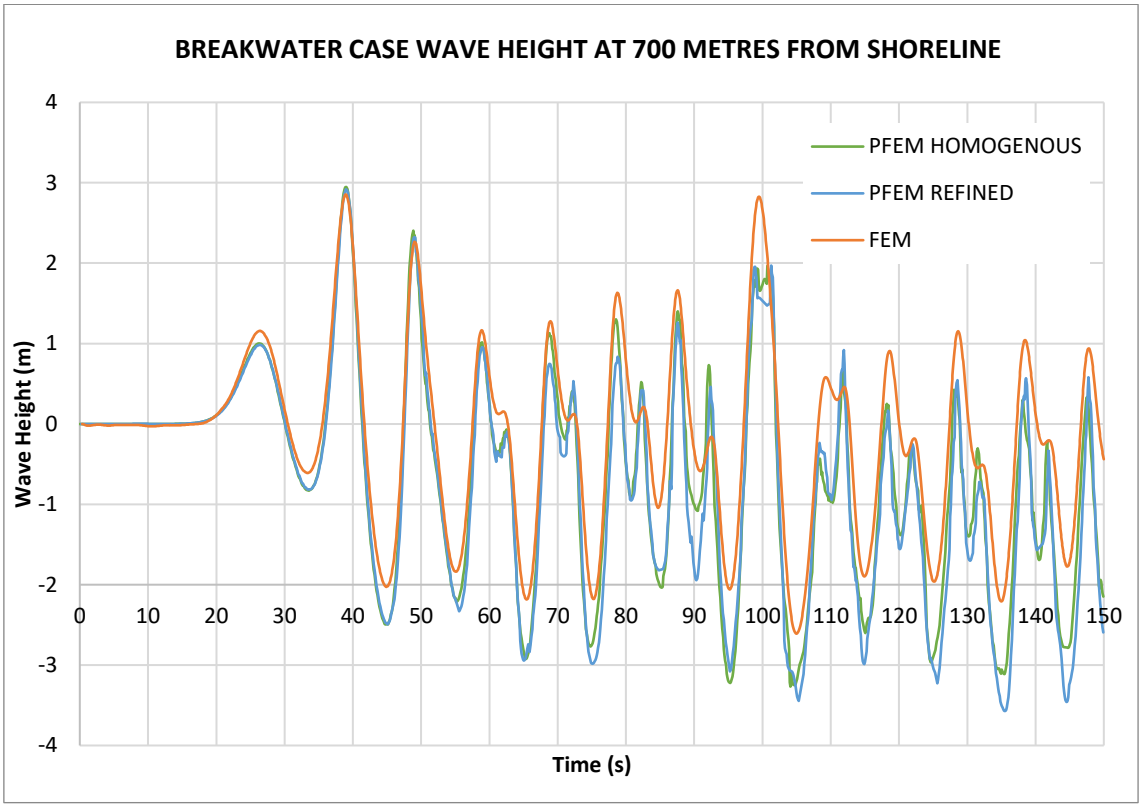

Analysing the results, the first thing that is noticed is the change in accuracy of the results compared to the previous analysis. On the one hand, the wave height measurement at 700 metres from the shoreline (Figure 101) shows how the accuracy of the performed simulation suffers an important decrease after approximately 60 seconds. This occurs when the wave regularly becomes affected by the breakwater reflection waves. On the other hand, the measurements at 500 metres from the shoreline, after the breakwater show high irregularities.

Looking at the different methods used, it is seen that PFEM homogenous and refined meshes had similar accuracies of results, with a slight improvement on the refined case. Regarding the comparison of PFEM and FEM case, it is visible how FEM have more regular wave height measurements and while at 700 metres from shoreline measurement point the measurements had higher crests and trough, on 500 metres it is the other way around.

Another important aspect to look at is the wave transmission, the fraction between the transmitted wave after the impact with the breakwater and the incident wave, before the breakwater. Table 19 shows this factor for the wave studied by comparing the maximum wave height measurements at 700 and 550 metres from the beach shoreline. It shows how the transmission of PFEM has bigger values compared to FEM and for this case, where there is some

overtopping on the breakwater, the transmission coefficient for this case has an approximate value of (K_t=*0.4*).

Table 19. The transmission coefficient of the different cases of the breakwater analysis

TRANSMISSION COEFFICIENT (Kt)	
PFEM HOMOGENOUS	0.4598239
PFEM REFINED	0.5390917
FEM	0.3592426

To look if the transmission coefficient obtained is reliable, the results obtained are compared to the theoretical ones of Van der Meer transmission coefficient formulation (Meer, 1995), as noted in Equation 7. First, it is needed to obtain the fraction between the freeboard (R_c) and the incident wave height (H_f) for each case (Equation 12). The freeboard is obtained from the channel geometry (R_c=1m) and the incident wave height from the measurements of the gauge located at 700 meters from the shoreline for the different cases. The obtained values are inside the limits corresponding to Equation 13. Then, the transmission coefficients of all studied cases are obtained (Equation 14).

Equation 12. Freeboard - Incident Wave Height fraction calculation

$$PFEM\ HOMOGENOUS\colon \frac{Rc}{Hf} = 0.339$$

$$PFEM\ REFINED\colon \frac{Rc}{Hf} = 0.342$$

$$FEM\colon \frac{Rc}{Hf} = 0.350$$

Equation 13. Transmission coefficient formula following Van Der Meer formulation

$$Kt = 0.46 - 0.3\frac{Rc}{Hf}\ , for - 1.33 < \frac{Rc}{Hf} < 1.2$$

Equation 14. Transmission coefficient calculation for each case study following Van Der Meer formulation

$$PFEM\ HOMOGENOUS\colon Kt = 0.358$$

$$PFEM\ REFINED\colon Kt = 0.357$$

$$FEM\colon Kt = 0.354$$

The obtained results by the numerical method (Table 19) compared to the theoretical ones of Van Der Meer formulation (Equation 14) has similar values, especially on the Eulerian FEM methods. Then, the good behaviour of the wave impact with the breakwater is proved.

7.4. CONCLUSIONS

The study showed how PFEM and Eulerian FEM can be used for the study of wave impact on breakwaters as the results obtained are physically meaningful. Nevertheless, the methods showed important accuracy issues in the results, particularly for the zone placed after the breakwater. The complexity of the situation makes the different numerical methods have notorious errors on the wave measurements, especially PFEM, due to the loss of regularity.

The different errors that appear are highly related to the complex water behaviour in contact with structures. This effect is easily noted because of the decrease in the system accuracy after 60 seconds in the measurements at the wave gauge located at 700 metres from the shoreline as this mainly happens due to the wave reflection the breakwater causes. When the reflected wave reaches again the wave gauge, the complexity of the situation makes the accuracy of the results decrease notoriously.

As the computational cost of the case is very high, to increase the system precision, the option of the usage of a refinement box was tested. Even there is a slight improvement in results, the accuracy improvement on the refinement case is non-sufficient. Then, it would be necessary to increase the mesh resolution and decrease the time-step size to obtain better results for complex cases when wave impacts with breakwaters.

Despite the reported differences, both methods (PFEM and Eulerian FEM) resulted in a similar estimation of the breakwaters transmission coefficient ($K \approx 0.4 \pm 0.05$).

8. CONCLUSIONS

The main objective of this work was to validate the use of Lagrangian numerical methods, the PFEM, for the simulation of waves propagation and their impact against breakwaters. This objective was achieved as the features of the numerical method with the support of GID and Kratos software allowed to perform all the desired analyses with good results. The system can be considered validated by comparing it with experimental results and to another numerical method based on Eulerian FEM.

The overall objective of this work was fulfilled by analysing different problems of waves propagation, solitary and wave trains, and their impact with breakwaters. The study allowed us to obtain some interesting conclusions about the strengths and weaknesses of the method. In this section, a detailed analysis of the specific issues arisen in the study is provided for each one of the four problems that have been studied.

Test and validate PFEM for regular solitary waves

Regular solitary waves are a simple case to observe the functioning of PFEM. To achieve this objective, two different analyses were performed. The first one consisted of a small-amplitude solitary wave analysis based on the study of a certain tsunami case. This analysis was run with the PFEM and compared to the experimental results conducted on an experimental laboratory channel in Braunschweig (Hitzegrad, 2019). The second analysis consisted of a big-amplitude solitary wave with a more complex beach geometry where the wave breaks. The case is also run with the PFEM and compared with a laboratory experiment carried out in Japan by Arikawa in the large Hydro Geo-Flume facility (Arikawa, 2009).

The PFEM showed to be able to reproduce with good accuracy the experimental results. The analyses proved the mesh and computational time-step convergence of the method and its importance to be found to do an optimal accurate and with low computational cost analysis.

It has been shown that to find an appropriate value for the mesh size, it is necessary to use an approximate good value for the time-step size, and otherwise. Thus, this method asks to do iterations between both inputs (mesh size and time-steps) to obtain the correct values. It is recommendable to iterate first with a range of values for the mesh size as it is more optimal to have an approximate correct value for the mesh density before doing the time-step size convergence analysis than the other way around.

To obtain the wave height measurement on the numerical channel on PFEM an additional function is added to Kratos scripts that work as a wave gauge at the desired point. The study shows how the function asks as an input a tolerance distance from the exact wave gauge location to obtain the measurements. This happens because PFEM nodes movement can cause that at certain time-steps, there is no node on the exact wave gauge location. Then, as PFEM data is stored at the nodes, the method would not be able of obtaining the wave height measurements. By applying a tolerance to this process, the function guarantee to find at least one node inside the limits. If there is more than one node, the function does the average between them. As consequence, too big tolerances can decrease the accuracy of the results as the function obtains the heights from nodes at some distance from the wave gauge. As the number of nodes to be

found by the function depend directly on the mesh size, the correct tolerance to choose depends on the mesh resolution of each case.

Finding the appropriate tolerance for each mesh size may be a long and difficult process and can be different for each study. There could be some improvements regarding this function. For example, the program could automatically find the correct tolerance value or, it should be possible to find a more optimum way of finding the wave height measurements on PFEM studies.

It is also seen how the discrepancy between numerical and experimental results increases along with the duration of analysis and with distance from the wave paddle. An easy way to counteract this tendency is to increase the analysis mesh density and decrease the computational time-step although it increases exponentially the computational cost.

The computational cost necessary to perform the analysis has been proved to be highly sensitive to the mesh and time-step sizes. Then, it is recommendable to run the cases with low values of time-step size and big values of mesh size to ensure the problem is set correctly set before putting the desired value.

A good strategy to reduce the computational cost of the analyses while keeping a good accuracy is to use mesh refinement boxes. As GID and Kratos allow the addition of refinement boxes, a refinement study is done on the second analysis. This refinement consists of implementing a different mesh size to a specific zone of the numerical channel, usually the one with more complex behaviour.

The study showed that the refinement process allows decreasing the computational cost while maintaining good accuracy. Nevertheless, the results showed a slight difference in the wave height measurements between the refinement cases and the ones of homogenous meshes. The wave peak on refined studies happens before compared to the other analyses. The reason for this error is not clear but it may be caused by the appearance of excessively deformed elements on the interface between the two zones mesh sizes. This factor should be studied to find alternatives or corrections that could avoid it.

Furthermore, the wave height measurements of the numerical channel showed slightly bigger results than the experimental ones. This discrepancy may be due to the infinite width of the study set on the numerical method while on the experimental one, the lateral width is limited and causes friction on the wave movement reducing its height. This error also increases with time of study as the effect is accumulated.

The big-amplitude solitary wave analysis validated the capacity of PFEM to perform studies of breaking waves. It was proven that this numerical method can correctly simulate fluid parts getting separated from the rest of the domain and its splashing with the fluid body.

Test and validate PFEM for regular wave trains

Wave train analysis is a different study to which the PFEM has been tested. The analysis consists of a piston wave generator on a long beach with a small slope generating a set of waves that do not break. The study validated PFEM for the study of wave trains as the results were meaningful

and the mesh density and computational time-step convergence was proven and found although it presented some imperfections and obstacles that need to be noted.

The study clearly shows the loss of accuracy of the numerical method on long periods of analysis due to the accumulation of errors and the loss of optimum mesh regeneration. The decrease of wave height due to the loss of water mass on the numerical channel also incentive the creation of these inaccuracies on the system meshes. An option to avoid this imperfection to happen could be to modify the system geometry to avoid water flowing out of the problem by introducing some slope on a long beach shore or by introducing water to the system at the same rate it flows out.

The study performed a refinement study which was proven satisfactory as it increased the accuracy of the problem with lower computational costs. It would be good to analyse the system with different refinement structures to obtain a better option. As on the solitary wave analysis, the refinement study presented some errors. It showed lower values of wave height measurement, especially on the wave trough.

The study conducted was of big dimensions and needed high precision to do the analysis correctly so, despite its size, low values of mesh size and computational time-steps were needed. Then, the computational cost needed was of the order of many days and the outputs were of big dimensions that could occupy all the memory available on Aquario. To avoid it, GID and Kratos software allows modifying the time-step for printing the results.

Compare PFEM and Eulerian FEM numerical methods.

The third analysis did a comparison between PFEM and FEM analysis for the same wave channel. The objective was to compare both methods, PFEM and FEM, and to observe and compare the two possible boundary mechanisms regarding the fluid-solid contact, slip (for FEM) and no-slip (for FEM and PFEM). However, important errors were obtained on this second stage of the objective.

PFEM system showed some important geometry conditions and limitations that need to be taken care of to run the problem correctly. It is possible to have water leakage if the paddle movement causes holes in the system boundaries or if it grabs wall nodes. This may cause a difference in geometry with the FEM analysis reducing the precision of the comparison. However, due to the big dimensions of the study and the small mesh size, this factor can be considered negligible. Then, the results showed may be considered accurate regarding this limitation. Furthermore, the study demonstrated that the optimum mesh used for the FEM and PFEM analysis may not be the same.

The results obtained by the PFEM gave a higher wave amplitude than the one given by the FEM although the wave period and length were very similar between the two methods. The difference increases with time and distance to the wave paddle. Unfortunately, for this analysis, it was complex to obtain conclusions about the effect of boundary conditions on the numerical results due to the excessive discrepancy between the different results.

Furthermore, the comparison between FEM no-slip and FEM slip boundary conditions was counter-intuitive as the no-slip boundaries had bigger wave height measurement results than the ones of the slip the friction caused by the no-slip boundary conditions should make the measurements lower. A hypothesis to explain this factor could be the elevation of a node on the no-slip analysis due to the solid-fluid contact, making the SWL to get elevated and the wave amplitude to increase due to the depth decrease.

To get the insights of the impact of breakwaters upon the wave height in the vicinity of the beaches.

This study also analysed the effects of wave train impacts with breakwaters with the two numerical methods, PFEM and Eulerian FEM. It has been seen that both methods are capable of reproducing the effect of the breakwater. It was proven that the numerical methods can be used for the study of wave impact on the breakwater with overtopping as the systems were capable of simulating water parts leaving and entering the fluid domain. The different analyses do not show important errors and the overall behaviour of the wave is correct.

When comparing the Eulerian FEM and PFEM results, it is seen the waves obtained by the Eulerian FEM are smoother than the ones of PFEM, with fewer irregularities, both in the incident-reflected and transmitted wave heights measurements.

The study also showed important accuracy issues related to the high complexity of the cases studied. The wave reflection and overtopping caused by the wave impact with the breakwater causes complex water movements difficult to predict. Even with the addition of the refinement box, the precision of the wave measurements is not enough. Then, it would be needed to increase the analysis mesh density and decrease the time-step size.

Overall, all analyses were capable of simulating the reduction of wave height of the breakwater. This coastal structure causes an important decrease in wave height. A useful parameter to study this effect is the called transmission coefficient, the fraction between the transmitted and the incident wave heights. The analyses studied these results by comparing the wave height measurements of the two wave gauges located closer to both sides of the breakwater. Both methods, PFEM and Eulerian FEM acquired good transmission coefficients when comparing them to the ones of the Van Der Meer formulation.

Further lines of investigation

This work focused on the study of the PFEM numerical method and its implementation of Kratos Multiphysics. Despite the discrepancy that has been commented on the document, the method showed good accuracy. It is a fast way of performing wave studies and it presents more freedom on the study features than the laboratory experimental ones although nowadays the numerical studies need to be complemented by experimental ones to be validated. For these reasons, I find it optimum to do further studies regarding the numerical method. During the project, some further lines of investigation were opened:

- Mesh refinement: as described, the refinement process involves the appearance of a certain error. The reason for this error should be studied to find adequate countermeasures.
- Multiple refining boxes: in the current state of the PFEM Kratos-GiD software, it is only possible to use a unique and fixed refining box. However, in some cases, it could be useful to use multiple refining boxes and even allow them to have a prescribed motion during the analysis
- PFEM wave height measurements: during this project, the wave height measurements on PFEM were performed by an added function to the Kratos scripts. It presented some complications regarding the setting of the correct tolerance. It is suggested to find a more optimum or automatic way of obtaining the correct tolerance or to find an alternative way of getting the wave height measurements.
- Computational time cost: during this study, many of the analyses needed high computational time costs, of the order of days. The investigation of mechanisms to optimize the computational cost-result accuracy is an important line of investigation.

REFERENCES

Airy, G., 1842. Tides and waves. *Encyclopedia Metropolitana,* Volume 5, pp. 241-396.

Arikawa, T., 2009. *Structural behavior under impulsive tsunami loading.* s.l.:s.n.

Conejo, A. S.-A., 2021. *Regular waves.* s.l.:s.n.

Cremonesi, M., Franci, A., Idelsohn, S. & Oñate, E., 2020. A State of the Art Review of the Particle Finite Element Method (PFEM). In: *Archives of Computational Methods in Engineering.* s.l.:s.n., p. 1709–1735.

Dadvand, P., Rossi, R. & Oñate, E., 2010. . An Object-oriented Environment for Developing Finite Element Codes for Multi-disciplinary Applications. In: *Arch Computat Methods.* s.l.:s.n., p. 253–297.

Donea, J., Huert, A., Ponthot, J. & Rodríguez-Ferran, A., 2004. Arbitrary Lagrangian–Eulerian Methods. In: *The Encyclopedia of Computational Mechanics.* s.l.:s.n., pp. 413-437.

Edelsbrunner, H. & Mücke, E. P., 1994. Three-dimensional alpha-shape. In: *ACM Transactions on Graphics,.* s.l.:s.n., pp. 43-72.

Edinburg Designs, 2016. *Wave Generators.* [Online]
Available at: http://www4.edesign.co.uk/waves/some-wave-1/

Hashemi, M., Ryzhakov, P. & Rossi, R., 2020. An Enriched Finite Element/Level-Set Method For Simulating Two-Phase Incompressible Fluid Flows With Surface Tension. In: *Computer Methods in Applied Mechanics and engineering.* s.l.:s.n.

Hirt, C. & Nichols, B., 1981. Volume of fluid (VOF) method for the dynamics of free boundaries. In: *Journal of Computational Physics.* s.l.:s.n., pp. 201-225.

Hitzegrad, J., 2019. *Experimental study on collapsing structures in extreme flow conditions.* Braunschweig: s.n.

Hughes, S. A., 1993. Physical models and laboratory techniques in coastal engineering. *World Scientific,* Volume 7.

Idelsohn, S. R., NestorCalvoa & EugenioOñate, 2003. Polyhedrization of an arbitrary 3D point set. In: *Computer Methods in Applied Mechanics and Engineering.* s.l.:s.n., pp. 2649-2667.

Meer, J. W. d., Brigantib, R., Zanuttighc, B. & Wangd, B., 2005. Wave transmission and reflection at low-crested structures: Design formulae, oblique wave attack and spectral change. In: *Coastal Engineering.* s.l.:s.n., pp. 915-929.

Meer, J. W. V. D., 1995. Conceptual design of rubble mound breakwaters. In: *Advances in Coastal and Ocean Engineering.* s.l.:s.n., p. 221.215.

Oliveira, T., 2012. *Generación de olas y estudio del rebase en un canal numérico basado en el PFEM.* s.l.:s.n.

Oñate, E., 2000. A stabilized finite element method for incompressible viscous flows using a finite increment calculus formulation. In: *Computer Methods in Applied Mechanics and Engineering.* s.l.:s.n., pp. 355-370.

Oñate, E. et al., 2022. Combination of the finite element method and particle-based methods for predicting the failure of reinforced concrete structures under extreme water forces. In: *Engineering Structures.* s.l.:s.n.

Oñate, E., Franci, A. & Carbonell, J., 2014. Lagrangian Formulation for Finite Element Analysis of Quasi Incompressible Fluids with Reduced Mass Losses. In: *International Journal for Numerical Methods in Fluids.* s.l.:s.n., pp. 699-731.

Osher, S. & Fedkiw, R. P., 2001. Level Set Methods: An Overview and Some Recent Results. In: *Journal of Computational Physics.* s.l.:s.n., pp. 463-502.

Rajendran, V., 2021. *What is the difference between Lagrangian and Eulerian elements and analysis in finite element analysis?.* [Online]
Available at: https://www.quora.com/What-is-the-difference-between-Lagrangian-and-Eulerian-elements-and-analysis-in-finite-element-analysis

Ryzhakov, P. & Oñate, E., 2017. A finite element model for fluid–structure interaction problems involving closed membranes, internal and external fluids. In: *Computer Methods in Applied Mechanics and Engineering.* s.l.:s.n., pp. 326, 422-445.

Ursell, F., Dean, R. G. & Yu, Y. S., 2006. Forced small-amplitude water waves: a comparison of theory and experiment. *Journal of Fluid Dynamics,* Volume 7(1), pp. 33-52.